

University of Nevada, Reno

Molybdenum Mineralization in Deep Drill Holes at the Cresson Mine
And Geology of Grouse Mountain: Cripple Creek District,
Teller County, Colorado

A thesis submitted in partial fulfillment of the
requirements for the degree of Master of Science in
Economic Geology

by

Crystal L. Robinson

Dr. Tommy B. Thompson/Thesis Advisor

December 2010

UMI Number: 1484050

All rights reserved

INFORMATION TO ALL USERS

The quality of this reproduction is dependent upon the quality of the copy submitted.

In the unlikely event that the author did not send a complete manuscript and there are missing pages, these will be noted. Also, if material had to be removed, a note will indicate the deletion.



UMI 1484050

Copyright 2011 by ProQuest LLC.

All rights reserved. This edition of the work is protected against unauthorized copying under Title 17, United States Code.



ProQuest LLC
789 East Eisenhower Parkway
P.O. Box 1346
Ann Arbor, MI 48106-1346



THE GRADUATE SCHOOL

We recommend that the thesis
prepared under our supervision by

CRYSTAL L. ROBINSON

entitled

**Molybdenum Mineralization in Deep Drill Holes at the Cresson Mine
And Geology of Grouse Mountain: Cripple Creek District,
Teller County, Colorado**

be accepted in partial fulfillment of the
requirements for the degree of

MASTER OF SCIENCE

Tommy B. Thompson, Ph. D., Advisor

Jonathan G. Price, Ph. D., Committee Member

Victor R. Vasquez, Ph. D., Graduate School Representative

Marsha H. Read, Ph. D., Associate Dean, Graduate School

December, 2010

Abstract

The Cripple Creek district in Teller County, Colorado has a long and distinguished mining history. From sheeted vein systems to large, low-grade disseminated deposits, ore is still being produced from the district, mainly at the largest operating mine in the district, the Cresson Mine. In 2003 the deepest holes drilled in the district were in the diatreme near Globe Hill (in the north) and the Cresson Pipe (in the south). These drill holes encountered molybdenum and base metal minerals in addition to continued but limited gold mineralization. Outboard of the diatreme there are several volcanic outliers. At the time of this study most had been mapped only in reconnaissance, and the question remained as to whether they were intrusive in origin or remnants of volcanic flows.

This study is two separate projects and will be addressed as such herein. The first portion deals with whether gold is related to molybdenum. Several methods were attempted to ascertain their relationship. Core and RC chips were logged onsite during the Summer, 2009, and twenty-six samples were collected for petrography to produce polished thin sections. The paragenesis was established from these sections, and fluid inclusions associated with the molybdenite were sought but not found. No gold-bearing minerals were observed in thin section but molybdenite was consistently later than base metals, and previous workers have documented that gold post-dates base metals. The billets for these samples were then stained to identify down-hole changes in potassium feldspar flooding, as potassic flooding is generally associated with gold in the district. Samples were taken at five-foot intervals every twenty feet for geochemical analysis, and correlation matrices of these data were calculated. The data showed that gold has a weak

to locally negative association with molybdenum. Finally, sulfur isotope analysis of molybdenite was conducted. Most of the $\delta^{34}\text{S}$ values lie within a narrow range of $0 \pm 5\%$, a range identified by Ohmoto and Goldhaber (1997) as characteristic of porphyry systems in the western U.S.

The second goal of this project was to examine the outliers to determine if they are intrusive or remnants of flows. Several outliers were explored, and two were mapped but Grouse Mountain was chosen for this report due to its complexity and degree of alteration. A geologic map, including alteration, was developed and samples were collected for petrography and chemical analyses. Two units not previously recognized at Grouse were found in this study. The first unit had previously been mapped as a hornblende phonolite or just a phonolite, but petrography has revealed it is a clinopyroxene-bearing phonolite. The second unit has been mapped as the Tallahassee Creek Conglomerate but is actually a breccia unit, known herein as “Grouse Mountain breccia.” Staining of billets from Grouse Mountain with sodium cobaltinitrite indicates that potassic alteration is abundant at Grouse.

The presence of altered Wall Mountain Tuff on the summit of Grouse Mountain, and the degree of alteration suggest that Grouse Mountain is intrusive in nature. Geochemical analysis indicates three distinct fluids based on elemental correlations. These fluids are a Au-Mo fluid, a Ag-Cu-Te fluid, and a Pb-Zn-Cd fluid. While the transition from one fluid to the next is likely gradual, it is not possible to determine the timing relationship between these fluids because correlation analyses only denote a spatial relationship.

Future exploration for the molybdenum within the diatreme should include drilling to delineate the extent and grade of the deposit. Since the molybdenum is mostly concentrated in the north and is more accessible there, drilling should begin in the north. Analysis of the sphalerites to determine if the molybdenum is hosted within the sphalerite lattice would be an important consideration for processing. For Grouse Mountain, samples from drilling should be examined to determine the extent and type of breccia body present. Additional drilling will not only define the breccia but should also aid in refining the surface geology.

Acknowledgements

This project has been made possible by the Center for Research in Economic Geology at University of Nevada, Reno and funding from Cripple Creek and Victor Gold Mining/AngloGold North America. I would like to thank my advisor, Dr. Tommy Thompson, for valuable input on this project and helpful insight when complications arose with the research. I am very grateful to all the geologists at the Cresson Mine, especially Emery Roy, George Papic, Tim Brown, and Andi Dillard for numerous geological discussions and valuable input as well as for making me feel at home during the summer I spent in Victor and, of course, Brenda Wolfe for her tireless efforts to create and maintain the property database.

I also owe a great debt of gratitude to my family and friends for helping me get my mind off work when I go into overload and for supplying a level of sanity to my world when I “just need to get out of town.” My committee members have been wonderful as well. I want to thank Jon Price for extremely helpful discussions regarding the geochemical aspects of the project and Victor Vasquez for his unfailing sense of humor. I would like to mention Sean Mulcahy at UNLV to thank him for his assistance with the SEM. Without his guidance the SEM work would have been much more difficult. Also, Simon Poulson was tremendously helpful regarding the stable isotope work. Finally, I would like to thank various geologic colleagues for sincere discussions regarding this project.

Table of Contents

<i>Abstract</i>	<i>i</i>
<i>Acknowledgements</i>	<i>iv</i>
<i>Introduction</i>	<i>1</i>
<i>Regional Geology</i>	<i>3</i>
<i>District History, Production, & Geology</i>	<i>5</i>
<i>Mineralization</i>	<i>12</i>
<i>Fluid Inclusions</i>	<i>16</i>
<i>Isotopes</i>	<i>17</i>
<i>Part 1: Molybdenum vs. Gold</i>	<i>19</i>
Methods	20
Results	26
Paragenesis.....	26
Potassic Alteration/Flooding.....	36
Geochemistry.....	39
SEM Analyses.....	42
Sulfur Isotope Analyses.....	42
Discussion	45
Future Work	47
Conclusion	48
<i>Part 2: Grouse Mountain</i>	<i>49</i>
Methods	49
Results	51
Mapping.....	51
Alteration.....	53
Geochemistry.....	53
Discussion	56
Future Work	58
Conclusion	58
<i>References</i>	<i>60</i>
Appendix A: Pearson's Correlation Coefficients.....	65
Appendix B: CC-2272, CC-2273, GHC-747-D & D2: Stained Billets.....	74
Appendix C: CC-2272, CC-2273, GHC-747-D & D2: Photomicrographs.....	77
Appendix D: CC-2272, CC-2273, GHC-747-D & D2: Geochemical Graphs.....	88
Appendix E: SEM Images and EDS Spectra.....	93

Appendix F: Geologic Map of Grouse Mountain	102
Appendix G: Pearson's Correlation Coefficients for Grouse Mountain.....	106
Appendix H: Grouse Mountain Stained Billets	109
Appendix I: Grouse Mountain Geochemical Graphs.....	112
Appendix J: Grouse Mountain Photographs and Photomicrographs	117

Tables

<i>Table 1. Geochemical associations (correlation coefficients) for gold and molybdenum in the diatreme.</i>	<i>40</i>
<i>Table 2. $\delta^{34}S$ values for molybdenite. CR samples are from this study, while J-1 and J-2 are from Jensen (2003). See Figure 4 for an index map showing the locations of the drill holes from which the samples were taken.</i>	<i>44</i>
<i>Table 3. Elemental correlations at Grouse (top) and elemental correlations with gold from the four drill holes in the diatreme (bottom) for comparison.....</i>	<i>54</i>

Figures

<i>Figure 1. Location and general geology.....</i>	<i>3</i>
<i>Figure 2. Geologic map of the Cresson open pit.....</i>	<i>10</i>
<i>Figure 3. Sub basins within the Cresson Diatreme</i>	<i>12</i>
<i>Figure 4. Index map showing location of drill holes.....</i>	<i>21</i>
<i>Figure 5. Paragenetic diagram for CC-2272</i>	<i>28</i>
<i>Figure 6. Paragenetic diagram for CC-2273</i>	<i>29</i>
<i>Figure 7. Paragenetic diagram for GHC-747-D & D2.....</i>	<i>30</i>
<i>Figure 8 A-F. A) Molybdenite entraining sphalerite and minor galena; B) Molybdenite interstitial to gangue minerals; C) Molybdenite and ankerite replacing adularia rhomb; D) Same view as C, crossed polars; E) Molybdenite replacing pyrite; F: view of pyrite grain with local molybdenite replacement.....</i>	<i>31</i>
<i>Figure 9. Cross section looking NE showing GHC-747-D & D2 drill holes</i>	<i>33</i>
<i>Figure 10. Cross section looking NE showing CC-2272 & CC-2273 drill holes.....</i>	<i>33</i>
<i>Figure 11. A) A zoned feldspar crystal; B) A close up view of the margin of a feldspar crystal with multiple zoning cut by a calcite veinlet.....</i>	<i>36</i>
<i>Figure 12. Stained billets from CC-2272, CC-2273, and GHC-747-D holes illustrating the presence and location of potassium flooding.....</i>	<i>38</i>
<i>Figure 13. Frequency diagram of sulfur isotope data.....</i>	<i>44</i>

Introduction

The Cresson Mine is situated within an alkaline Oligocene diatreme complex in the Cripple Creek district, Teller County, Colorado (Fig. 1). The district is widely known for its abundant telluride mineralization; however, drilling in 2003 has revealed the presence of molybdenite and sphalerite at depth in the Cresson open pit. The presence of molybdenum and base metal sulfides in drill core may indicate an additional economic resource at depth. If an economic molybdenum deposit does exist, the question remains of whether or not the molybdenum mineralization is related to the gold mineralization or if these were two separate events. This study examines the nature and timing of molybdenum mineralization to see how it compares with the well-studied gold mineralization and base metal events in the district.

There are also several volcanic or intrusive outliers present in the vicinity of the Cripple Creek diatreme-intrusive complex that may host mineralization. The origin of these outliers has not been established but could provide vital clues as to their economic potential. If the outliers are erosional features resulting from volcanic flows, then they are not likely candidates for economic mineralization. However, if they are intrusive, then the potential for mineralization at depth may exist. This study looks at one of the outliers, Grouse Mountain, and at its chemical composition, alteration, origin, and economic potential. A comparison of elemental associations at Grouse with elemental associations in the diatreme will be presented. The information is discussed with emphasis on its relevance to future exploration.

The importance of the project is threefold. First, exploration must continue if a mine is to remain profitable, and understanding the characteristics associated with

mineralization outboard of the diatreme would greatly facilitate such exploration. Secondly, discovery of a molybdenum or base metal deposit at Cresson could extend the life of the mine if the resource is large enough to be economic. Last but not least, from an academic standpoint, unearthing such a deposit at depth in a telluride-rich diatreme system could encourage exploration at depth in other similar systems if the gold mineralization and molybdenum mineralization are linked. If molybdenum and base metal mineralization resulted from a separate event independent of gold mineralization or as a result of certain magmatic and tectonic regimes, the applications to exploration in other deposits without such a setting may be limited. Either way, information obtained in this study should prove invaluable in exploring for other base metal sulfide deposits at depth in alkaline diatreme complexes.

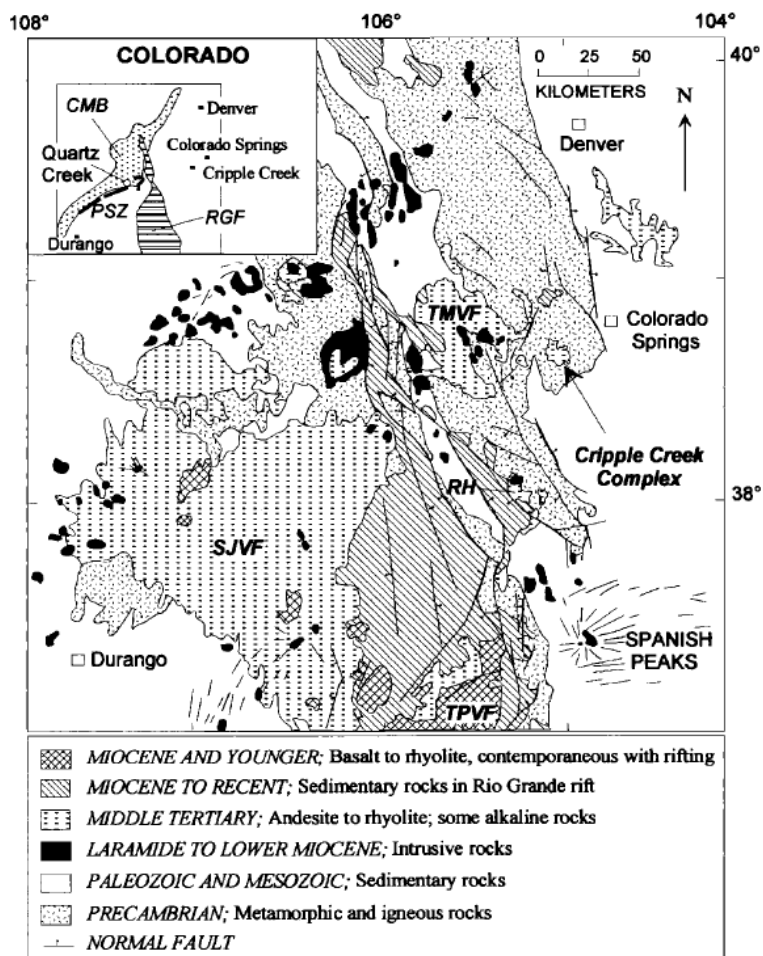


Figure 1. Location and general geology from Kelley et al., 1998.

Regional Geology

The geologic history of the region that encompasses the Cripple Creek district began with the accretion of metamorphic and gneissic terranes, including the Idaho Springs Formation, to the Archean Wyoming craton in the neighborhood of 1.8-1.7 Ga (Reed et al., 1987; Jensen, 2003). Following the accretion event, N-NE to N-NW shear zones and faults and prominent NE basement structural trends, such as those found in the Cripple Creek district, developed (Tweto and Sims, 1963). Pluton emplacement continued throughout the Precambrian as these structural fabrics formed, giving rise to

granodiorites (1.7 Ga; Wobus et al., 1976), the Silver Plume magmatic suite (Karlstrom and Humphreys, 1998), the Cripple Creek Quartz Monzonite (1.43 Ga; Hutchinson and Hedge, 1968), and the Pikes Peak Granite (1.04 Ga; Hedge, 1970). Pulses of alkaline magmatism in the region occurred throughout the mid Proterozoic and in Cambrian to Ordovician time (Jensen, 2003).

During a period of time between the Precambrian and Cambrian there was a hiatus in sedimentation across the western United States known as the Great Unconformity (Powell, 1876). The Great Unconformity is represented in this region by sedimentary deposits overlying the Precambrian units. Sedimentation resumed in the Paleozoic and continued through the Mesozoic. The type of sedimentation varied with time: Cambrian to Mississippian fluvial and marine deposits represent a low energy environment, while Pennsylvanian to Permian sediments were coarse and arkosic to conglomeratic and resulted from tectonism related to the ancestral Rocky Mountains. Multiple transgressions and regressions are apparent in the geologic record during this time period, indicating that the region was at or near sea level.

Alkaline magmatism persisted intermittently throughout Cretaceous-Tertiary time, including the Oligocene alkaline magmas present in the Cripple Creek district. At about 70-40 Ma the Laramide Orogeny affected the region resulting in a regional compressional tectonic setting. Thickening, uplift, and magmatism along the Colorado mineral belt resulted from Laramide compression (Tweto and Sims, 1963; Bookstrom, 1990). At about 55-40 Ma the region became tectonically inactive due to flattening of the subducting slab, a remnant of the Farallon plate (Lipman, 1981; Kelley et al., 1998). Subsequently, an Eocene erosional surface developed across the region around 55-37 Ma

due to uplift of about 2 km and erosion of approximately 4 km (Karlstrom and Humphreys, 1998). Remnants of this erosional surface can still be seen in Colorado today.

At about 40-35 Ma the tectonic regime changed from compression to extension and igneous activity in the region resumed (Kelley et al., 1998). The recommencement of igneous activity is attributed to a decreased rate of convergence and a steeper angle of subduction (Christiansen et al., 1992). Extension within the Rio Grande rift had initiated by 32 Ma (possibly as early as 38 Ma in southern New Mexico; Aldrich et al., 1986) but the timing of extension in the northern portion of the rift is not well defined and is roughly constrained to a period between 32-27 Ma (Kelley et al., 1998). Magmatism in the Cripple Creek area occurred in the Oligocene during the transition from compressional to extensional tectonics. According to Jensen (2003), volcanism in the Cripple Creek district spanned from 31.8-28.4 Ma.

District History, Production, & Geology

Over a century of geologic work has been done in the Cripple Creek district. Early studies by Cross and Penrose (1895), Lindgren and Ransome (1906), and Loughlin and Koschmann (1935) were extensive and still represent the main source of information on the district. More recent studies have built upon the previous knowledge as mining continues and more of the deposit is revealed. Jensen (2003) presents a detailed history, a reclassification of rock types, a summary of alteration and magmatism as they relate to gold deposits in the region, and a comparison of Cripple Creek to other alkaline gold deposits. Many other workers have examined fluid inclusions, isotopes, geochemistry,

and petrography (Dwellely, 1984; Thompson et al., 1985; Trippel, 1985; Birmingham, 1987; Burnett, 1995; Jensen, 2003; McIntosh, 2004). In light of these thorough reports on the subject, only a brief summary of district history, geology, and deposit characteristics will be given here.

The Cripple Creek District has had a long and distinguished mining history. The area was recognized as an abnormality as early as 1873 (Endlich, 1874) and even though slow identification of telluride mineralogy and two hoaxes (Jensen, 2003) hindered early development of the region, production estimates as of 2001 are between 20.5 M oz to 22 M oz of gold for the district (Jensen, 2003). The majority of the production in the district is historic, though the Cresson Mine is still operating today. As of 2002, reserves were estimated at 142.2 Mt of gold (average grade of 1.1 g Au/t) with identified resources of 240 Mt (1.03 g Au/t) (Yernberg, 2002).

The site of mining activity in the Cripple Creek district today is an Oligocene diatreme complex (Fig. 2). The diatreme trends northwest to southeast and is situated between Proterozoic metamorphics and three Proterozoic intrusions (Kelley et al., 1998). Within the diatreme, the Cripple Creek breccia is the most important unit and the most common host for much of the disseminated deposit that is being mined; however, rocks within the district that host gold mineralization can span many lithologies and compositions. Evidence for a diatreme in the region includes diatremal breccias (Cripple Creek Breccia), carbonized trees and organic matter at depths up to 300 m (Lindgren and Ransome, 1906), fluidized features such as accretionary lapilli (Lindgren and Ransome, 1906; Thompson et al., 1985), and fluvial and lacustrine sediments (locally interbedded with Cripple Creek Breccia) that represent shallow standing bodies of water (Koschmann,

1949; Thompson et al., 1985). The basin filled by the diatreme breccia is shallow on the eastern margin with a steeply dipping western wall. The presence of carbonaceous material and lacustrine sediments at depth support basin subsidence as the diatreme formed (Thompson et al., 1985). A generally accepted sequence of events for the formation of the Cripple Creek diatreme involves eruptive volcanism and diatreme development followed by sedimentation and subsidence and a later period of intrusions and brecciation with continued diatreme development (Thompson et al., 1985).

The Cripple Creek district was volcanically active from 31.8-28.4 Ma, producing alkaline intrusions that became more mafic with time and igneous compositions that ranged from felsic phonolites to ultramafic lamprophyres and silicocarbonatites (Jensen, 2003). Rocks within the district are commonly silica undersaturated and sodium-rich. They also contain high amounts of large ion lithophile elements, high field strength elements, light rare earth elements, and CO₂ (Jensen, 2003). Phonolite is by far the most abundant igneous rock type, and ultramafics are the least common (Kelley et al., 1998).

Following is a brief description of rock types in the district, from oldest to youngest. Detailed classifications and descriptions of district lithologies, as well as chemical analyses, can be found in Birmingham (1987) and Jensen (2003). Numerous names and classification schemes have been applied to units in the Cripple Creek district. Most were formulated before the advent of modern chemical analyses and often various nomenclatures were used for the same intrusion type. Therefore, for clarity, the classification and descriptions presented herein are dominantly from Jensen (2003).

The earliest rocks in the district are Precambrian sillimanitic schists and granites that form the basement rock into which the diatreme intruded. They may locally be

present as xenoliths in later igneous intrusions. Diatremal breccias formed throughout the history of the diatreme and are generally described as matrix supported, poorly sorted with sizes ranging from microscopic to several meters in diameter (matrix may be well sorted; Thompson et al., 1985), and heterolithic to locally monolithic with subrounded to angular clasts (Jensen, 2003). The Cripple Creek Breccia is the main diatremal breccia in the district. Early phonolites were emplaced in the breccia. They are porphyritic and composed mostly of alkali feldspar (plagioclase phonolites; Birmingham, 1987). Plagioclase is common, and early phonolites are locally cut by more mafic rocks and a younger generation of phonolites (Jensen, 2003). Equigranular phaneritic rocks encompass nepheline syenites, nepheline monzosyenites, and nepheline monzodiorites, which are the phaneritic equivalent of phonolites, tephriphonolites, and phonotephrites (Jensen, 2003). In the literature these rock types are often called syenites.

Mafic alkaline intrusions crosscut equigranular phaneritic rocks and as classified by Jensen (2003) include tephriphonolites to phonotephrites, basaltic trachyandesites, and trachybasalts. These mafic intrusions are generally porphyritic and contain augite, plagioclase, and lesser hornblende. They are differentiated from lamprophyres by the presence of plagioclase (Jensen, 2003). Late stage phonolites followed the mafic alkaline intrusions and are chiefly composed of sanidine. They are generally finer-grained than early phonolites, are referred to as aphanitic phonolites in the literature, and are radioactive enough that they may be distinguished from early phonolites on this characteristic alone (Jensen, 2003). Lamprophyres are the youngest igneous rocks in the district and are composed of mafic to ultramafic dikes and breccia pipes such as the

Cresson Pipe. They are generally magnetic and porphyritic (Jensen, 2003). Though they are volumetrically minor they are commonly associated with ore in the district.

The Cripple Creek system shows a trend from felsic to mafic lithologies through the eruption of mafic alkaline intrusions. A reversal back to more felsic compositions is apparent when the late stage phonolites are erupted and evolution of the magmas once again tends towards mafic lithologies (lamprophyres). Before the separation of early and late phonolites by Jensen (2003) early workers believed the trend toward mafic compositions was due to magma mixing (Thompson et al., 1985). Jensen (2003) used fractional crystallization and assimilation/fractional crystallization models to determine the parent magma was most likely phonotephritic and that the magma chamber was zoned, with the most evolved compositions erupting first and producing the sequence from early phonolites to mafic alkaline intrusions. Magmatic recharge then occurred and late phonolites were derived through Rayleigh crystallization (Jensen, 2003).

Some information is available regarding the nature of the region and deposit at depth. A study by Kleinkopf et al. (1970) shows that the Cripple Creek district is centered over gravity and magnetic lows and the authors interpret this to be the result of a large batholithic mass at depth (Thompson et al., 1985). Geophysical anomalies can also delineate alteration trends in the area and may correlate with geochemical anomalies (Kelley et al., 1998).

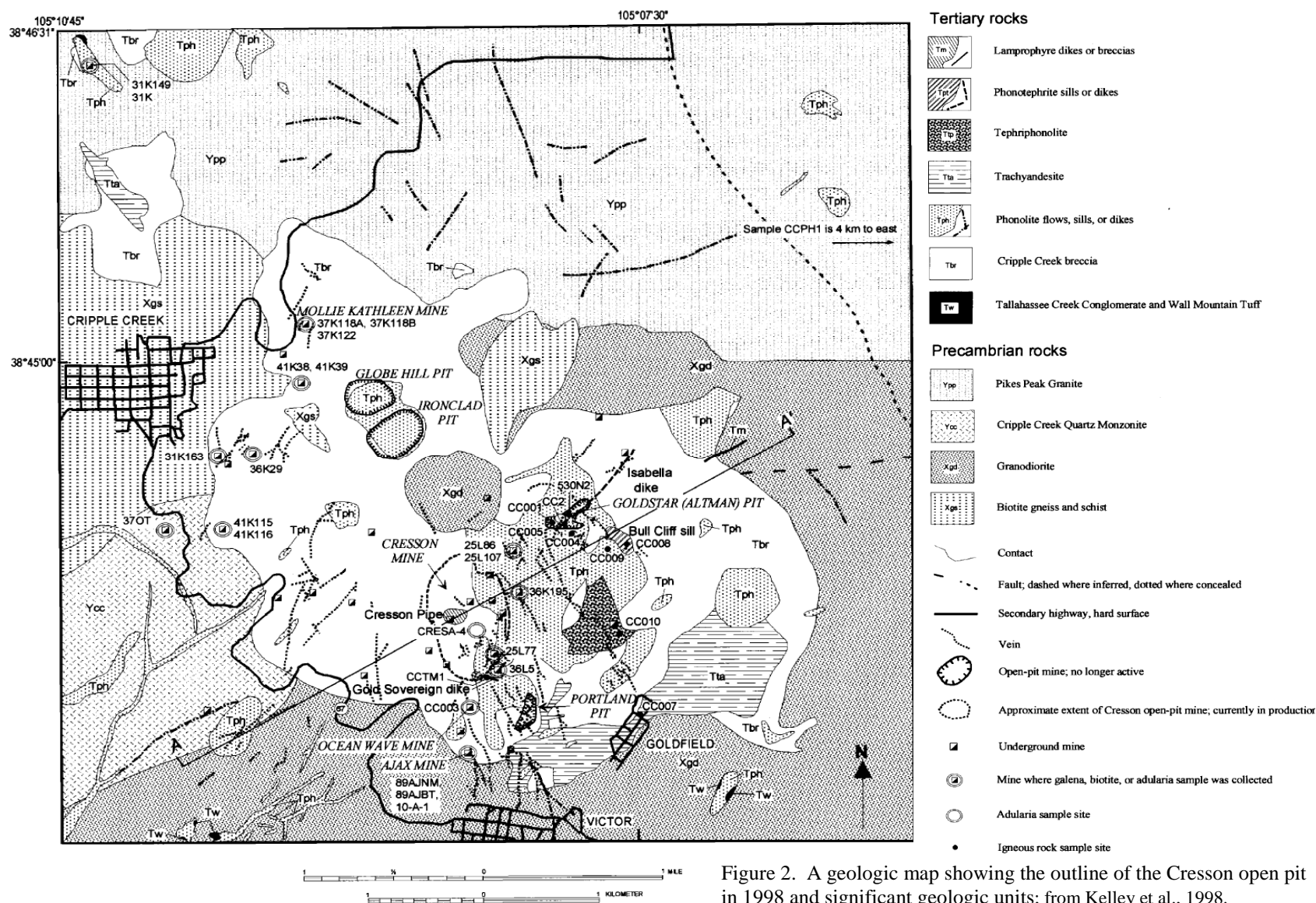


Figure 2. A geologic map showing the outline of the Cresson open pit in 1998 and significant geologic units; from Kelley et al., 1998.

Early on, mines in the district experienced problems with the presence of a strange gas that was slightly warmer than normal mine temperatures and roughly 85% nitrogen, 10% carbon dioxide, and 5% oxygen (Lindgren and Ransome, 1906). Both nitrogen and carbon dioxide cause suffocation so testing the carbon dioxide content alone was often not enough to ensure the air was safe for mining. The gas had a negative effect on miners and production because mining activity could only commence on high-pressure days when the gas was less of a problem. Strangely enough, the mines in the eastern part of the district had fewer problems with gas (Lindgren and Ransome, 1906). Lindgren and Ransome (1906) suggested a separation between the eastern and western parts of the district based on the lack of migration of the gas from west to east and on the fact that dewatering of the western portion did not immediately produce the same effect in the eastern portion. From further work, it is now apparent that the district is actually separated into at least three sub-basins (Fig. 3) separated from one another by granitic and schistose ridges (Loughlin and Koschmann, 1935).

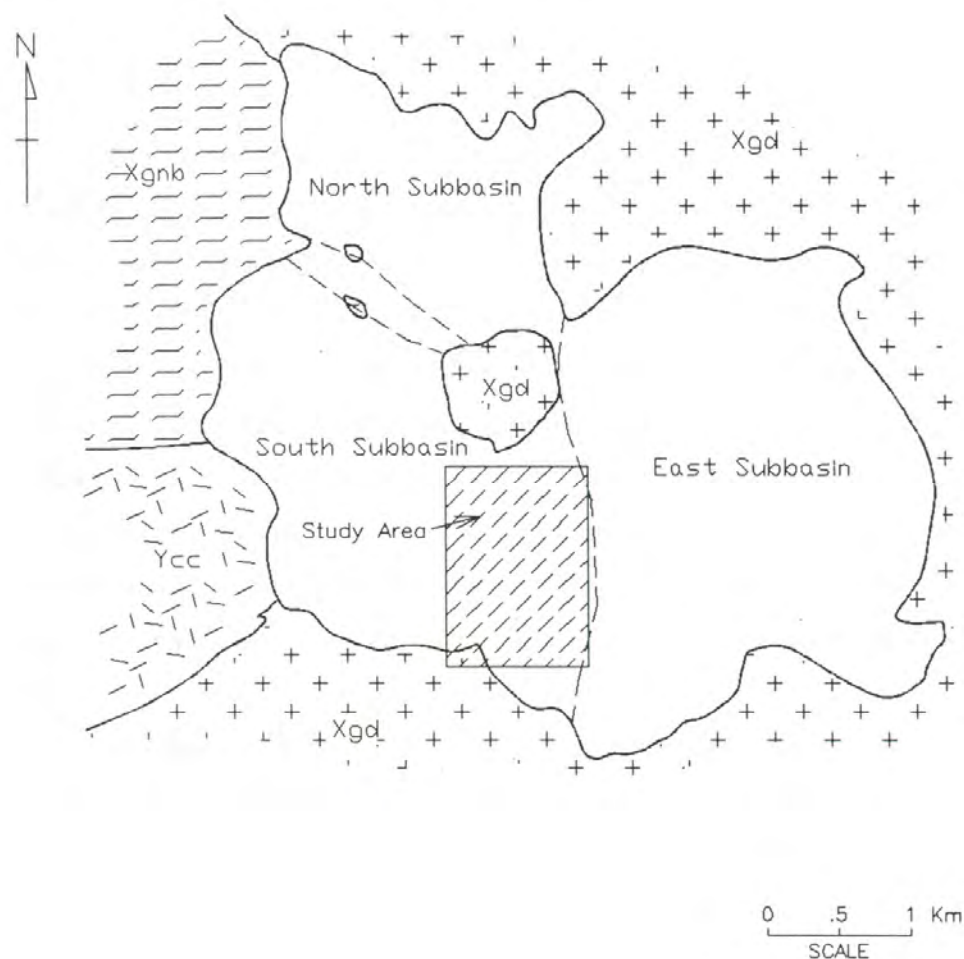


Figure 3. Sub basins within the Cresson Diatreme from Burnett (1995). Study area refers to the study area for Burnett's thesis.

Mineralization

There are two main types of economic gold deposits recognized in the Cripple Creek district: Vein deposits and disseminated deposits. Host rocks in the district range from phonolite to ultramafic rocks to the surrounding Precambrian country rock (Fig. 2). Intrusive rocks (phonolitic to ultramafic rocks) are alkali-rich and dominantly silica poor. Although they are volumetrically minor, a disproportionate amount of gold mineralization is associated with lamprophyric intrusions (Jensen, 2003). The primary control on the distribution of gold deposits is a northwest trending fissure zone deep in

the crust and an increase in grade is commonly found where northwest and northeast structures intersect (Kelley et al., 1998).

Most of the historic production in the district was derived from vein deposits; however, the Cresson mine is currently exploiting a low-grade disseminated deposit. Gold in historic vein deposits occurred as tellurides (with calaverite being the most common telluride), while at Cresson it is found in microcrystalline form or as gold-rich (1-10ppm) pyrite (Kelley et al., 1998; Jensen, 2003). Accessory minerals corresponding to gold mineralization are quartz, fluorite, carbonate, sulfate and pyrite; however, veins at depth in the Cresson open pit with similar mineralogy do not appear to have significant gold values. In contrast, veins at the Ajax mine contain appreciable mineralization down to a depth of at least 3,075 ft (Thompson et al., 1985). Geochemically, gold shows a positive correlation with arsenic, tellurium, antimony, thallium, and copper (Jensen, 2003). Gold mineralization is also intimately associated with potassic alteration (more specifically, K feldspar flooding, pyrite, and sericite) and potassium metasomatism that altered sodium-rich rocks to potassium-rich rocks (Thompson et al., 1985; Kelley et al., 1998; Jensen and Barton, 2007). Glassy potassium feldspar is usually found as an alteration halo to gold-rich veins, with potassium feldspar-pyrite alteration outboard.

Base metal mineralization has been noted in the district but to date has not been economic. Because base metals have not been mined in the district they have not been as well studied as gold mineralization. Pyrite is the most abundant sulfide in the district and base metals are generally associated with tellurides in vein deposits (Kelley et al., 1998). Because base metals are found with tellurides, ore controls and host rocks for base metals are similar to those described above for vein deposits. A rough zoning is evident at the

district scale: Copper is more abundant to the north as supergene turquoise, and tetrahedrite, galena, and sphalerite are more common at the margins of the district (Jensen, 2003). Lindgren and Ransome (1906) recognized lead-zinc veins containing galena and sphalerite in the western portion of the district from Poverty Gulch to Squaw Gulch and indicate that significant silver values are linked to tetrahedrite. Base metals in the district also tend to increase with depth. Veins (potassium feldspar-sericite-ankerite±pyrite±base metals with low-grade gold) and grains of sphalerite and galena are present at the 1000 m level of the Ajax and Vindicator and are also present in zones of biotite alteration at Ajax (Jensen, 2003). The same type of vein is found at the 2400 ft level of the Cresson Mine, Ironclad-Globe Hill, and the Molly Kathleen (Koschmann, 1965; Jensen, 2003). Disseminated galena and sphalerite are also found in zones of potassium feldspar-illite-pyrite alteration at the 7000 ft elevation in the Ajax, Portland, and Vindicator mines (Jensen, 2003).

Molybdenum is generally found in the form of molybdenite (MoS_2) and associated with other base metal sulfides such as galena and sphalerite. Preliminary geochemical results indicate anomalous concentrations of molybdenum in the Grassy Valley region (ALS Chemex, 2004). Significant molybdenite in the form of “moly paint” has been identified in the deepest holes drilled in the district and geochemical analyses from these drill holes support this observation. Molybdenite is locally present in stockwork veinlets in core from deep drill holes. Jensen (2003) suggests that the presence of molybdenum at deep levels may signify a transition to a base metal system at depth with a molybdenum or copper-rich core and that the presence of stockwork molybdenum veins indicates a molybdenum core is most likely the case.

Mineralization in the Cripple Creek district, both precious and base metal, post-dated diatreme formation and igneous intrusions, as it is seen to crosscut lamprophyres, the youngest intrusions in the district. Lindgren and Ransome (1906) and Loughlin and Koschmann (1935) proposed at least three stages of mineralization for the district, while Thompson et al. (1985) recognized five stages of mineralization at the Ajax mine. According to Kelley et al. (1998), the three stages of mineralization proposed by Lindgren and Ransome (1906) and Loughlin and Koschmann (1935) are as follows:

Stage 1: Quartz, biotite, potassium feldspar, dark purple fluorite, dolomite, and coarse-grained pyrite;

Stage 2: Milky to smoky quartz, light purple fluorite, and fine-grained pyrite, dolomite, ankerite, celestite, barite, molybdenite, sphalerite, galena, tetrahedrite, roscoelite, and tellurides with tellurides consistently later than base metals; and

Stage 3: Native gold, smoky to colorless quartz, fluorite, chalcedony, fine-grained pyrite, and calcite

The five stages recognized by Thompson et al. (1985) at the Ajax mine are:

Stage 1: Quartz, fluorite, adularia, pyrite, and dolomite-marcasite

Stage 2: Base metals, quartz, and pyrite

Stage 3: Quartz, fluorite, pyrite, hematite, and rutile

Stage 4: Quartz, pyrite, rutile, calaverite, and acanthite

Stage 5: Quartz, fluorite, and dolomite

It should also be noted that while each vein may not show the same proportions of each stage of mineralization, the mineralogy is consistent from vein to vein (Thompson et al., 1985).

Fluid Inclusions

Numerous fluid inclusion studies have been done in the Cripple Creek district. Each study concentrated on a specific region of the deposit or a particular mineralogy and much of the work has been focused on gold mineralization. A comprehensive review of fluid inclusion data in the district can be found in McIntosh (2004; Appendix C). Most workers in the district recognize a high temperature (~250-500 deg C), high salinity (~30-50 wt. % NaCl) fluid at depth (Stage 1; Thompson et al., 1985), a lower temperature (~100-250 deg C) lower salinity (~0-8 wt. % NaCl) fluid (Stage 2 & 3; Thompson et al., 1985) (Lane, 1976; Burnett, 1995; Beaty et al., 1996; McIntosh, 2004), or both (Thompson et al., 1985; Pontius, 1996; Rosdeutscher, 1998; Mote, 2000) depending on the location and mineralogy of their samples.

In general, higher temperature, higher salinity fluids are present at depth, grading into lower temperature, lower salinity fluids closer to the surface. Daughter products such as halite, sylvite, and hematite are noted in the earlier, higher temperature, higher salinity inclusions while they are absent in lower temperature inclusions. Carbon dioxide may also be trapped in the inclusions. Several types of inclusions have been found: liquid + vapor, liquid + vapor + daughters, and vapor only, any of which may or may not have CO₂. Many studies support boiling in the upper portions of the deposit (Thompson et al., 1985; Trippel, 1985; Seibel, 1991; Burnett, 1995; Thompson, 1996; Jensen, 2003).

Two studies, Saunders (1986) and Nelson (1989) did not find indications of boiling at depth in the Cresson diatreme but Thompson et al. (1985) documents boiling to a depth of 7,777 ft at the Ajax mine in the southern portion of the diatreme.

Isotopes

Several isotopic studies have been completed within the Cripple Creek district examining oxygen, deuterium, and sulfur isotopes. Oxygen isotopes have indicated a dominantly magmatic origin for the mineralizing fluids and potential mixing with isotopically lighter meteoric waters along the margins of the deposit (Silberman, 1992; Beaty et al., 1996; Seibel, 1996; Kelley et al., 1998; Rosdeutscher, 1998; Thompson, 1998; Jensen, 2003; McIntosh, 2004). McIntosh (2004) studied carbonate veins throughout the district and discovered a zone of strong magmatic signatures (heavy $\delta^{18}\text{O}$) centered about the Ajax/Portland mines that became less prominent outboard. Oxygen isotopic signatures also tend towards lighter values as depth decreases, which may indicate an increase in meteoric input to the system (Silberman, 1992; Jensen, 2003).

Beaty et al. (1996) and Jensen (2003) recognized a zoning in $\delta^{18}\text{O}$ values in and around vein systems. Beaty et al. (1996) found that alteration increased the $\delta^{18}\text{O}$ signature by about 5‰ immediately adjacent to a vein, with an increase in $\delta^{18}\text{O}$ persisting up to 30 m outboard and decreasing with increasing distance from the vein. Jensen (2003) describes feldspars closest to veins as having high $\delta^{18}\text{O}$ values (>12‰), while feldspars further away are lighter (9 to 12‰). Calculations from Jensen (2003) of fluids in equilibrium with veins indicate the fluids are enriched in $\delta^{18}\text{O}$ from about 2 to 8‰ (with an average of 5‰) and show that the fluids are from a magmatic source or that they

have been buffered through isotopic exchange with igneous wall rocks. On a larger scale, Beaty et al. (1996) found that altered phonolites proximal to veins have lower values (7 to 14.31‰) than “silicified rock from the upper levels of the hydrothermal system” (about 18‰) and that late stage quartz has the highest $\delta^{18}\text{O}$ values (21-24‰). The authors suggest this trend is due to cooling and increased fractionation of the ore fluids.

In general, sulfur isotopes in the Cripple Creek district show distinct trends, with light sulfide (-21.1 to -6.8 from Thompson, 1996; -10.4 to -3.9‰ from Rosdeutscher, 1998; -18.6 to 2.91‰ from Jensen, 2003; -16 to 0‰ from McIntosh, 2004) and heavy sulfate (6 to 16‰; Jensen, 2003). Light sulfides and heavy sulfates are consistently found at all levels of the deposit: shallow (Cresson Pit), deep (Ajax-Portland), and within hydrothermal breccias (Ironclad-Globe Hill) (Jensen, 2003). Thompson (1996) has found that sulfur isotopes from galena become distinctly lighter at shallow levels and attributes this to galena forming from condensing H_2S in a zone of shallow boiling. Jensen (2003) notes that later phase minerals such as stibnite and cinnabar tend to display lighter $\delta^{34}\text{S}$ values (-16‰) and may have been vapor transported. Rosdeutscher (1998) examined 23 pyrites and found no association between sulfur isotopes and depth.

Most workers in the district agree that the sulfur isotopic signatures represent a magmatic source. However, some event has occurred that has caused the values to shift to more negative sulfides and heavier (positive) sulfates. Thompson (1996) states that the change from a H_2S dominated system to a SO_4^{2-} system was due to oxidation, likely from boiling or mixing with meteoric water. McIntosh (2004) suggests that while oxidation may be a component (because oxygen and sulfur values are outside of the range expected for epithermal deposits) it was not the only contributor because if it was, both $\delta^{18}\text{O}$ and

$\delta^{34}\text{S}$ should change with depth (heavy O should follow heavy S values), and this relationship was not found when graphing the data (Fig. 15; McIntosh, 2004). Therefore, McIntosh (2004) states that oxidation (through boiling, precipitation of sulfates, sulfides, and carbonates, fluid mixing, or reactions with wall rocks; Ohmoto and Goldhaber, 1997) probably occurred in conjunction with mixing, though oxidation was primarily responsible for the shift in sulfur values. $\delta^{34}\text{S}$ data from Jensen (2003) indicate at least two fluid sources were present along the margin of the district.

Sulfide data from base metal stages at the Pointer-Index mines show very light sulfur values, while sulfides from near surface exposures in the western part of the diatreme display the heaviest $\delta^{34}\text{S}$ signatures (Jensen, 2003). It is interesting to note that the two molybdenite samples analyzed by Jensen (2003) fall into the range for porphyry deposits ($0 \pm 5\%$; Ohmoto and Goldhaber, 1997). Temperatures were calculated from sulfate-sulfide pairs by Jensen (2003) and resulted consistently in temperatures greater than 300°C with the exception being galena-pyrite pairs in the Cresson Pit, which commonly gave lower temperatures.

Part 1: Molybdenum vs. Gold

The project at hand is really two different studies: 1) A comparison of gold mineralization with molybdenum mineralization and 2) Exploration of Grouse Mountain. Therefore, each will be addressed separately herein. This is necessary for brevity and for presentation of the data in a coherent manner.

Methods

The first step in comparing molybdenum mineralization with the well-studied gold mineralization in the district was macroscopic examination of the mineralization. This was completed through relogging of drill core for CC-2272, CC-2273, GHC-747D, GHC-747-D2, and GHR-747 (RC hole) (Fig. 4). This was necessary to become familiar with the lithology and mineralogy in the district, as well as to collect samples for petrographic work. The relogging and sample collection was completed onsite at the Cresson mine in the summer of 2009.

From the samples collected, 26 were selected for petrographic work. Polished thin sections were created for each of the 26 samples, and examination of petrographic relationships was conducted in transmitted and reflected light, with the goal of identifying paragenetic relationships between sulfides, gangue, and alteration events. The samples were chosen to be representative of the drill holes examined during the summer and on the basis of which would be most helpful in establishing paragenetic relationships. The expectation was also to observe directly the association of gold and molybdenite, but gold was not encountered in these sections.

Because potassium flooding is common in the district and generally associated with high gold grades, the billets for each of the 26 samples were stained to identify the extent of potassium flooding. The billets were also examined to see if the flooding was confined to the clasts, the matrix, or present in both. The goal was to see if the location or amount of potassium flooding changed significantly with depth in the drill holes. After assessing the potassium flooding, several billets were selected to be representative of the various drill holes. All 26 stained billets are presented in Appendix B.

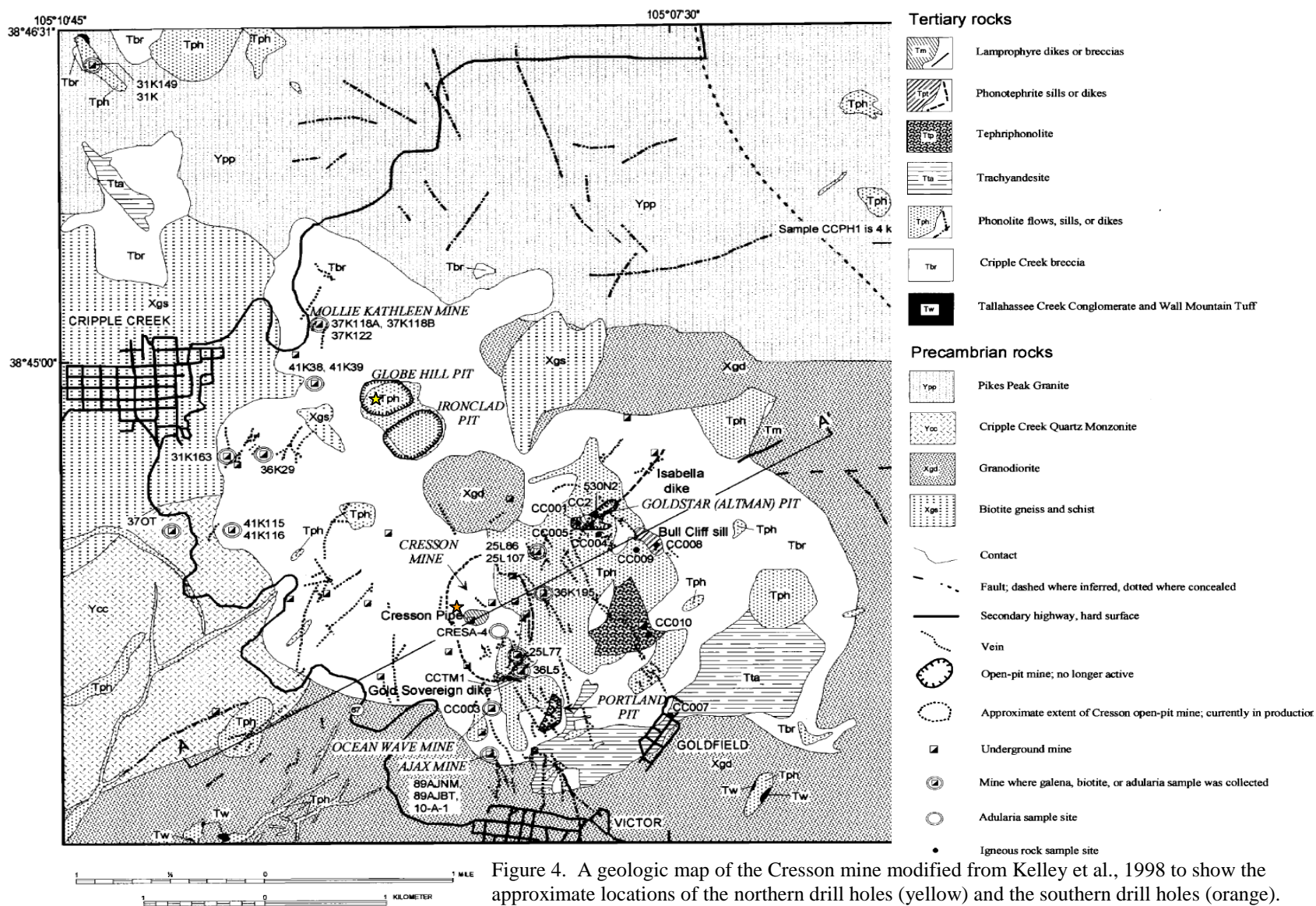


Figure 4. A geologic map of the Cresson mine modified from Kelley et al., 1998 to show the approximate locations of the northern drill holes (yellow) and the southern drill holes (orange).

Five-foot geochemical samples were taken from CC-2273 every 20 feet for four acid total digestion analyses through the ALS Chemex lab in Reno, Nevada. The package used was ME-MS61m, which provides data on 48 elements and differs from ME-MS61 because ME-MS61m includes a separate analysis for mercury. Similar downhole geochemistry was available for GHC-747-D2 and limited, erratic geochemistry was provided for CC-2272. Fire assay results were available for all drill holes and the analyses were carried out either at ALS Chemex or on-site at the Cresson mine. The results provided data on 50 elements total (for a list of these elements see the top row of the matrices in Appendix A), including mercury and gold, and any changes in these elements throughout the length of the drill hole. Correlation matrices were calculated from these data to establish Pearson's Correlation Coefficients (Appendix A) for each pair of elements. Based on the correlation matrices, specific elements were identified that exhibited significant positive correlations with gold, molybdenum, and base metal sulfides. These correlations were then graphed separately to determine the strength of the relationship.

Small (<0.01 mm) fluid inclusions were observed locally in thin section, generally occurring in calcite, quartz, or recrystallized gypsum, and rarely in fluorite. Some inclusions were also observed in feldspars contained in the wallrock. The inclusions observed were dominantly liquid + vapor or liquid + vapor + daughters and commonly elongate. NaCl crystals were evident in several inclusions but it was not possible to identify the daughter minerals present due to the small size of the inclusions. The inclusions were not analyzed in this study partly because they were not very abundant and mostly because it was not possible to directly associate them with the molybdenite.

In all cases where inclusions were located they were either paragenetically much earlier or later than the molybdenite.

Because fluid inclusions were not a viable method for obtaining a temperature to compare with the temperature for gold mineralization, attention was turned to sulfur isotopes. There are abundant data on the sulfur isotopes in the district and the $\delta^{34}\text{S}$ numbers span from ~3 to -21‰ for sulfides (see Previous Work: Isotopes section above) but the two molybdenum samples analyzed by Jensen (2003) fall into the range for porphyry copper deposits in the western U.S. (Ohmoto and Goldhaber, 1997). As the gold mineralization has already been associated with an epithermal signature, sulfur isotope analysis of molybdenum appeared promising for identifying the source of molybdenum mineralization and to see if more analyses correspond with the two published analyses.

Originally, the idea was to generate separates of molybdenite and separates of other sulfides individually according to paragenesis to see if certain generations of the other sulfides fell only in the porphyry range as well. To do this, the billets from which the polished sections were taken and the paragenesis established were polished. Initially, the author attempted to polish them on a polishing wheel but due to plucking issues this method did not work well. Instead, the sections were polished by hand. An attempt was made to extract the minerals from the polished billets by chipping and scratching the material out (to preserve the paragenesis because if the material was crushed and separated the paragenetic information would have been lost) but this method did not provide enough material for analysis. Therefore, the focus of the isotope work shifted to the molybdenite, to see if it fell into the epithermal range (associated with gold) or only

in the porphyry range (separate system). Portions of selected samples were then crushed, soaked in hydrochloric acid to remove any carbonate, and hand-sorted under a binocular stereoscope. However, after making the separates it was found that they were still impure because a mineral of unknown composition, likely either a sulfate or iron carbonate, was intergrown at a very fine scale with the molybdenite. The mineral had a tabular form in thin section and under the binocular scope appeared to be quite soft but identification based on optical properties was not possible.

SEM analysis was required to identify the mineral intergrown with molybdenite to see if the mineral, likely a sulfate or a carbonate, would affect the analysis. If the mineral were a sulfate, EDS spectra showing the composition would indicate if it could be dissolved to obtain clean molybdenum separates for sulfur isotope work. SEM work was conducted at University of Nevada, Las Vegas (UNLV) in April 2010. The semi-quantitative analyses were completed on a JEOL JSA-5600 scanning electron microscope equipped with an Oxford Link Pentafet 6587 energy dispersive X-ray spectrometer at 20-25 kV with a 20 mm working distance, a spot size of 40 μ m, and a sixty-second acquisition time (Mulcahy, Sean; personal communication). The mineral in question was found to be ankerite. EDS spectra were obtained and images were generated to show the nature of the intergrowth between molybdenite and the ankerite. The EDS analyses were reported as normalized atomic and weight percentages.

Various other regions of interest were also analyzed with the SEM at UNLV. One of these contained a mineral that appeared bright red under crossed polars. The author believed it might be an arsenic mineral due to its coloration and proximity to arsenopyrite. Upon analysis it was discovered to be ankerite as well. Also, distinct

generations of pyrite were observed in thin section and one grain with an anhedral core and a defined rim was subjected to analysis. As-Au-rich pyrite has been documented by other workers (Burnett, 1995) but was not observed in the anhedral core or the rim of the grain analyzed.

It has been noted that high-iron sphalerites commonly contain trace amounts of other elements in their structure due to distortion of the lattice by iron (Huston et al., 1995; Orberger et al., 2003; Cook et al., 2009). In porphyry copper deposits it is not uncommon to find sphalerites hosting molybdenum (Tommy Thompson; personal communication). Due to the discrepancy between the amount of molybdenite seen in thin section versus the amount of molybdenum evidenced by geochemical work, it appears that some molybdenum is hosted elsewhere and may be incorporated into the sphalerite lattice. Another possible explanation could be that the thin sections were not representative of the 5 ft interval analyzed for geochemistry.

Initially, the plan was to obtain EDS spectra for the sphalerites to determine the trace elements present. However, the detection limits of the SEM were not sensitive enough to determine the trace element concentration. It is possible that a microprobe could detect the trace elements if the concentrations were above 300-500 ppm but there are no published works documenting average concentrations of molybdenum in sphalerites in porphyry systems. The best method to identify the types and amounts of trace elements would be to analyze the sphalerites on a microprobe with much lower detection limits or to utilize a LA-ICP-MS. As the concentration of molybdenum in sphalerite was not the focus of this study and because of funding limitations and a lack of available data for comparison, these analyses were not carried out at this time.

The sulfur isotope analyses were carried out by Simon Poulson at the University of Nevada, Reno Stable Isotope Lab in June of 2010 on an Eurovector model 3028 elemental analyzer interfaced to a Micromass IsoPrime stable isotope ratio mass spectrometer, after the method of Giesemann et al. (1994) and Grassineau et al. (2001) with $\delta^{34}\text{S}$ values reported in ‰ units vs. VCDT (Simon Poulson, personal communication). Fourteen samples were analyzed to determine their $\delta^{34}\text{S}$ ratio. The samples were obtained by the process of hand separation described above and the utmost care was taken to obtain samples free of contamination, as fine-grained pyrite was commonly intergrown with some of the molybdenite.

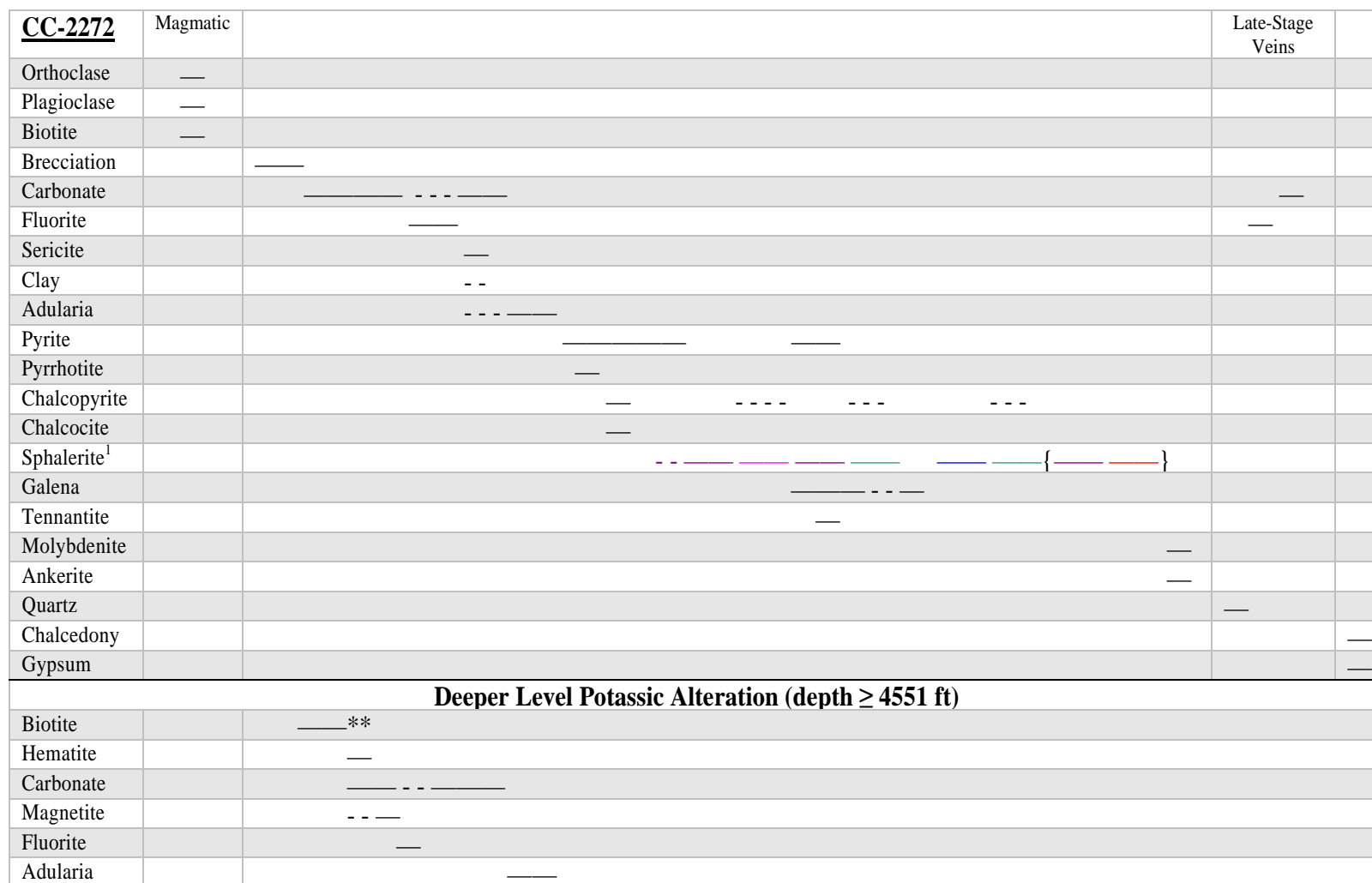
Results

Paragenesis

Several relationships observed in thin section indicate that molybdenite is later than the base metal events (Figs. 5, 6, and 7). Molybdenite was observed entraining sphalerite and galena, rimming and replacing gangue minerals, crosscutting and replacing adularia, and rimming and replacing pyrite (Fig. 8). Molybdenite is generally intergrown with a tabular mineral (ankerite) on which SEM work was conducted to ascertain its identity. Molybdenite is a minor component in dark rims around breccia clasts in both the northern and southern drill holes.

When compared with previous paragenetic descriptions, molybdenite in this study appears to occur after Thompson's (1985) stage two and before his stage five and at the end of Lindgren and Ransome (1906) and Loughlin and Koschmann's (1935) stage two, in both cases after base metals and coprecipitated with ankerite. As no gold or telluride

minerals were observed in thin section or hand sample, it is not possible to definitively say whether molybdenite was before, after, or contemporaneous with gold from petrographic analysis alone. Petrographically, they appear to have been deposited very close in time if the placement of gold from other paragenetic studies is taken in conjunction with this study.



1) Generations of Sphalerite:
 — = Low to no Fe, no cp — = High Fe, cp dis
 — = Low Fe, cp disease — = Mod Fe, no cp
 — = High Fe, no cp

{ ... } indicates sequence repeats six times
 ** indicates mineral is secondary

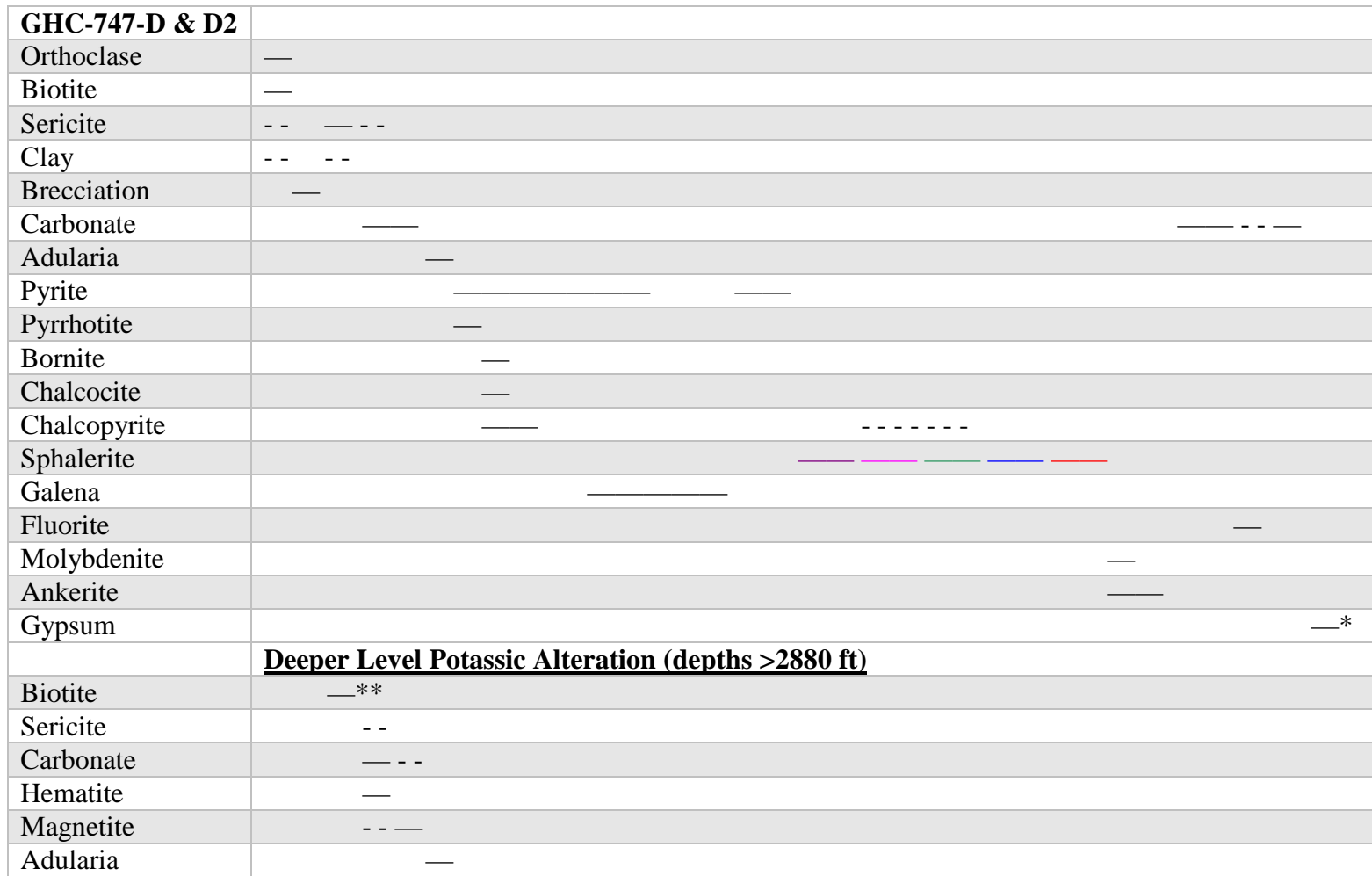
Figure 5. Paragenetic diagram for CC-2272. See text for discussion.

CC-2273	
Orthoclase	—
Plagioclase	—
Sericite	-- ———*
Clay	-- - - - - *
Brecciation	—
Carbonate	- - - ——— ———
Adularia	- - ———
Arsenopyrite	———
Pyrite	- - ——— ———
Pyrrhotite	—
Chalcocite	—
Bornite	—
Covellite	—
Chalcopyrite	——— - - -
Sphalerite ¹	——— ———
Galena	———
Ankerite	———
Deeper Level Potassic Alteration (depth ≥ 4362 ft)	
Biotite	———**
Hematite	—
Carbonate	- - - ———
Magnetite	- - —
Adularia	- - ———

1) Generations of Sphalerite:
 ——— = Low to no Fe, no cp
 ——— = Low Fe, cp disease

* indicates mineral is minor at 61 and absent at 65
 ** indicates mineral is secondary

Figure 6. Paragenetic diagram for CC-2273. See text for discussion.



1) Generations of Sphalerite:
 — = Low Fe, no cp
 — = Low Fe, cp disease
 — = High Fe, no cp
 — = High Fe, cp disease
 — = Mod Fe, no cp

* indicates mineral is only present at 2456 ft
 ** indicates mineral is secondary

Figure 7. Paragenetic diagram for GHC-747-D & D2. See text for discussion.

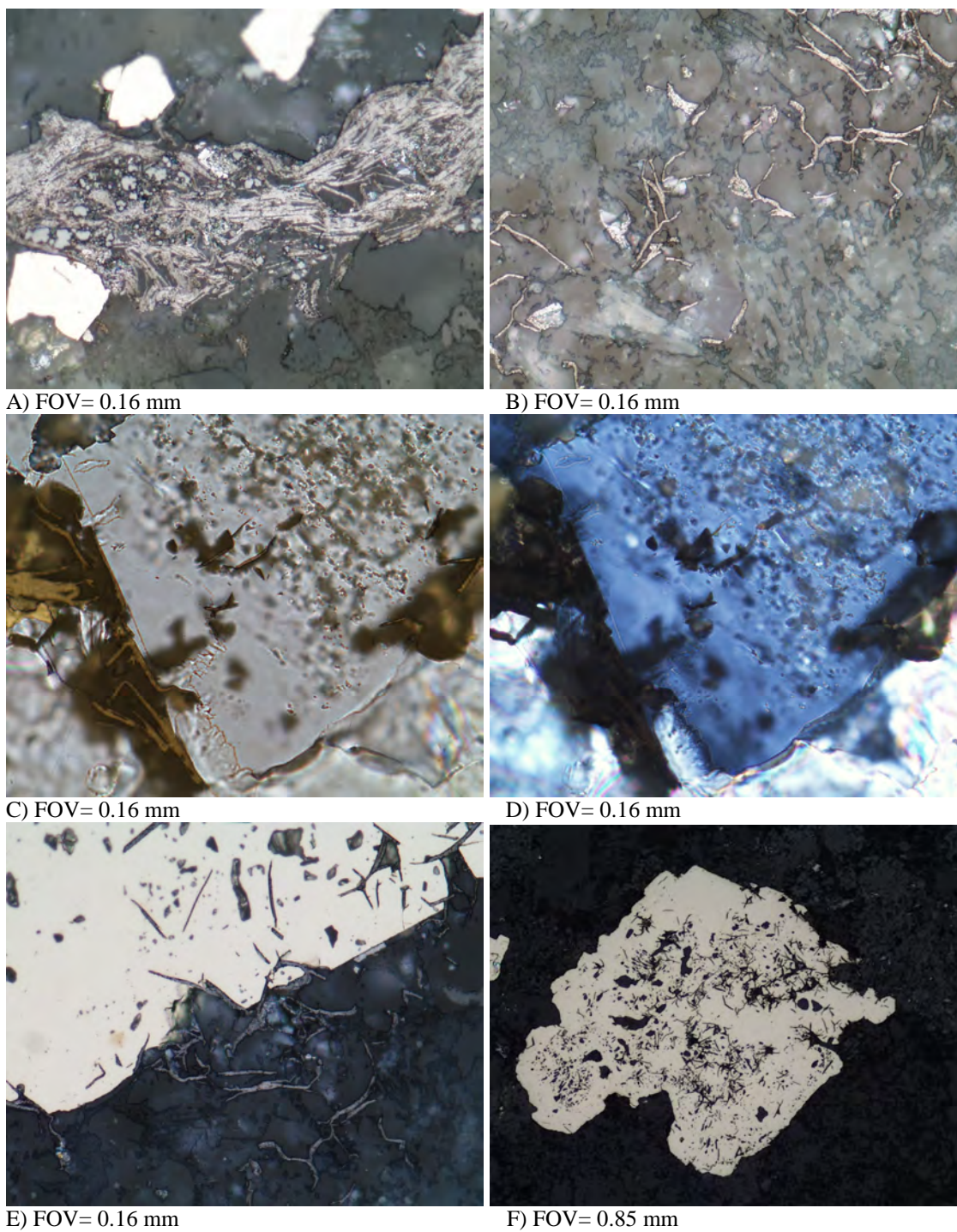


Figure 8 A-F. A) Molybdenite entraining sphalerite and minor galena; B) Molybdenite interstitial to gangue minerals; C) Molybdenite and ankerite replacing adularia rhomb; D) Same view as C, crossed polars; E) Molybdenite replacing pyrite; F: view of pyrite grain with local molybdenite replacement.

Work by Burnett (1995) identified a general paragenesis for the upper portion of the Cresson Mine, As-Au-rich pyrite, and looked at fluid inclusions in adularia. He encountered little to no base metal sulfides and documented adularia forming early in the paragenetic sequence before deposition of gold. He also documents fluid inclusion temperatures as $>224^{\circ}\text{C}$ with salinities of 7.3 wt. % equiv. NaCl (Burnett, 1995). Results of this study also support an early adularia event. No evidence was found to support As-Au-rich pyrite at the depths sampled in this study but only one pyrite grain and one rim were analyzed with the SEM so the results should not be considered conclusive.

The paragenetic diagrams in Figures 5, 6, and 7 all show upper level versus deeper level alteration and the depths at which the deeper level alteration begins. Biotite-carbonate-hematite-magnetite \pm sericite alteration in the deeper levels appears to be contemporaneous with the carbonate-sericite \pm fluorite \pm clay alteration present at shallower levels. The change in the alteration assemblages between these zones is abrupt and a gradational change was not observed in the thin sections analyzed. The change is most likely due to evolution of the fluids with depth. However, when considering the alteration variation in these sections it is important to note the character of the drill holes used in this study. While the northern drill holes (GHC-747-D & D2) were vertical (Fig. 9), the southern drill holes (CC-2272 & CC-2273) were wedged off at an angle in an attempt to intersect the Cresson Pipe (Fig. 10).

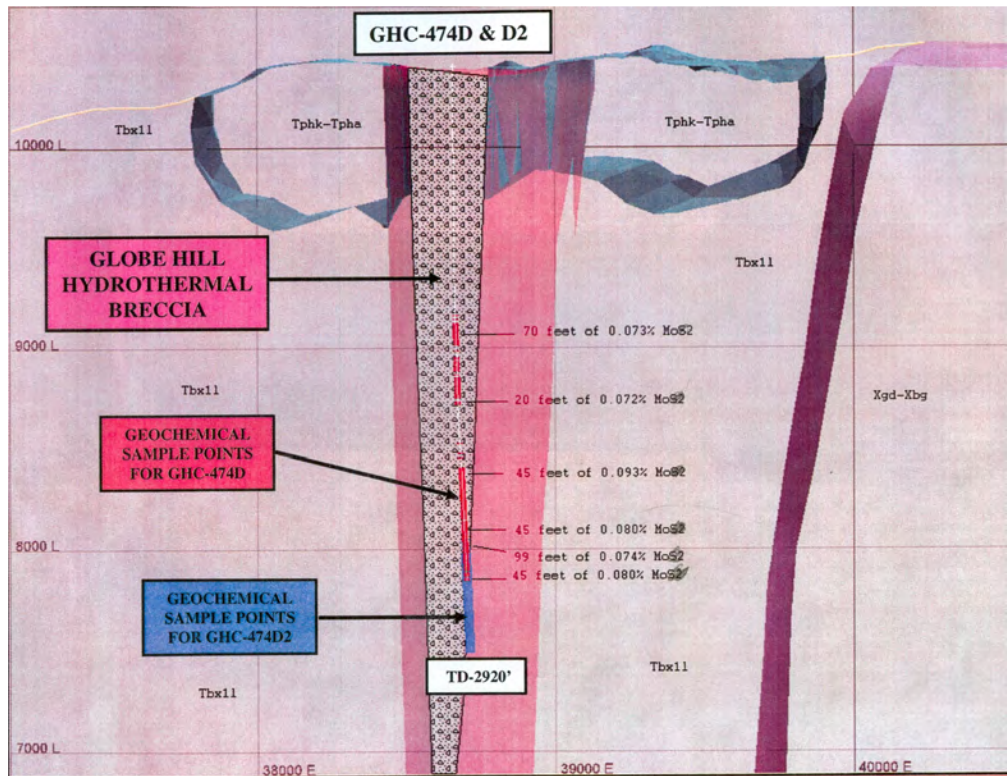


Figure 9. Cross section looking NE showing the character of the GHC-747-D and GHC-747-D2 drill holes (from Cripple Creek & Victor/AngloGold (Colorado) Corporation, internal company presentation).

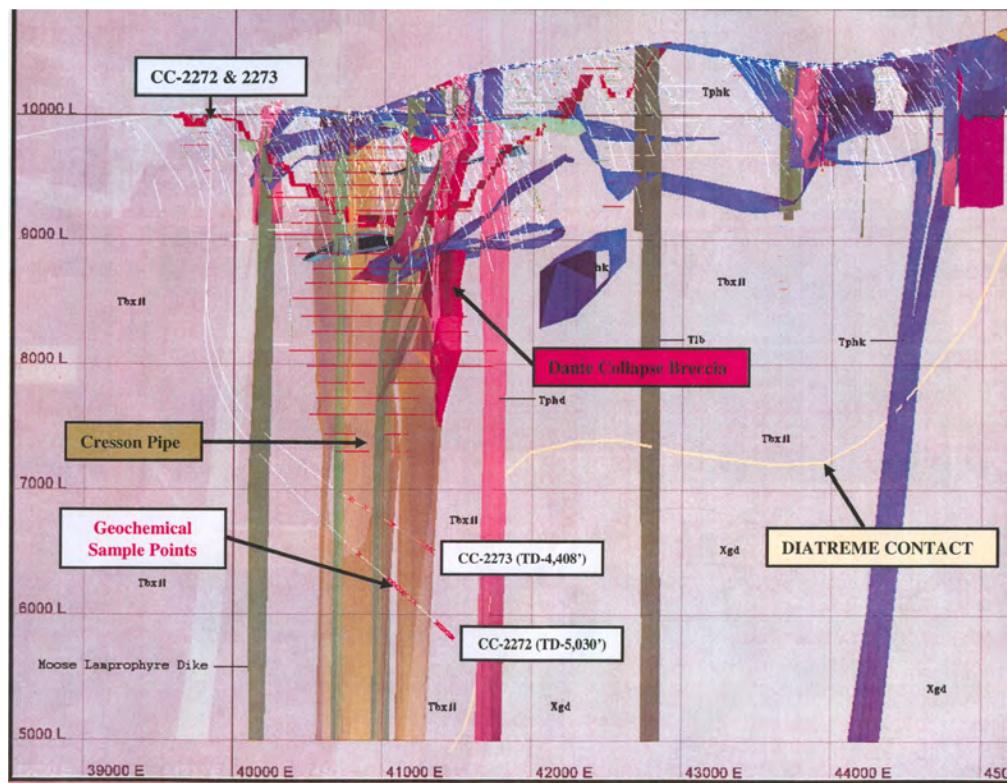


Figure 10. Cross section looking NE showing the character of the CC-2272 and CC-2273 drill holes (from Cripple Creek & Victor/AngloGold (Colorado) Corporation, internal company presentation).

Potassic alteration in the form of adularia appears to have precipitated at the same time at all levels where it is documented in this study. It is commonly observed in rhombic form in vugs and along vein margins, locally displaying a small 2V angle, but may also occur flooding the matrix, rimming orthoclase, or lining wallrock along late-stage quartz-calcite veins. It is generally associated with biotite and calcite in the deeper levels. Rhombic adularia is common along vein margins and may have resulted from early fracture development followed by adularia deposition in the open space. These veins are subsequently filled by euhedral sulfides (likely carried through the veins by subsequent fluids as they generally show signs of transport) and a final flooding of late-stage vein material (calcite-quartz).

An early event of adularia-carbonate alteration occurred before sulfides because carbonate and adularia grains can be found rimmed by pyrite and sphalerite and the early generation of pyrite that appears “pockmarked” has that texture because it contains inclusions of carbonate and/or adularia indicating incomplete replacement of these minerals. Dissolution of pyrite could create voids, and subsequent infill by carbonate-adularia could also create the pockmarked texture but the presence of carbonate grains rimmed by pyrite, the fact that none of the sulfides are cross cut by adularia-early carbonate, and the rimming and/or replacement of gangue mineralogy by sulfides suggests that this was not the case.

Petrographic work has also revealed that there are a lot more base metals present at these depths than were previously described in the core logs. Disseminated chalcopyrite was also found to be quite common in polished thin section and hand sample but was not recognized in previous core logs. Much of the dark, disseminated sulfides

found in the core that were described as molybdenite were actually galena or sphalerite. This leads to an interesting question: Where is the molybdenum? Geochemical analyses for select samples indicate high concentrations (>200-400 ppm) of molybdenum that should be visible in the samples, but only small, localized, wispy molybdenite is present. There are two possibilities that could result in this scenario: 1) the sections chosen are not representative of the interval from which geochemistry was obtained or 2) the molybdenum is accommodated in the structure of some other mineral. Sphalerite has been shown to accommodate small amounts of molybdenum in its structure (Huston et al., 1995; Orberger et al., 2003; Cook et al., 2009) and abundant sphalerite is usually found in these sections. While analysis of the sphalerites was attempted in this study as outlined in the Methods section, it was not successful and technical recommendations for further study on this subject are given in the Future Work section.

Trace element concentration also affects feldspars in these sections. Feldspars observed in thin section are locally zoned (Fig. 11). Generally, they have a rim of material that is optically different from the core and appears as a distinct yellow under crossed polarized light, though there may be several zones in some crystals. This change in optical properties is likely due to the incorporation of some trace element in the feldspar lattice (possibly barium; Jensen, 2003).

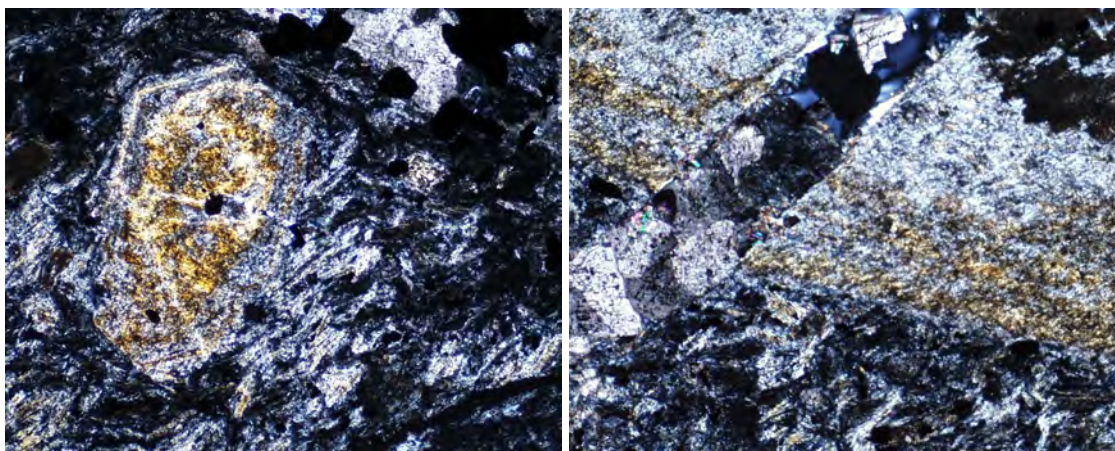


Figure 11. A) On the left, a zoned feldspar crystal; B) On the right, a close up view of the margin of a feldspar crystal with multiple zoning cut by a calcite veinlet (Both photos: FOV= 1.7 mm, crossed nicols).

Significant differences were also observed between the mineralogy in the northern vs. southern drill holes. The northern drill holes not only contained much more carbonate, they also tended to have more disseminated chalcopyrite. The southern drill holes contained little disseminated chalcopyrite but considerably more sphalerite. Both the northern and southern drill holes contained chalcopyrite in sphalerite but due to the amount of chalcopyrite present it was likely a coprecipitated or replacement product and not derived from exsolution.

Potassic Alteration/Flooding

The billets for the 26 samples selected for petrography were stained to identify potassium flooding in the samples. Microscopic characteristics of the potassic alteration are described in the Petrography section above. The stained billets were then examined to see if potassium flooding was confined to the clasts, the wallrocks, or both. Broad inferences were made for each individual hole but comparison were not possible between the various drill holes because in the southern portion of the district CC-2272 is collared at 2772 ft and CC-2273 is collared at 2745 ft, while the GHC-747-D and GHC-747-D2

holes in the northern part of the diatreme bottom at 2920 ft. Stained billets from these drill holes represent a depth of 2436-2880 ft for the northern drill holes and 2745-4813 ft for the southern drill holes. This allows very little overlap, hardly enough for confident comparison of potassic flooding at similar depths. Combining CC-2272 and CC-2273 billets may be feasible given the close proximity of the holes (When the CC-2272 and CC-2273 holes were drilled, it was with the intention of identifying the terminus of the Cresson Pipe so the holes were wedged off at an angle in an attempt to intersect the Cresson Pipe; Fig. 10), but there is no guarantee that potassium alteration and/or brecciation was consistent enough throughout the diatreme to combine the northern and southern drill holes.

Of the 26 stained billets, four were selected from CC-2272, CC-2273, and GHC-747-D/D2 holes. The GHC-747-D and GHC-747-D2 holes are treated as a single hole because they ran together at depth during drilling (Fig. 9). These samples were selected from the stained billets to represent the rough patterns in potassic alteration seen throughout each drill hole (Fig. 12). The patterns are classified as “rough” due to the limited number of samples in each given area and the lack of other nearby drill holes of similar depth to compare them against. Still, there were commonly several samples in a row within a drill hole with potassium flooding preferentially in the matrix, or preferentially in the clasts and it is from these groups that one sample was selected to represent that group and be incorporated in Figure 12. The stained billets for all drill holes are presented in Appendix B.





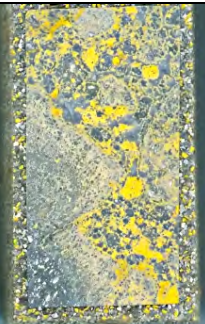

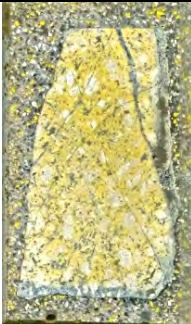





<i>Southern Drill Holes</i>		<i>Northern Drill Holes</i>
CC-2272	CC-2273	GHC-747-D & D2
		
3008: Mostly in matrix and in up to 60% of clasts	3380: In clasts, minor in matrix	2436: In clasts only
		
4551: In matrix and in clasts in vein; not found in clasts in wallrocks	3628: Mostly in clasts, lesser in matrix	2571: Mostly in matrix, minor amounts in clasts
		
4645: In matrix only	3854: In matrix & about 50% of clasts	2644: In clasts only
		
4742: In matrix of wall rocks and locally in clasts in veins; not found in clasts in wallrocks	4362: Very minor, present in both clasts and matrix	2880: Mostly in matrix, locally in clasts

Figure 12. Stained billets illustrating the presence and location of potassium flooding. The numbers preceding the description of each billet represent the depth of the sample.

Geochemistry

Within the diatreme there are many highly correlated elemental associations. Since the correlation matrix addresses spatial and not necessarily temporal relationships, the majority of this can be attributed to the fact that virtually all the fluids used the same or similar pathways and there were undoubtedly multiple episodes of fluid introduction. It is also difficult to recognize a specific rock signature because the host rock is the Cripple Creek Breccia, a predominantly heterolithic breccia.

The reason for examining elemental correlations within the diatreme is to compare the elements generally associated with gold with the elements that show a strong association with molybdenum. If both gold and molybdenum have a strong correlation or are associated with the same elements they may have been derived from similar fluids. However, if there is no observed correlation between gold and molybdenum or between molybdenum and the elements associated with gold then the two were likely from different systems. It is important to note that the correlations do not necessarily show that the elements precipitated together, only that they are commonly found in association.

From the geochemical data analyzed, gold and molybdenum in the diatreme show the spatial correlations given in Table 1. The values in parentheses are the Pearson's correlation coefficient from Appendix A. The values in red are the elements cited by Jensen (2003) as being associated with gold. The remaining listed values are other significant elements or elements that show a strong (>0.60) correlation with the element listed. Values in italics illustrate a negative correlation.

Element	CC-2272	CC-2273	GHC-747-D	GHC-747-D2
Sample Size	19	82	176	103
Au	As (0.913), Te (0.958), Tl (0.508), Sb (0.808), Cu (0.025), Co (0.635), Hf (0.658), Ni (0.644), Mo (-0.262)	As (0.355), Te (0.097), Tl (-0.009), Sb (0.333), Cu (0.459), Hg (0.846), Mo (0.305)	As (0.747), Te (0.434), Tl (0.039), Sb (0.287), Cu (0.463), Mo (0.147)	As (0.625), Te (0.220), Tl (0.612), Sb (0.255), Cu (0.391), Mo (0.039)
Mo	As (-0.272), Te (-0.052), Tl (-0.329), Sb (-0.050), Cu (-0.500), Ag (0.823), Bi (0.885), Pb (0.707), Re (0.925), S (-0.034), Se (0.843), Sn (0.605), Zn (0.049), Li (-0.627)	As (0.440), Te (0.138), Tl (-0.002), Sb (0.997), Cu (0.897), Ag (0.948), Bi (0.757), Cd (0.991), Ge (0.764), Hg (0.704), In (0.898), La (0.990), Pb (0.996), S (0.710), Se (0.798), Sr (0.762), Zn (0.975)	As (0.171), Te (0.196), Tl (0.113), Sb (-0.048), Cu (0.267), S (-0.205), Zn (0.075)	As (0.181), Te (0.265), Tl (0.082), Sb (0.204), Cu (0.266), Re (.710), S (0.211), Zn (0.382)

Table 1. Geochemical associations (correlation coefficients) for gold and molybdenum in the diatreme.

From Table 1 it is apparent that the correlation coefficients are somewhat variable from drill hole to drill hole. It is also evident that gold does not always show a strong correlation with the associated elements identified by Jensen (2003). However, overall gold generally has a ~0.30 or greater correlation with the associated elements. Molybdenum is only weakly (~0.30 at the highest) correlated with gold (Table 1, Appendix D), and CC-2272 actually shows a negative correlation (-0.26). With the exception of copper and antimony in CC-2273, molybdenum exhibits low correlations

with the elements associated with gold, including several negative or near zero values. The lack of a correlation between molybdenum, gold, and the elements associated with gold seems to suggest that molybdenum mineralization was a separate event.

Molybdenum correlates strongly with silver and lead in the southern drill holes but the same association is not seen in the northern drill holes. Interestingly, molybdenum only shows a strong association with sulfur in CC-2273 and a negative association in CC-2272 and GHC-747-D. This is strange considering there is more visible molybdenite in the northern drill holes than in the southern drill holes and visible molybdenite can be found in each drill hole. Based on the data at hand and the fact that the correlations relate to spatial distributions (without temporal constraints) this could be interpreted as evidence that some of the molybdenum is hosted in another mineral. Sphalerite can host molybdenum and molybdenum shows strong to moderate correlation with zinc in CC-2272 and GHC-747-D2. However, these are also the drill holes with reasonable sulfur-molybdenum correlations. The lack of correlation between sulfur and molybdenum in CC-2273 and GHC-747-D could occur because the sulfur numbers used in the correlation include all sulfur in all sulfide minerals in the sample and therefore the sulfur is part of other sulfides in addition to molybdenite.

Broad geochemical zoning for the base metals is readily distinguished by the variation in mineralogy between the northern and southern drill holes. It is important to keep in mind that the northern drill holes only reach a depth of 2880 ft and the southern drill holes begin about 2745 and extend to a depth of 5030 ft, so there is a significant difference in depth between the northern and southern holes that could relate to the zoning patterns seen here. There is less Zn (as sphalerite) and more Cu (as chalcopyrite)

in the northern drill holes. At depth to the south the Zn content increases and the copper content decreases overall. In the northern drill holes Cu is generally on the order of 100-200 ppm with local variation, while in the southern drill holes Cu is commonly in the 10-50 ppm range, with local higher values. Zn is extremely variable in the southern drill holes. It generally ranges from ~50-300 ppm but contains local values up to 10,000 ppm. In the northern drill holes it is usually ~100-300 ppm with fewer values above this range. However, the rare local spikes in the northern drill holes can range up to 3,800 ppm.

SEM Analyses

SEM analysis was necessary to identify the mineral intergrown with molybdenite before preparing separates for sulfur isotope analysis. Six EDS spectra were acquired for the mineral intergrown with molybdenite and all showed peaks of iron, manganese, magnesium, carbon, and oxygen (most closely resembles ankerite) with rare peaks of titanium that may be due to the influence of the surrounding matrix. In addition, EDS for molybdenite was also obtained to confirm its identity. Three EDS spectra were obtained for a mineral that appeared to be an arsenic mineral (due to optical properties and association with arsenopyrite) but the spectra indicated that the mineral was the same as that intergrown with molybdenite. Near the arsenopyrite a pyrite grain with a distinct rim was identified and spectra were obtained for the rim and the core of the grain. Neither contained arsenic or gold and the rim was a euhedral overgrowth of uncontaminated pyrite. All SEM images and EDS spectra can be found in Appendix E.

Sulfur Isotope Analyses

Fourteen samples of molybdenite taken from the drill holes were analyzed to ascertain their $\delta^{34}\text{S}$ ratios. No usable samples were obtained from CC-2273. All of the

analyses fell within the range of -6.6 to 0.5% , and with two exceptions the data occur in the range of $0 \pm 5\%$. Table 2 displays numerical values for the results. A frequency diagram depicting the results is illustrated in Figure 13. Given that the $\delta^{34}\text{S}$ values for most other minerals (base metals and sulfides associated with gold) fall within the range of 0 to -22% (epithermal deposits) it is interesting to note that most of the $\delta^{34}\text{S}$ values for molybdenum are clustered within the range identified for porphyry deposits in the western U.S (Ohmoto and Goldhaber, 1997). Though much care was taken to ensure a clean separate, the two exceptions that fall outside this range could have experienced minor contamination by pyrite, as pyrite typically has low (negative) $\delta^{34}\text{S}$ values and is locally intricately intergrown with the molybdenite.

The discrepancy between molybdenite sulfur values and other, more negative values found for the remaining sulfides may be due to S-SO₄ partitioning. Heavier (positive) values tend to be sequestered by SO₄ minerals, while lighter (negative) values reflect sulfides. Sulfate minerals were not found with the molybdenite but are commonly associated with other (negative) sulfides. This could indicate that S-SO₄ partitioning occurred during deposition of the sulfides with negative values but was not active during molybdenite mineralization. The lack of sulfates present with molybdenite also indicate that the molybdenite $\delta^{34}\text{S}$ values are closer to the values present in the ore fluids, as the molybdenite sulfur did not experience S-SO₄ partitioning. Since negative values have been obtained for pyrites associated with gold and for other base metal sulfides, this seems to reflect that molybdenum mineralization occurred separately from gold and base metal mineralization.

Sample	Drill Hole	Depth (ft)	$\delta^{34}\text{S}$ (‰)
CR-1	GHC-747-D2	2641	-0.3
CR-2	GHC-747-D2	2870.5	-1.5
CR-3	GHC-747-D	2456	-2.6
CR-4	GHC-747-D	2436.5	0.5
CR-5	GHC-747-D2	2571	-2.1
CR-6	GHC-747-D2	2880	-2.5
CR-8	GHC-747-D2	2644	-3.5
CR-9	CC-2272	4742.5	-5.0
CR-10	CC-2272	4450.5	-4.6
CR-11	CC-2272	4434	-4.3
CR-12	CC-2272	4465.5	-4.4
CR-13	CC-2272	4457	-5.5
CR-14	CC-2272	4643.5	-6.6
CR-15	CC-2272	4555.5	-3.8
J-1	See Jensen, 2003	See Jensen, 2003	-2.4
J-2	See Jensen, 2003	See Jensen, 2003	-1.2

Table 2. $\delta^{34}\text{S}$ values for molybdenite. CR samples are from this study, while J-1 and J-2 are from Jensen (2003). See Figure 4 for an index map showing the locations of the drill holes from which the samples were taken.

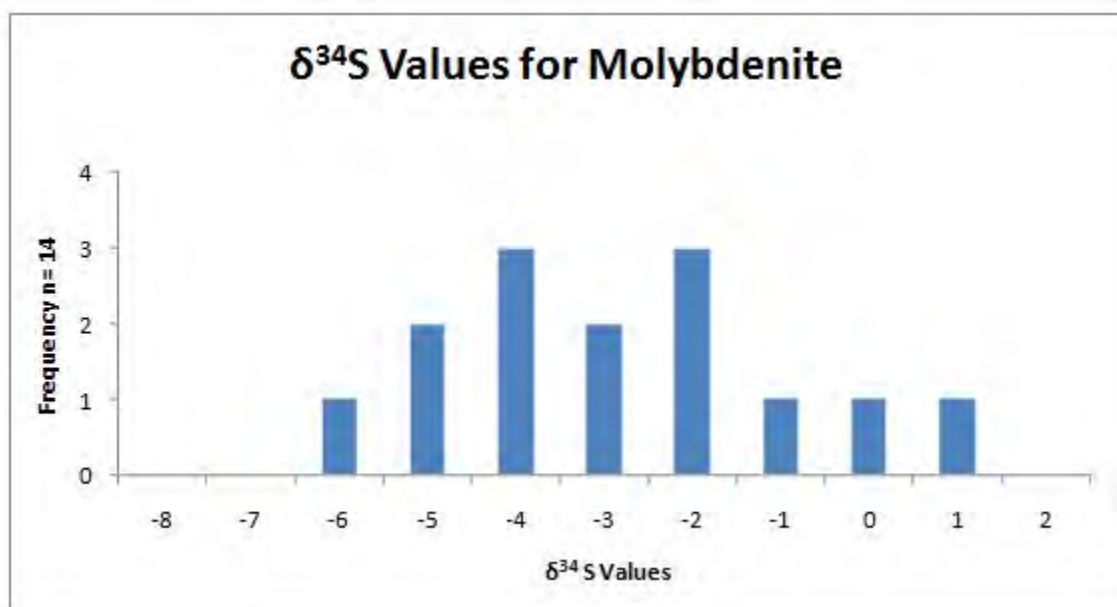


Figure 13. Frequency diagram illustrating the results of sulfur isotope data from this study.

Discussion

The main questions associated with this portion of the project were whether or not the molybdenum mineralization is associated with the gold mineralization event, is molybdenum related to the base metal event, and if a molybdenum deposit exists what is its extent? It was not possible to obtain temperatures for molybdenum mineralization from fluid inclusions or isotope pairs to compare with temperatures for gold mineralization; gold was not observed in association with molybdenum in thin section (but the two appeared to have been deposited very close in time), and potassic alteration, though generally found in association with gold mineralization, was an early event so all of these methods rendered inconclusive results. However, isotopic analyses of the molybdenite show that the sulfur values fall into the range identified by Ohmoto and Goldhaber (1997) for porphyry systems in the western U.S. This indicates that while the gold event is epithermal, the molybdenum mineralization is likely a separate event, possibly a porphyry system. The presence of local stockwork molybdenite veins supports this theory.

Geochemically, the molybdenite shows weak (~ 0.30) to no association with gold in the diatreme and locally a negative association. However, it was difficult to eliminate the rock signature within the diatreme because of the presence of the heterolithic (locally monolithic) Cripple Creek Breccia. Also, many fluids utilized the same pathways within the diatreme, further complicating matters. In comparison, the elements identified by Jensen (2003) as being associated with gold in the diatreme only had a similarly weak (~ 0.30) correlation with gold in the drill holes studied.

Molybdenum locally shows a high correlation with typical base metals such as zinc and lead but in thin section molybdenum consistently appeared much later than the base metal phases. There were many phases of base metal mineralization and the variety of minerals indicates that the composition of the fluids fluctuated over time. Some isotope results have been presented by other workers (see Background: Isotopes section) but none of these results have been obtained while taking paragenesis into account. It is possible that some of the base metals were related to the epithermal gold mineralization, while other phases were associated with the molybdenum event.

The extent of the molybdenum deposit cannot be outlined without more drilling. Given the isotope results obtained in this study, it seems possible that a stockwork Mo system has been encountered. From the current concentrations in various areas (at depth near the Cresson Pipe, in Globe Hill, in Grassy Valley) it appears that there is potential for an economic deposit but this cannot be confirmed or delineated without future drilling. The feasibility of a potential deposit will depend on the results obtained from drilling and the market price of molybdenum at the time the appropriate information is acquired.

Future Work

The first priority for the molybdenum would be to determine if the deposit is economic. To do this, additional drilling, possibly deep drilling, would be needed to outline the resource. The primary areas to focus on are the Globe Hill region and potentially Grassy Valley. Concentrating the drilling to the north will likely yield the best results, as this is where the highest concentrations were encountered in the drill holes examined for this study. While significant molybdenum was intercepted near the Cresson Pipe in the southern portion of the diatreme, the mineralization was deeper and the concentrations less than in the northern portion. Therefore, if an economic deposit does exist it will likely be more accessible and higher grade to the north.

As noted above in the Methods section, it is possible that some of the molybdenum identified from geochemical analyses could be incorporated into the sphalerite lattice. If this is to be studied in the future, either a microprobe with low detection limits or LA-ICP-MS should be used to identify the trace elements because they are present in very low concentrations. Several generations of sphalerite indicate fluctuation in fluid composition and multiple stages of deposition with varying iron and copper content. To determine the trace elements present in sphalerite focus should probably be directed to the high-iron sphalerites, as these are likely to have the most lattice distortion and therefore the highest ability to host trace elements.

It would also be beneficial to the understanding of the system to determine the relationship between base metals and molybdenite. The question here is whether any of the base metals are related to the molybdenum mineralization or if they are all related to the gold mineralization. Careful petrography and isotope work on individual phases

would aid greatly in making this determination. Also, because the fluid composition is variable vertically within the deposit it would be advantageous to select several samples from different levels of the deposit and compare them to one another.

Conclusion

Regarding the relationship of the molybdenum mineralization versus gold mineralization, several methods were attempted to discern their association or lack thereof. Geochemistry showed little to no spatial association between molybdenum and gold. Conclusive data were finally obtained from sulfur isotopes. The data showed that the molybdenum mineralization is likely a separate event and could represent a porphyry system. Previous work has indicated that the gold is epithermal so the two appear to represent different systems. The extent of the molybdenum mineralization cannot be outlined with the data at hand. More drilling is needed, particularly in the northern portion of the diatreme to confirm and define the deposit. Initially, the focus should be on the northern portion because the concentrations were highest there and the holes encountered mineralization at much shallower levels there than in the southern portion of the diatreme. The association between molybdenum and the base metals remains unclear, though from petrography molybdenum appears to be consistently later than base metals. Isotope data from this study and previous studies show most base metals with more negative values than those obtained for molybdenite with the exception of some pyrite values.

Future work for the molybdenum portion of the project should focus on identifying the extent of mineralization with additional drilling and in the process, using

the drilling information to determine if the deposit constitutes an orebody. Determining whether the molybdenum is in the form of molybdenite or encapsulated in the sphalerite lattice should also be an area of focus. If the molybdenum is hosted in sphalerite it would directly affect the economic potential of the deposit because it would be a lot more difficult to process the molybdenum. The relationship of base metals to molybdenum should also be examined further because not only could it aid in the understanding of the deposit but some of the base metals could be processed as well, should they be found in sufficient concentrations.

Part 2: Grouse Mountain

Methods

Grouse Mountain is a volcanic outlier southwest of the Cresson Mine. A map focusing on both geology and alteration was needed to classify the outlier and assess its mineral potential. Previous geologic maps existed (Wobus et al., 1976) but were not detailed enough for the present level of study. During the summer of 2009, George Paptic, an AngloGold company geologist, and I developed a detailed geologic map focusing on alteration as well as lithology. The field maps were then digitized into ArcMap 9.3 and unit descriptions were prepared from field notes.

Samples were collected in the field for petrographic work and geochemical analyses. Thirty-three samples were collected in regions that appeared to have the potential for mineralization. At each locality two samples were taken; one that would be assayed in-house at the Cresson Mine and one to be sent to ALS Chemex for ME-MS61m analysis. The same analysis package that was used on the drill holes within the diatreme was chosen for these samples in order to facilitate the comparison of elements

inboard of the diatreme with those at Grouse. Before the samples were taken to ALS Chemex, billets were cut from each sample to aid in petrographic work. Additional hand samples were gathered in the field for petrographic work and cut into billets.

A correlation matrix was calculated from the geochemical results and elements that correlated with one another were identified. The main rock type in the samples was phonolite, so the elements and amounts normally present in phonolites within the district were recognized as the rock signature. Graphs were constructed from the data showing the relationship of the correlated elements. These graphs and the strength of association between various elements helped distinguish the different events at Grouse Mountain.

Nine billets were selected for petrographic work. The billets were chosen to confirm the identity of units or to further classify the alteration. One unit in particular had previously been mapped as the Tallahassee Creek Conglomerate but appeared to contain clasts of phonolite. Since the phonolite is younger than the Tallahassee Creek Conglomerate, if phonolite were found in the unit then the unit in question could not be the Tallahassee Creek. Several samples were cut and a billet was selected to examine the lithology of the unit. Another unit in question had been mapped over the summer as hornblende phonolite. According to Jensen (2003) many of the phenocrysts identified in hand sample as hornblende are actually clinopyroxene, commonly augite. Therefore, sections were taken to examine the phenocrysts and the alteration in these units. Several other samples were chosen to look at the type and variation in alteration.

The billets cut from all the samples sent for geochemical analysis, including the samples selected for petrography, were stained to determine the location, amount and extent of potassic alteration in the form of feldspar flooding. The billets were etched with

hydrofluoric acid and stained using sodium cobaltinitrite. The acid leaches the rock and the sodium cobaltinitrite replaces the potassium sites, resulting in a bright yellow color in regions of potassium flooding. A light yellow color may result from porous clays selectively uptaking the solution and is probably not due to potassic flooding. The stained billets for Grouse Mountain can be found in Appendix E.

Results

Mapping

Over the summer of 2009, several volcanic outliers near the Cresson Mine were visited. Two were mapped: one with a relatively uncomplicated mineralogy and little alteration and Grouse Mountain. Due to the complexity of Grouse Mountain, it is the focus of this report. A completed geologic map of Grouse Mountain is available in Appendix F, featuring an inset that expands the region mapped in detail. Most of the detailed mapping at Grouse was carried out in the northeast corner due to time limitations. Abundant cover in the form of soil, grasses, shrubs, and trees also hindered the mapping process. The map of Grouse Mountain includes the location of prospect pits, shafts, samples that made grade, dikes, structures, and stained billet locations, in addition to descriptions of lithology and general alteration.

Two notable lithologic discoveries were made during the mapping process. First, a unit that had previously been identified as Tallahassee Creek Conglomerate was found to contain clasts of phonolite (Appendix J). This is significant because the Tallahassee Creek is well documented as being older than the phonolite. Since it is a conglomerate, it cannot contain clasts of a unit younger than itself. Other characteristics such as angular

clasts, poor sorting through the majority of the unit, local puzzle-breccia texture, and minor localized bedding also indicated that the unit was not a conglomerate. Several samples were cut from the material and thin sections made to see if the suspected phonolite actually was phonolite. In thin section it is very clear that the clast is indeed phonolite (Appendix J) and that in several places the unit previously mapped by other workers as the Tallahassee Creek Conglomerate is in fact a breccia unit.

The second important discovery involves a unit that is commonly mapped as “hornblende phonolite.” This lithology does not appear on previous maps but a significant amount was found in the field area in the summer of 2009. When thin sections were taken from this unit it was discovered that the phenocrysts were not hornblende but were clinopyroxene (Appendix J). Jensen (2003) noted that many of the “hornblende phonolites” mapped in the Cresson open pit were actually in his mafic alkaline intrusion category, which includes phonotephrites-tephriphonolites, basaltic trachyandesites, and trachybasalts. He also notes that when altered (as they generally are at Grouse) only the plagioclase remains intact and that makes it difficult to differentiate these rocks from plagioclase phonolites (Jensen, 2003).

Alteration

Due to the abundance of cover in the region, alteration was only mapped in a general sense and descriptions of the alteration are included with the lithologic descriptions for each unit. As it can be impossible to identify potassic flooding in the field, billets were cut from the samples collected and stained to determine the extent of potassic alteration. The locations of these billets can be found on the Grouse Mountain map in Appendix F and the stained billets are presented in Appendix H. There is also a fairly consistent ring of breccia about 10-30 ft wide at the contact of the Altered Clinopyroxene Phonolite with the Phonolite. The breccia there is composed almost exclusively of phonolitic clasts and an iron-rich, goethite matrix. Thin sections of this breccia show that moderate amounts of sericite are present in the phonolite clasts.

One of the main questions regarding Grouse Mountain deals with its character. Part of the goal of this project was to determine if the volcanics at Grouse represent an intrusive or if they are remnants of a volcanic flow. Altered Wall Mountain Tuff, which is younger than the phonolites in the district, has been found at the crest of Grouse Mountain. The Grouse Mountain breccia also shows potassic alteration chemically the same as the Wall Mountain Tuff but concentrated in breccia clasts, not in the matrix. The presence of altered Wall Mountain Tuff surrounded by phonolite at the top of Grouse indicates that the phonolites rose up through the Wall Mountain and that the nature of Grouse is that of an intrusive.

Geochemistry

Elemental associations determined from geochemical work have facilitated identification of three distinct hydrothermal fluids. Because the majority of the samples

collected at Grouse represented various types of phonolite, it was easier to separate the rock signature at Grouse than within the diatreme, as the samples from the diatreme contained many rock types. When looking at the geochemical data for Grouse and the comparison to elements within the diatreme it is important to keep in mind that the samples at Grouse were surface samples and the samples from within the diatreme came from depth. Therefore, not only could the samples represent different levels within the system but the Grouse samples have also been exposed to weathering that could leach out the more mobile elements.

Grouse	Au	Mo	Ag	Pb	Zn
<i>Sample Size</i>	33	33	33	33	33
	As (0.332), Te (0.276), Tl (0.503), Sb (0.509), Cu (0.190), Mo (0.595), S (0.334), Ag (0.240)	As (0.375), Au (0.595), Hg (0.307), S (0.185), Sb (0.597), Tl (0.584)	Cu (0.808), Pb (0.593), Sb (0.533), Te (0.928)	Ag (0.593), Cd (0.485), Ta (0.594), Te (0.354), Zn (0.549)	Ba (0.734), Cd (0.940), Fe (0.307), Mn (0.741), Pb (0.549), Ta (0.706)

Au (Diatreme)	CC-2272	CC-2273	GHC-474-D	GHC-474-D2
<i>Sample Size</i>	19	82	176	103
	As (0.913), Te (0.958), Tl (0.508), Sb (0.808), Cu (0.025), Ag (-0.043), Co (0.635), Hf (0.658), Ni (0.644), Mo (-0.262)	As (0.355), Te (0.097), Tl (-0.009), Sb (0.333), Cu (0.459), Ag (0.525), Hg (0.846), Mo (0.305)	As (0.747), Te (0.434), Tl (0.039), Sb (0.287), Cu (0.463), Ag (0.219), Mo (0.147)	As (0.625), Te (0.220), Tl (0.612), Sb (0.255), Cu (0.391), Ag (0.166), Mo (0.039)

Table 3. Elemental correlations at Grouse (top) and elemental correlations with gold from the four drill holes in the diatreme (bottom) for comparison.

From the correlation coefficients (Table 3), it is apparent that gold at Grouse Mountain shows at least a mild to moderate positive correlation with the elements

associated with gold in the diatreme (As, Sb, Tl, Te, and Cu). Strangely enough, gold also has a positive correlation with molybdenum at Grouse, and that association is the highest correlation of all associated elements. Gold does not generally associate with molybdenum in the diatreme and locally has a mild negative correlation. Gold at Grouse also correlates weakly with silver and sulfur. In the diatreme, a weak association with silver is also common, though locally (Table 3, CC-2272) there may be no association.

Three different hydrothermal fluid signatures have been discerned at Grouse Mountain based on the correlation coefficients. The first fluid described here is dominated by gold and molybdenum. Gold and molybdenum show a significant (0.595) correlation with one another and are also both associated to a lesser extent with thallium, antimony, arsenic, sulfur, and silver. The second fluid is delineated by abundant silver, copper, and tellurium. Silver is strongly associated with copper and tellurium and to a lesser degree with lead and antimony. The third fluid is defined by lead, zinc, cadmium, and a weak correlation with silver. Tantalum shows a high correlation with lead, zinc, and cadmium but also correlates with high immobile trace elements, indicating it is likely a rock forming component (probably phonolitic) and not associated with a hydrothermal fluid. It is also important to note that tantalum and niobium normally follow one another and a strong correlation is found between tantalum and niobium here. However, niobium shows only weak correlations with lead, zinc, and cadmium while tantalum shows high correlations with the same elements. This probably indicates that the link between lead, zinc, cadmium, and tantalum is coincidental.

It should be noted that these fluids are not described in any particular order, as a temporal relationship cannot be defined from the correlation coefficients alone. A clue to

the temporal relationship could be provided by the evolution of the fluids over time. For example, the gold-molybdenum fluid shows a weak association with silver and the silver-copper-tellurium fluid shows a weak association with lead. This could illustrate a gradual change in the fluid through time but it is not possible to demonstrate whether the process began with the gold-molybdenum fluid or the lead-zinc-cadmium-tantalum fluid.

Discussion

Though other outliers were examined and one other was mapped, the decision to focus on Grouse Mountain was made because of its complexity. The primary question regarding Grouse was whether it represented an intrusive or if it was a remnant of a volcanic flow. Due to the presence of altered Wall Mountain Tuff on the summit and the degree of alteration in virtually all the rock types mapped, Grouse Mountain appears to be intrusive. The degree of alteration indicates fluid flow occurred at Grouse and given the assay and geochemical results the fluids were not barren.

Two significant discoveries were made while mapping Grouse. The first is the identification of clinopyroxene-bearing phonolite that had previously been mapped only as phonolite or hornblende phonolite. Clinopyroxene-bearing phonolites have been recognized in the diatreme by Jensen (2003), where they had previously been mapped as hornblende phonolites, and according to Jensen (2003) are probably phonotephritic in composition. The second discovery was that a unit previously mapped as the Tallahassee Creek Conglomerate was really a breccia, hereafter called "Grouse Mountain Breccia." It is not possible to determine the breccia type (vent opening, hydrothermal, diatremal, etc.) without information as to its character at depth. In order to construct a reliable cross

section, drilling information will be required because the amount of cover and lack of outcrop makes most surface contacts in the region uncertain.

Geochemistry was completed at Grouse to determine if the elements associated with gold in the diatreme were also associated with gold at Grouse. The elements linked to gold in the diatreme show a similar relationship to gold at Grouse. However, at Grouse molybdenum seems to show an association with gold while molybdenum is not significantly associated with gold in the diatreme. In addition, three different fluids were recognized from the geochemical work. Overall, this differs from the diatreme because the same fluids could not be identified there with any certainty. This could be because there were more hydrothermal events in the diatreme that used the same pathway. The greater variety of elemental associations within the diatreme supports this idea. It could also be because the samples at Grouse represent a different level of the system than the samples in the diatreme. The diatreme samples used in this study were from the deepest holes drilled in the district, while the samples at Grouse were surface samples (and could have been subjected to weathering and/or leaching, though every effort was made to obtain the freshest samples). In addition, there was a much smaller sample size for Grouse than for the diatreme.

Future Work

Future work on Grouse Mountain should involve commencement of a drilling campaign. With the information obtained from drilling reliable cross sections could be developed and the surface maps refined without the interference of vegetation. The construction of cross sections based on drilling would help determine the extent and character of the breccia body. The samples that made grade at Grouse were generally located along phonolite contacts and within the phonolite breccia so these areas should be given special consideration when designating areas for drilling.

Conclusion

Grouse Mountain appears to be intrusive and not the remnant of a volcanic flow. The presence of Wall Mountain Tuff (altered) and the degree of alteration of the units mapped support this conclusion. In addition, the extent of alteration, including but not limited to potassium feldspar flooding, suggest that significant fluid flow has occurred at Grouse. Three distinct assemblages were identified at Grouse based on geochemical analyses: gold-molybdenum, silver-copper-tellurium, and lead-zinc-cadmium-tantalum. The trace elements associated with gold in the diatreme are also associated with gold at Grouse, with the exception of molybdenum, which shows a correlation with gold at Grouse but not within the diatreme.

Two units were identified at Grouse through the mapping portion of this study that had not been recognized previously. The first was a unit that had been mapped as phonolite or hornblende phonolite but through petrographic work it is clear that the unit is actually a clinopyroxene-bearing phonolite. The second unit had formerly been mapped

as the Tallahassee Creek Conglomerate but during the course of mapping for this project it was discovered that the unit in question contained clasts of phonolite and due to its physical characteristics (poor sorting, only localized bedding, dominantly angular fragments, and local puzzle breccia texture) resembled a breccia more than a conglomerate. Thin section work confirmed the identity of the phonolite in a sample from this unit. For Grouse Mountain future work should consist of drilling. The data obtained from drilling would help produce reliable cross sections and refine the surface map. It would also facilitate identification of the type of breccia present at Grouse.

References

- Aldrich, M.J. Jr., Chapin, C.E., and Laughlin, A.W., 1986, Stress History and Tectonic Development of the Rio Grande Rift, New Mexico: *Journal of Geophysical Research*, v. 91, No. B6, p. 6199-6211.
- ALS Chemex, 2004, Grassy Valley Monitor Wells ME-MS-61 Multielement Geochemistry and Leco Analyses Completed 2005: Unpublished Report Prepared for Cripple Creek & Victor Gold Mining Company/AngloGold North America, 2 p.
- Beaty, D.W., Kelley, K.D., Silberman, M.L., and Thompson, T.B., 1996, Oxygen Isotope Geochemistry of a Portion of the Cripple Creek Hydrothermal System: *Soc. Economic Geologists Guidebook Series*, v. 26, p. 55-64.
- Birmingham, S.D., 1987, The Cripple Creek Volcanic Field, Central Colorado: M.S. Thesis, University of Texas, Austin, 295 p.
- Bookstrom, A.A., 1990, Igneous Rocks and Carbonate-Hosted Ore Deposits of the Central Colorado Mineral Belt: *Soc. Economic Geologists Monograph* 7, p. 45-65.
- Burnett, W.J., 1995, Fluid Chemistry and Hydrothermal Alteration of the Cresson Disseminated Gold Deposit, Colorado: unpublished Colorado State University M.S. Thesis, 168 p.
- Chapin, C.E. and Lowell, G.R., 1979, Primary and Secondary Flow Structures in Ash-Flow Tuffs of the Gribbles Run Paleovalley, Central Colorado: *Geological Society of America Special Paper* 180, p. 137-154.
- Christiansen, R.L., Yeats, R.S., Graham, S.A., Niem, W.A., Niem, A.R., and Snavely, P.D. Jr., 1992, The Post-Laramide Geology of the U.S. Cordilleran Region: *Geological Society of America, Geology of North America*, v. G3, p. 261-406.
- Cook, N.J., Ciobanu, C.L., Pring, A., Skinner, W., Shimizu, M., Danyushevsky, L., Saini-Eidukat, B., and Melcher, F., 2009, Trace and Minor Elements in Sphalerite: A LA-ICPMS Study: *Geochimica et Cosmochimica Acta*, v. 73, Issue 16, p. 4761-4791.
- Cripple Creek & Victor/AngloGold (Colorado) Corp., 2005, Cripple Creek Presentation, Internal company powerpoint presentation.
- Cross, W. and Penrose, R.A.F. Jr., 1895, Geology and Mining Industries of the Cripple Creek District, Colorado: U.S. Geological Survey 16th Annual Report, Part 2, p. 1-209.

- Dwellely, P.C., 1984, Geology, Mineralogy, and Fluid Inclusion Analysis of the Ajax Vein System, Cripple Creek Mining District, Colorado: unpublished M.S. Thesis, Colorado State University, 167 p.
- Economic Geology Consulting, 2003, Petrography of CC-2272-Series and GHC-747-D-Series Samples, Cripple Creek, Colorado: Unpublished Report Prepared for Cripple Creek & Victor Gold Mining Company/AngloGold North America, 44 p.
- Endlich, F.M., 1874, Report Upon the Geology of the San Luis District, Section A: *in* Hayden, F.V. ed., Annual Report of the Geologic and Geographical Survey of the Territories, embracing Colorado, being a report of progress of the exploration for the year 1873: Government Printing Office, Washington, D.C., p. 305-322.
- Giesemann A., Jager H.J., Norman A.L., Krouse H.P. and Brand W.A., 1994, On-line sulfur-isotope determination using an elemental analyzer coupled to a mass spectrometer: Analytical Chemistry, vol. 66, p. 2816-2819.
- Grassineau N.V., Matthey D.P. and Lowry D., 2001, Sulfur Isotope Analysis of Sulfide and Sulfate minerals by Continuous Flow-Isotope Ratio Mass Spectrometry: Analytical Chemistry, vol. 73, p. 220-225.
- Hedge, C.E., 1970, Whole-Rock Rb-Sr Age of the Pikes Peak Batholith, Colorado: U.S. Geological Survey Professional Paper 700-B, p. B86-B89.
- Huston D. L., Sie S. H., Suter G. F., Cooke D. R. and Both R. A. (1995) Trace elements in sulfide minerals from eastern Australian volcanic-hosted massive sulfide deposits; Part I, Proton microprobe analyses of pyrite, chalcopyrite, and sphalerite, and Part II, Selenium levels in pyrite; comparison with delta ³⁴S values and implications for the source of sulfur in volcanogenic hydrothermal systems: Economic Geology 90, p. 1167–1196.
- Hutchinson, R.M., and Hedge, C.E., 1968, Depth-Zone Emplacement and Geochronology of Precambrian Plutons, Central Colorado Front Range: Geological Society of America Special Paper 115, p. 424-425.
- Jensen, E.P., 2003, Magmatic and Hydrothermal Evolution of the Cripple Creek Gold Deposit, Colorado, and Comparisons with Regional and Global Magmatic-Hydrothermal Systems Associated with Alkaline Magmatism: Unpublished University of Arizona Ph.D. dissertation, 846 p.
- Jensen, E.P. and Barton, M.D., 2007, Geology, Petrochemistry, and time-space evolution of the Cripple Creek district, Colorado: The Geological Society of America Field Guide 10, p. 63-78.

- Karlstrom, K.E. and Humphreys, E.D., 1998, Persistent Influence of Proterozoic Accretionary Boundaries in the Tectonic Evolution of Southwestern North America: Interaction of Cratonic Grain and Mantle Modification Events: *Rocky Mountain Geology*, v. 33, No. 2, p. 161-179.
- Kelley, K.D., Romberger, S.B., Beaty, D.W., Pontius, J.A., Snee, L.W., Stein, H.J., and Thompson, T.B., 1998, Geochemical and Geochronological Constraints on the Genesis of Au-Te Deposits at Cripple Creek, Colorado: *Economic Geology*, v. 93, p. 981-1012.
- Koschmann, A.H., 1947, The Cripple Creek District, Teller County, *in* Vanderwilt, J.W., Ed., *Mineral Resources of Colorado*: Denver, State of Colorado Mineral Resources Board, plate 26.
- Koschmann, A.H., 1949, Structural Control of the Gold Deposits of the Cripple Creek District, Colorado: *U.S. Geological Survey Bulletin* 955-B, 60 p.
- Kleinkopf, M.D., Peterson, D.L., and Gott, G., 1970, Geophysical Studies of the Cripple Creek Mining District, Colorado: *Geophysics*, v. 35, p. 490-500.
- Lane, C.A., 1976, *Geology, Mineralogy, and Fluid Inclusion Geothermometry of the El Paso Gold Mine, Cripple Creek, Colorado*: Unpublished M.S. Thesis, University of Missouri-Rolla, 103 p.
- Lindgren, W. and Ransome, F.L., 1906, *Geology and Gold Deposits of the Cripple Creek District, Colorado*: *U.S. Geological Survey Professional Paper* 54, 516 p.
- Lipman, P.W., 1981, *Volcano-Tectonic Setting of Tertiary Ore Deposits, Southern Rocky Mountains*: *Arizona Geological Society Digest*, v. 14, p. 199-213.
- Loughlin, G.F. and Koschmann, A.H., 1935, *Geology and Ore Deposits of the Cripple Creek District, Colorado*: *Colorado Scientific Society Proceedings*, v. 13, No. 6, p. 217-435.
- McIntosh, A.N., 2004, *Stable Isotopic Evidence for Fluid Mixing in the Tertiary Alkalic-Type Epithermal Au-Te Deposit, Cripple Creek, Colorado*: Unpublished M.S. thesis, Socorro, New Mexico Institute of Mining and Technology, 124 p.
- Mote, A.S., 2000, *Fluid Inclusion Study of Veins within Granite Island, Cripple Creek Mining District, Cripple Creek, Colorado*: Unpublished B.S. Thesis, University of Georgia, 17 p.
- Mutschler, F.E., Wright, E.G., Ludington, S., and Abbott, J.T., 1981, *Granite Molybdenite Systems*: *Economic Geology*, v. 76, No. 4, p. 874-897.

- Nelson, S.E., 1989, Geology, Alteration, and Mineral Deposits of the Cresson Diatreme, Cripple Creek District, Colorado: Unpublished M.S. Thesis, Colorado State University, Fort Collins, 147 p.
- Ohmoto, H., and Goldhaber, M.B., 1997, Chapter 11: Sulfur and Carbon Isotopes *in* Barnes, H.L., ed., *Geochemistry of Hydrothermal Ore Deposits*, 3rd Ed.: New York, John Wiley and Sons Inc., p. 517-612.
- Orberger B., Pasava J., Gallien J.-P., Daudin L. and Trocellier P. (2003) Se, As, Mo, Ag, Cd, In, Sb, Pt, Au, Tl, Re traces in biogenic and abiogenic sulfides from Black Shales (Selwyn Basin, Yukon territories, Canada): a nuclear microprobe study: *Nucl. Instr. Meth. Phys. Res. B210*, p.441-448.
- Pontius, J.A., 1996, Gold Deposits of the Cripple Creek Mining District, Colorado, USA: *Soc. Economic Geologists Guidebook Series*, v. 26, p. 29-37.
- Powell, J.W., 1876, *Exploration of the Colorado River of the West*: Smithsonian Institution, 291 p.
- Reed, J.C., Bickford, M.E., Premo, W.R., Aleinikoff, J.N., and Pallister, J.S., 1987, Evolution of the Early Proterozoic Colorado province: Constraints from U-Pb Geochronology: *Geology*, v. 15, p. 861-865.
- Rosdeutscher, J.A., 1998, Characterization of Distal Gold Mineralization and Alteration in the Cripple Creek District, Colorado [abs.]: *Geological Society of America Abstracts with Programs*, v. 30, No. 7, p. 301.
- Silberman, M.L., 1992, Verbal and Written Update of Oxygen Isotope Work on the Pharmacist Vein System, Cripple Creek, Colorado, reference in Pontius, 1996.
- Saunders, J.A., 1986, Petrology, Mineralogy, and Geochemistry of Representative Gold Telluride Ores from Colorado: Unpublished Ph.D. Dissertation, Colorado School of Mines, 171 p.
- Seibel, G.E., 1991, Geology of the Victor Mine, Cripple Creek Mining District, Colorado: Unpublished M.S. Thesis, Colorado State University, 133 p.
- Thompson, T.B., 1996, Fluid Evolution of the Cripple Creek Hydrothermal System, Colorado: *Soc. Economic Geologists Guidebook Series*, v. 26, p. 45-54.
- Thompson, T.B., Trippel, A.D., and Dwelley, P.C., 1985, Mineralized Veins and Breccias of the Cripple Creek District, Colorado: *Economic Geology*, v. 80, p. 1669-1688.

- Trippel, A.D., 1985, Hydrothermal Mineralization and Alteration at the Globe Hill Deposit, Cripple Creek District, Colorado: Unpublished M.S. Thesis, Colorado State University, 93 p.
- Tweto, O., and Sims, P.C., 1963, Precambrian Ancestry of the Colorado Mineral Belt: Geological Society of America Bulletin, v. 74, p. 991-1014.
- Wobus, R.A., Epic, R.C., and Scott, G.R., 1976, Reconnaissance Geologic Map of the Cripple Creek-Pikes Peak Area, Teller, Fremont, and El Paso Counties, Colorado: U.S. Geological Survey Miscellaneous Field Studies Map, MF-805.
- Yernberg, W.R., 2002, Cresson Mine Completes two-year Expansion: Mining Engineering, vol. 54, No. 12, p. 22-23.

Appendix A:
Pearson's Correlation Coefficients

The following charts contain Pearson's Correlation Coefficients for the elements listed on the chart for the respective drill holes. Arbitrary cutoff values of 0.75 to 1 and -0.75 to -1 were chosen to represent positive (blue) and negative (red) correlations, respectively. Further statistical approaches will define these cutoffs specifically but for the current presentation arbitrary cutoffs were chosen to highlight the strongest correlations. The raw geochemical data are proprietary and are not included in this report. The reader interested in such data should contact the AngloGold Exploration Manager of the Colorado division, currently Tim Brown.

CC-2272: Pearson's Correlation Coefficients

CC-2272	Au	Ag	Al	As	Ba	Be	Bi	Ca	Cd	Ce	Co	Cr	Cs	Cu	Fe	Ga	Ge	Hf	Hg	In	K	La	Li	Mg	Mn
Au	1																								
Ag	-0.04289	1																							
Al	0.021455	-0.2374	1																						
As	0.912897	-0.04503	0.007325	1																					
Ba	0.198288	0.072602	-0.47948	0.161247	1																				
Be	-0.30181	-0.43238	0.054247	-0.31061	0.17583	1																			
Bi	-0.25149	0.957729	-0.17117	-0.25086	-0.03405	-0.32571	1																		
Ca	-0.08819	0.179629	-0.73296	-0.0831	0.655397	0.169163	0.094153	1																	
Cd	-0.20433	0.312428	-0.04246	0.101443	0.038075	-0.32689	0.293406	0.039272	1																
Ce	-0.23525	-0.14769	-0.66022	-0.26535	0.297181	0.309541	-0.1184	0.524687	-0.30623	1															
Co	0.63478	-0.0079	-0.42884	0.547728	0.379595	0.223488	-0.13689	0.274766	-0.35792	0.234698	1														
Cr	-0.13934	-0.35709	-0.07671	-0.12998	0.050931	0.750696	-0.28546	0.283364	-0.38775	0.37633	0.339268	1													
Cs	-0.10562	-0.04526	0.025031	-0.13606	0.276667	0.764054	-0.04837	0.271758	-0.20071	0.039175	0.302009	0.558779	1												
Cu	0.024818	-0.47028	-0.13765	0.150557	0.076204	0.539529	-0.45351	0.256374	-0.09346	0.415891	0.409575	0.632047	0.15136	1											
Fe	0.091384	0.025426	-0.38614	0.001603	0.329184	0.629839	-0.00035	0.498044	-0.37799	0.436154	0.752974	0.643795	0.651277	0.568177	1										
Ga	0.047281	-0.08394	0.800531	-0.03691	-0.39846	0.079642	-0.00978	-0.07948	-0.52291	-0.38399	-0.11529	0.194415	-0.35476	-0.307	0.194415	1									
Ge	-0.20355	-0.11447	-0.39022	-0.19632	0.016147	0.317908	-0.12766	0.405632	-0.09738	0.589804	0.237843	0.353282	0.205817	0.452179	0.524678	-0.42523	1								
Hf	0.698346	-0.13339	0.459283	0.67527	-0.087	-0.50172	-0.24051	-0.35654	0.108891	-0.49637	-0.09528	-0.37991	-0.46158	-0.18859	-0.55202	0.415832	-0.50776	1							
Hg	-0.01472	0.144232	-0.18077	0.332275	0.01383	-0.37923	0.098772	-0.14826	0.913411	-0.44487	-0.37695	-0.38755	-0.28688	-0.07811	-0.53452	0.032378	-0.24351	0.423668	1						
In	-0.07088	0.207063	-0.17087	0.171832	0.094946	0.170265	0.170309	0.376422	0.526969	-0.00373	0.109926	0.210596	0.174286	0.492246	0.254181	-0.20437	0.278283	-0.10972	0.36015	1					
K	-0.17292	0.136749	-0.07375	-0.03171	-0.09437	-0.22515	0.198312	-0.22499	0.442852	0.10486	-0.29081	-0.13013	-0.2454	-0.2225	-0.35257	0.012193	-0.04	0.054229	0.508852	-0.17578	1				
La	-0.22575	-0.09542	-0.65948	-0.28988	0.435512	0.205065	-0.09637	0.601602	-0.21705	0.933811	0.11182	0.212105	0.040674	0.247753	0.313906	-0.44175	0.502276	-0.43488	-0.45673	-0.01199	0.082275	1			
Li	-0.14052	-0.6378	0.048983	-0.15622	0.003199	0.694829	-0.60096	0.164962	-0.21322	0.268321	0.062389	0.642952	0.508002	0.457856	0.332292	0.155806	0.394807	-0.22131	-0.2453	0.206408	-0.19995	0.296563	1		
Mg	0.304599	-0.06666	-0.0843	0.229911	0.395445	0.539244	-0.14551	0.258091	-0.1728	0.025719	0.563346	0.372683	0.835791	0.104949	0.650912	0.208738	0.126033	-0.16909	-0.21143	0.063343	-0.1936	0.061821	0.441436	1	
Mn	-0.32742	0.001435	-0.48094	-0.37712	0.242329	0.218781	0.036997	0.259259	0.049844	0.286637	0.053447	0.026744	0.353129	-0.24247	0.190178	-0.18429	0.111886	-0.59712	-0.17395	-0.18111	0.089572	0.378887	0.254405	-0.397836	1
Mo	-0.26152	0.823206	-0.0449	-0.27151	0.013011	-0.2935	0.884741	-0.00981	0.154907	-0.18458	-0.13398	-0.25427	-0.01204	-0.49962	-0.04052	0.02588	-0.26475	-0.23921	0.042699	0.007564	0.029085	-0.16853	-0.62701	-0.13295	0.08045
Na	0.178844	-0.60275	0.384506	-0.00352	-0.01218	0.100792	-0.58446	-0.09475	-0.44847	-0.13437	-0.09082	0.079609	-0.16195	0.147005	-0.13894	0.277996	-0.20123	0.428102	-0.30404	-0.32271	-0.35522	-0.10587	0.226292	-0.12207	-0.40245
Nb	0.060556	0.522619	-0.08364	0.101942	-0.25239	-0.59437	0.518896	-0.11282	0.234953	-0.05879	-0.33469	-0.44773	-0.51112	-0.49418	-0.52003	0.12858	-0.34084	0.365933	0.303501	-0.04184	0.384623	-0.0437	-0.50904	-0.42437	-0.11343
Ni	0.644301	0.365461	-0.27859	0.535009	0.239204	-0.04341	0.244429	0.075942	-0.14833	-0.08309	0.835661	0.010432	0.252229	-0.00819	0.55808	-0.11064	0.091123	0.011245	-0.23088	0.051958	-0.12383	-0.14044	-0.18907	0.571881	0.075831
P	0.248533	-0.19836	-0.56262	0.192981	0.268959	0.326918	-0.26317	0.352429	-0.4503	0.693938	0.74399	0.448242	0.233496	0.442684	0.689134	-0.51989	0.556275	-0.33485	-0.43844	-0.10354	-0.04183	0.503139	0.163566	0.378838	0.209522
Pb	-0.21817	0.855296	-0.20544	-0.1826	0.133315	-0.54444	0.806729	0.18455	0.540639	-0.18078	-0.28542	-0.52702	-0.20321	-0.56869	-0.23271	-0.15931	-0.10581	-0.1095	0.691035	0.112761	0.238441	-0.05054	-0.58769	-0.21726	0.137546
Rb	-0.34303	-0.18549	-0.19471	-0.25954	0.231603	0.467584	-0.07088	0.150201	0.21863	0.422224	-0.13511	0.305219	0.276143	0.16685	0.107878	0.069792	0.18377	-0.25758	0.210825	0.058159	0.629056	0.445654	0.429151	0.262461	0.370162
Re	-0.25939	0.697715	-0.04978	-0.24936	0.03323	-0.13223	0.812947	-0.04168	0.096421	-0.15756	-0.06633	-0.08164	0.041436	-0.37021	0.013384	0.057537	-0.37545	-0.23328	0.027421	0.001267	0.121423	-0.19221	-0.56638	-0.09055	0.059859
S	-0.45733	-0.12363	-0.16518	-0.40577	-0.09652	0.623661	-0.02391	0.29624	-0.25461	0.508876	0.191964	0.750816	0.360792	0.677788	0.64261	-0.32024	0.552134	-0.64302	-0.3732	0.321599	-0.18077	0.304497	0.361472	0.05047	-0.0735
Sb	0.807965	0.235563	-0.00729	0.908742	0.136487	-0.44821	0.033178	-0.0559	0.345203	-0.44563	0.417756	-0.30013	-0.09415	-0.10105	-0.06939	0.034684	-0.21444	0.618096	0.473228	0.219885	0.098283	-0.41231	-0.2817	0.269987	-0.25734
Se	-0.14442	0.575624	0.178988	-0.20881	-0.17719	-0.22341	0.673264	-0.27757	0.035243	-0.26178	-0.05743	-0.24604	-0.05495	-0.42032	-0.01302	0.247954	-0.1554	-0.11118	-0.00777	-0.11083	-0.04236	-0.28342	-0.45928	-0.04067	0.033265
Sn	-0.46415	0.42481	0.048954	-0.61511	-0.06574	0.054334	0.550542	-0.05542	-0.12063	0.06976	-0.21849	-0.11299	0.137072	-0.41032	0.087991	0.196447	0.232696	-0.41791	-0.44949	-0.18049	0.024651	0.108925	-0.12003	-0.00969	0.153721
Sr	-0.11811	-0.38567	-0.1933	-0.08554	0.216442	0.781706	-0.3767	0.410786	-0.24565	0.434535	0.442486	0.724035	0.55921	0.822397	0.767899	-0.28899	0.51252	-0.49565	-0.32808	0.42849	-0.4698	0.339271	0.663338	0.439356	0.135321
Ta	0.114416	0.235084	-0.17002	0.281197	-0.14178	-0.35311	0.239262	-0.07636	0.282099	0.010662	-0.18347	-0.20898	-0.33217	-0.24234	-0.42888	0.020375	-0.3301	0.324172	0.467976	0.063472	0.443452	-0.02473	-0.30205	-0.24615	0.023584
Te	0.958412	0.160614	-0.09775	0.890039	0.283276	-0.28368	-0.04947	0.010521	-0.15042	-0.20584	0.744714	-0.1039	-0.02027	0.026459	0.236754	-0.06368	-0.17838	0.512258	-0.02298	0.024772	-0.18318	-0.21905	-0.24723	0.368083	-0.2763
Th	0.331039	-0.21102	0.436561	0.180483	0.082374	-0.13469	-0.24946	-0.16705	-0.09921	-0.36887	-0.25257	-0.3119	-0.07001	-0.37951	-0.41027	0.658961	-0.45605	0.684929	0.036708	-0.26012	-0.08099	-0.19268	0.090303	0.114798	-0.21582
Ti	0.422909	0.037325	-0.51264	0.389531	0.440428	0.297018	-0.07408	0.313159	-0.21662	0.266997	0.885344	0.323726	0.485595	0.242647	-0.727003	-0.4064	0.270787	-0.32014	-0.25375	0.054354	-0.16523	0.179001	0.118256	0.699347	0.422889
Tl	0.507982	-0.25307	0.335275	0.731247	-0.04655	-0.11485	-0.33894	-0.34123	0.357906	-0.26364	0.065467	-0.08746	-0.13628	0.173762	-0.27892	0.26948	-0.22031	0.684222	0.710246	0.194228	0.251587	-0.29377	0.064501	0.121028	-0.33703
U	0.113359	-0.3499	0.349498	0.178293	-0.23389	0.031529	-0.34248	0.04305	0.005157	-0.23183	-0.22479	0.274851	-0.09334	0.28011	-0.19636	0.297202	-0.14713	0.498427	0.185349	0.262675	-0.10609	-0.25188	0.25472	-0.16622	-0.56942
V	0.403735	-0.08179	-0.21454	0.356601	0.445123	0.444009	-0.19913	0.244482	-0.05885	0.015902	0.692606	0.304123	0.697083	0.199616	0.646864	-0.01311	0.137884	-0.1775	-0.15876	0.152611	-0.17921	0.054645	0.419449	0.921594	0.419771
W	-0.07918	0.345445	-0.45425	-0.0113	0.118718	-0.13335	0.303352	0.063401	0.280226	0.352023	0.10789	-0.11187	-0.09494	-0.10234	0.558209	-0.39634	0.246717	-0.32002	0.15046	0.048889	0.410771	0.367277	-0.04824		

CC-2272: Pearson's Correlation Coefficients Con't

CC-2272	Mo	Na	Nb	Ni	P	Pb	Rb	Re	S	Sb	Se	Sn	Sr	Ta	Te	Th	Ti	Tl	U	V	W	Y	Zn	Zr
Au																								
Ag																								
Al																								
As																								
Ba																								
Be																								
Bi																								
Ca																								
Cd																								
Ce																								
Co																								
Cr																								
Cs																								
Cu																								
Fe																								
Ga																								
Ge																								
Hf																								
Hg																								
In																								
K																								
La																								
Li																								
Mg																								
Mn																								
Mo	1																							
Na	-0.51638	1																						
Nb	0.340914	-0.27956	1																					
Ni	0.199851	-0.29934	-0.08394	1																				
P	-0.25903	-0.12078	-0.26562	0.447715	1																			
Pb	0.708562	-0.53853	0.451152	0.07525	-0.35093	1																		
Rb	-0.25298	-0.17747	-0.00291	-0.1712	0.109775	-0.13791	1																	
Re	0.92475	-0.43056	0.313314	0.205831	-0.21903	0.490157	-0.06902	1																
S	-0.03371	-0.04615	-0.43964	-0.11658	0.436249	-0.25121	0.122854	0.028879	1															
Sb	-0.05033	-0.19775	0.212227	0.608275	-0.00124	0.13276	-0.22278	-0.07589	-0.54307	1														
Se	0.843202	-0.35274	0.174584	0.323728	-0.20397	0.468644	-0.27041	0.766328	-0.07729	-0.01846	1													
Sn	0.605154	-0.1871	-0.03893	0.078291	-0.11372	0.40488	0.039603	0.500827	0.156124	-0.42409	0.719196	1												
Sr	-0.36112	0.022188	-0.66134	0.06584	0.463551	-0.464	0.16489	-0.30967	0.724236	-0.2726	-0.30999	-0.1738	1											
Ta	0.131718	-0.37838	0.831281	-0.07616	-0.10833	0.132446	0.203046	0.229262	-0.3988	0.827251	0.008609	-0.34744	-0.43855	1										
Te	-0.05205	-0.00402	0.052194	0.786192	0.31567	-0.0638	-0.36952	-0.05748	-0.35322	0.827251	0.008609	-0.35705	-0.07182	0.091202	1									
Th	-0.28157	0.644325	0.194531	-0.13287	-0.39654	-0.16165	0.025638	-0.25814	-0.59389	0.182647	-0.16982	-0.0854	-0.40022	0.050422	0.158523	1								
Ti	-0.01091	-0.38286	-0.35621	0.779367	0.739202	-0.1444	0.022745	0.021606	0.143435	0.344169	0.024144	-0.11889	0.43955	-0.1094	0.562966	-0.39911	1							
Tl	-0.32852	-0.06271	0.155431	0.084081	-0.05775	-0.22561	0.117384	-0.28716	-0.35549	0.648593	-0.16592	-0.5204	-0.08017	0.407294	0.425975	0.232975	0.043732	1						
U	-0.43418	0.607711	0.071342	-0.37557	-0.27663	-0.40824	-0.03913	-0.30481	0.070524	0.085593	-0.44874	-0.4446	0.014071	0.110854	-0.02902	0.470153	-0.48618	0.226199	1					
V	-0.21673	-0.18203	-0.49101	0.658842	0.411034	-0.17944	0.209215	-0.18829	0.021413	0.377668	-0.13507	-0.14321	0.481237	-0.29416	0.479338	-0.02084	0.800147	0.158918	-0.27385	1				
W	0.191542	-0.7448	0.240516	0.20298	0.228572	0.46375	0.287026	0.063818	-0.03181	0.071352	0.119513	0.11853	0.012594	0.240613	0.019807	-0.50701	0.333064	0.080633	-0.71378	0.187194	1			
Y	-0.16984	-0.14915	-0.23594	0.075575	0.784491	-0.18776	0.340686	-0.12454	0.631054	-0.34169	-0.2122	0.051414	0.578464	-0.09659	-0.17386	-0.44323	0.466245	-0.28585	-0.15306	0.220608	0.194707	1		
Zn	0.049213	-0.35855	0.264438	-0.22552	-0.43363	0.50645	0.193967	-0.00864	-0.26183	0.373578	-0.12875	-0.2874	-0.23519	0.318029	-0.1029	-0.04215	-0.24833	0.42252	0.103549	-0.07537	0.261452	-0.21625	1	
Zr	-0.23017	0.51868	0.394264	-0.09928	-0.4109	-0.1275	-0.25227	-0.21977	-0.63975	0.484119	-0.09785	-0.3367	-0.558	0.300108	0.39006	0.755048	-0.45699	0.571793	0.549765	-0.2941	-0.40319	-0.62713	0.132646	1

CC-2273: Pearson's Correlation Coefficients

CC-2273	Au	Ag	Al	As	Ba	Be	Bi	Ca	Cd	Ce	Co	Cr	Cs	Cu	Fe	Ga	Ge	Hf	Hg	In	K	La	Li	Mg	Mn
Au	1																								
Ag	0.524795	1																							
Al	-0.08048	-0.52348	1																						
As	0.355115	0.37881	-0.01849	1																					
Ba	-0.07235	-0.34041	0.2584	-0.14484	1																				
Be	-0.20137	-0.26909	0.235272	-0.0999	-0.08111	1																			
Bi	0.189618	0.812039	-0.44393	0.164842	-0.46079	-0.07785	1																		
Bd	-0.05816	0.445983	-0.88025	-0.14009	-0.20521	-0.23118	0.41611	1																	
Cd	0.271549	0.943406	-0.55279	0.386611	-0.31873	-0.24196	0.765595	0.511203	1																
Ce	0.162492	0.498504	-0.42667	0.135561	-0.08906	-0.25513	0.340066	0.567869	0.521568	1															
Co	-0.22843	-0.19652	-0.48952	-0.33229	0.129819	-0.02292	-0.19259	0.62263	-0.14411	0.22867	1														
Cr	-0.22996	-0.1545	-0.52798	-0.31574	0.160609	-0.07037	-0.17541	0.665519	-0.03681	0.252594	0.978308	1													
Cs	-0.15909	-0.12435	-0.34816	-0.28959	-0.04987	0.142867	-0.11162	0.396863	-0.0885	0.080536	0.680985	0.628317	1												
Cu	0.458817	0.924641	-0.69972	0.25222	-0.28435	-0.26671	0.707636	0.683286	0.902578	0.593752	0.14188	0.173351	0.102119	1											
Fe	-0.17125	-0.01729	-0.52042	-0.29152	0.04726	0.083142	0.068379	0.676703	0.028671	0.329624	0.912407	0.867368	0.616893	0.308743	1										
Ga	0.123455	-0.13366	0.75611	0.163285	0.132239	0.178007	-0.08563	-0.76889	-0.17692	-0.20736	-0.6651	-0.69767	-0.41079	-0.35717	-0.58459	1									
Ge	0.101145	0.723759	-0.67617	0.142748	-0.334	-0.09169	0.650195	0.778732	0.776316	0.655939	0.30406	0.340868	0.302535	0.830944	0.447049	-0.46571	1								
Hf	-0.18676	-0.21006	-0.09999	-0.27223	0.388019	-0.19318	-0.26864	0.21906	-0.15383	0.176597	0.517077	0.562174	0.186916	-0.03245	0.431334	-0.10428	-0.04731	1							
Hg	0.845603	0.856836	-0.39243	0.344886	-0.21192	-0.26789	0.52724	0.285478	0.697949	0.3795	-0.17224	-0.14622	-0.11921	0.819542	-0.05129	-0.07166	0.484173	-0.16391	1						
In	0.22964	0.885841	-0.6113	0.251107	-0.27977	-0.16587	0.821053	0.621875	0.548969	0.016123	0.033157	0.03875	0.897383	0.242366	-0.21533	0.820955	-0.1319	0.637421	0.820955	1					
K	-0.06633	-0.28781	0.467691	0.254093	-0.00397	0.234666	-0.2771	-0.61483	-0.3029	-0.58486	-0.41056	-0.41291	-0.31202	-0.45947	-0.49089	0.271699	0.48627	-0.26543	-0.20986	-0.42077	1				
La	0.286902	0.934526	-0.55048	0.390902	-0.30904	-0.25626	0.729645	0.522118	0.986761	0.627307	-0.12236	-0.0758	-0.08528	0.903825	0.045111	-0.18572	0.788066	-0.12164	0.696539	0.900135	-0.34142	1			
Li	-0.07453	-0.17898	0.089917	-0.09751	0.076273	0.495777	-0.18387	-0.10293	-0.15728	-0.0768	0.177336	0.110758	0.430052	-0.10459	0.194465	0.15429	-0.06055	-0.055	-0.15625	-0.0453	-0.04628	-0.15067	1		
Mg	-0.22823	-0.15598	-0.5134	-0.32473	0.154391	-0.07129	-0.16323	0.658611	-0.0957	0.275462	0.988066	0.978781	0.650969	0.179025	0.902322	-0.64957	0.333835	0.561423	-0.14934	0.063946	-0.47424	-0.07395	0.161323	1	
Mn	0.162213	0.127878	0.358376	0.241707	-0.11787	0.191465	0.188739	-0.2831	0.116687	0.062491	-0.51498	-0.5428	-0.29997	-0.01322	-0.29334	0.484662	0.016544	-0.43507	0.096173	0.168332	0.080126	0.102934	0.06888	-0.496	1
Mo	0.305388	0.948219	-0.54271	0.439634	-0.32733	-0.26545	0.757449	0.483921	0.990797	0.547392	-0.15924	-0.11289	-0.10525	0.897156	0.01064	-0.16674	0.764076	-0.1652	0.704339	0.89752	-0.29734	0.990276	-0.15701	-0.1149	0.112729
Nb	-0.08803	-0.2134	0.548328	-0.24023	0.257957	0.019609	-0.21128	-0.56319	-0.20589	-0.23353	-0.35091	-0.39024	-0.18379	-0.32977	-0.35423	0.626784	-0.48956	0.129549	-0.18079	-0.27129	0.003725	-0.19897	0.226166	-0.34196	0.047759
Ni	0.057474	-0.21562	0.590729	0.030244	0.419439	0.015358	-0.24091	-0.64754	-0.23659	-0.26747	-0.54323	-0.5231	-0.42798	-0.3977	-0.55456	0.799543	-0.5742	0.212951	-0.12542	-0.29158	0.277716	-0.24804	0.109696	-0.49873	0.257709
P	-0.23463	-0.16821	-0.51449	-0.30816	0.144226	-0.071	-0.19566	0.646351	-0.10533	0.254182	0.987242	0.987234	0.662504	0.161723	0.872525	-0.67328	0.329738	0.551374	-0.15716	0.032736	-0.42872	-0.08363	0.143274	0.993169	-0.5374
Pb	-0.22222	-0.13633	-0.4825	-0.29228	0.24968	-0.10604	-0.18424	0.645951	-0.06789	0.304287	0.956541	0.969946	0.550922	0.189729	0.871697	-0.65232	0.332857	0.622869	-0.13258	0.060133	-0.46188	-0.03981	0.097723	0.964439	-0.49599
Pb	0.283667	0.947806	-0.54285	0.399917	-0.31386	-0.25999	0.762552	0.495132	0.994889	0.53168	-0.14507	-0.09519	-0.0913	0.898871	0.017965	-0.17674	0.77228	-0.14751	0.69843	0.903752	-0.30707	0.989609	-0.15787	-0.09851	0.09464
Rh	-0.12082	-0.22712	0.472507	0.012747	-0.25695	0.374079	-0.01545	-0.5351	-0.2379	-0.51907	-0.45067	-0.49683	-0.25285	-0.39141	-0.38679	0.421956	-0.41665	-0.31931	-0.25225	-0.24999	0.708045	-0.27907	0.197343	-0.50354	0.267288
Re	0.088021	0.549699	-0.39902	0.009129	-0.54602	-0.02644	0.818016	0.407751	0.4946	0.234445	-0.21774	-0.19186	-0.13767	0.463397	-0.01005	-0.1604	0.478553	-0.39199	0.340243	0.577266	-0.21054	0.458341	-0.23469	-0.20552	0.219655
S	0.391597	0.735812	-0.26214	0.373568	-0.42288	-0.07172	0.698596	0.16703	0.682704	0.322673	-0.37315	-0.39407	-0.28921	0.598911	-0.11148	0.094595	0.428865	-0.39084	0.593277	0.670762	-0.14408	0.675171	-0.0738	-0.36296	0.344685
Sb	0.333418	0.949787	-0.55011	0.438083	-0.31365	-0.26784	0.729263	0.486037	0.990147	0.543663	-0.14183	-0.09703	-0.09155	0.909127	0.018656	-0.17809	0.756363	-0.14787	0.729147	0.890294	-0.29699	0.990694	-0.1493	-0.098	0.083805
Sc	-0.18024	-0.12699	-0.41536	-0.30282	0.401675	-0.17919	-0.16913	0.571442	-0.07358	0.320212	0.831648	0.870929	0.38201	0.157287	0.761808	-0.48324	0.227419	0.762034	-0.1114	0.051215	-0.46787	-0.04587	0.044485	0.86724	-0.45301
Se	0.260237	0.747035	-0.3994	0.291152	-0.07374	-0.24974	0.492133	0.337594	0.804671	0.315902	-0.06242	-0.02149	-0.08777	0.739525	0.025918	-0.09827	0.500176	0.036732	0.596918	0.708625	-0.1241	0.786006	-0.00967	-0.01899	-0.01547
Sn	-0.07968	-0.04565	-0.03075	-0.05498	-0.54759	0.16926	0.027611	0.109495	-0.03889	-0.04031	0.168889	0.087743	0.424918	0.011567	0.148833	-0.24343	0.220537	-0.47084	-0.07317	0.010266	0.001107	-0.04195	0.162304	0.108483	0.110554
Sr	0.386931	0.746041	-0.54266	0.303495	0.193576	-0.40083	0.44314	0.517559	0.75418	0.602531	0.128518	0.188293	-0.01456	0.797763	0.230914	-0.2077	0.594644	0.272239	0.657181	0.722983	-0.40629	0.774425	-0.12059	0.190149	-0.08269
Ta	0.015141	-0.21076	0.24296	-0.0407	0.693201	-0.06232	-0.3099	-0.34334	-0.20441	-0.13761	-0.10008	-0.07302	-0.17444	-0.2405	-0.13458	0.450977	-0.43805	0.469828	-0.10488	-0.21547	0.077676	-0.20971	0.135244	-0.06429	-0.08891
Te	0.097321	0.213357	-0.05331	-0.02614	-0.5925	0.302909	0.506006	0.136349	0.139146	0.035961	-0.05734	-0.14452	0.03103	0.207319	0.206419	-0.03176	0.282245	-0.40974	0.136202	0.285338	-0.02912	0.128776	0.028579	-0.09806	0.316597
Th	0.061258	0.046005	0.148943	0.051276	0.425257	-0.13142	-0.11332	-0.22413	0.080697	0.044726	-0.24121	-0.18619	-0.23712	-0.01699	-0.26374	0.491049	-0.23699	0.438871	0.082696	-0.00071	0.017029	0.08161	-0.01038	-0.18106	-0.05688
Ti	-0.1397	-0.10945	0.071779	-0.10244	-0.42796	0.204986	0.062231	0.15326	-0.11074	0.011249	0.211866	0.188834	0.133206	-0.03098	0.263276	0.24535	0.219941	-0.21707	-0.1501	-0.02659	-0.04508	-0.10777	0.022541	0.171882	0.217506
Tl	-0.00945	0.020047	0.210379	0.014892	-0.55158	0.167195	0.173187	-0.07017	-0.00475	-0.05228	-0.22004	-0.25012	-0.06837	-0.05028	-0.13761	0.034285	0.119203	-0.43331	-0.03887	0.003062	0.119319	-0.00334	-0.01316	-0.25137	0.349013
V	-0.06173	-0.00448	-0.02942	0.051227	-0.54292	0.261544	0.107331	0.092542	0.004035	-0.02333	0.12068	0.03382	0.33323	0.042491	0.157396	-0.17764	0.245768	-0.51111	-0.04449	0.070757	0.032239	-0.00314	0.133992	0.061098	0.148935
W	-0.10765	-0.006																							

CC-2273: Pearson’s Correlation Coefficients Con’t

CC-2273	Mo	Na	Nb	Ni	P	Pb	Rb	Re	S	Sb	Sc	Se	Sn	Sr	Ta	Te	Th	Ti	Tl	U	V	W	Y	Zn	Zr
Au																									
Ag																									
Al																									
As																									
Ba																									
Be																									
Bi																									
Ca																									
Cd																									
Ce																									
Co																									
Cr																									
Cs																									
Cu																									
Fe																									
Ga																									
Ge																									
Hf																									
Hg																									
In																									
K																									
La																									
Li																									
Mg																									
Mn																									
Mo	1																								
Na	-0.19582	1																							
Nb	-0.23821	0.653569	1																						
Ni	-0.12326	-0.35973	-0.51481	1																					
P	-0.08063	-0.29517	-0.45031	0.962655	1																				
Pb	0.996402	-0.1843	-0.23614	-0.1062	-0.06422	1																			
Rb	-0.23995	0.276652	0.318799	-0.5041	-0.52946	-0.24894	1																		
Re	0.483178	-0.33213	-0.30451	-0.2331	-0.24121	0.478513	0.087953	1																	
S	0.709549	-0.03734	-0.0695	-0.39888	-0.35732	0.686556	0.063701	0.538206	1																
Sb	0.997217	-0.18782	-0.23814	-0.10487	-0.06265	0.994829	-0.25399	0.445561	0.693491	1															
Sc	-0.08721	-0.17488	-0.1593	0.853231	0.926531	-0.0709	-0.51769	-0.23464	-0.32226	-0.07206	1														
Se	0.798122	0.043585	0.003196	-0.02476	0.041226	0.808136	-0.05545	0.197972	0.457091	0.812804	0.088044	1													
Sn	-0.04624	-0.29035	-0.64859	0.121496	-0.02706	-0.04702	0.088467	0.126794	-0.03979	-0.05118	-0.34855	-0.2527	1												
Sr	0.761955	-0.16973	-0.05602	0.170083	0.266759	0.762607	-0.507	0.141626	0.440792	0.776523	0.370517	0.737362	-0.41877	1											
Ta	-0.20498	0.520014	0.780247	-0.07912	0.005593	-0.19847	-0.01237	-0.4572	-0.1468	-0.19214	0.27256	0.102665	-0.80439	0.226198	1										
Te	0.137696	-0.25539	-0.40317	-0.13995	-0.18889	0.121893	0.333796	0.563863	0.375145	0.115196	-0.3298	-0.11056	0.53393	-0.22715	-0.65343	1									
Th	0.071616	0.445681	0.723168	-0.18882	-0.14107	0.081218	-0.02914	-0.25358	-0.01538	0.084856	0.11373	0.285896	-0.70933	0.345403	0.829232	-0.60517	1								
Ti	-0.11805	-0.32429	-0.54658	0.173127	0.169356	-0.12065	0.131749	0.21081	-0.0828	-0.13189	-0.0593	-0.28219	0.641958	-0.38422	-0.74919	0.616993	-0.76046	1							
Tl	-0.00236	-0.17907	-0.26908	-0.25623	-0.30661	-0.01378	0.33307	0.347727	0.156315	-0.02329	-0.42693	-0.21827	0.601424	-0.40577	-0.70965	0.704562	-0.65559	0.691971	1						
U	-0.00396	-0.34371	-0.64071	0.068852	-0.07462	-0.00927	0.117583	0.179034	0.012257	-0.01197	-0.40448	-0.24058	0.938066	-0.39266	-0.76707	0.621386	-0.65178	0.634267	0.531454	1					
V	0.047639	-0.14271	-0.04616	0.727264	0.837045	0.060485	-0.52588	-0.24213	-0.20974	0.063017	0.953271	0.220851	-0.51591	0.529546	0.414904	-0.40935	0.262481	-0.22669	-0.54731	-0.53924	1				
W	-0.10975	-0.14969	0.177795	-0.27661	-0.27969	-0.12395	0.281384	-0.0175	0.005002	-0.11907	-0.21844	-0.03501	-0.16319	-0.11175	0.125868	-0.10596	0.125387	-0.22329	-0.06875	-0.10099	-0.11779	1			
X	0.082218	-0.16554	-0.26507	-0.13818	-0.16008	0.077023	0.201286	0.485234	0.265617	0.05047	-0.25171	-0.10788	0.441904	-0.24178	-0.55867	0.568999	-0.52769	0.631521	0.609768	0.407383	-0.33763	-0.10489	1		
Y	0.974858	-0.19306	-0.16796	-0.12118	-0.08138	0.979001	-0.22845	0.429053	0.694269	0.976477	-0.07174	0.820841	-0.08785	0.771993	-0.1314	0.077229	0.140461	-0.16993	-0.05342	-0.03439	0.070777	-0.07607	0.025918	1	
Zr	-0.23506	-0.0201	-0.13431	0.609631	0.58128	-0.21783	-0.18502	-0.35494	-0.48128	-0.22563	0.586918	-0.15611	-0.0412	-0.03849	0.05893	-0.27986	0.141395	0.591144	-0.554	-0.136	0.524184	-0.21189	-0.08819	-0.22796	1

GHC-747-D: Pearson's Correlation Coefficients

GHC-747-D	Au	Ag	Al	As	Ba	Be	Bi	Ca	Cd	Ce	Co	Cr	Cs	Cu	Fe	Ga	Ge	Hf	Hg	In	K	La	Li	Mg	Mn
Au	1																								
Ag	0.21893674	1																							
Al	0.183042737	-0.092821	1																						
As	0.746935622	0.18049	0.31012	1																					
Ba	-0.02305853	0.055466	0.214514	0.048499	1																				
Be	-0.136083294	0.09713	0.574015	-0.028071	0.114623	1																			
Bi	-0.156507709	0.442615	-0.286674	-0.097073	0.038935		1																		
Ca	-0.001210265	0.081032	-0.873822	-0.196831	-0.110235	-0.602923	0.337041	1																	
Cd	-0.081459168	0.002927	0.118696	-0.098064	-0.009191	0.147611	0.076212	-0.144819	1																
Ce	-0.351126388	-0.245116	-0.328377	-0.393593	0.082318	-0.052085	0.317608	0.254338	0.092415	1															
Co	0.388498964	0.075099	0.663548	0.425702	0.115577	0.387706	-0.253395	-0.491042	0.0811188	-0.459431	1														
Cr	0.19658597	-0.04524	0.406506	0.278251	0.032542	0.193654	-0.231678	-0.444682	0.0176486	-0.282243	0.47326	1													
Cs	-0.085649558	0.150159	0.647593	-0.055629	0.147926	0.607189	-0.211977	-0.625465	0.1235287	-0.026878	0.537256	0.134273	1												
Cu	0.462943203	0.308288	0.388168	0.390475	0.189002	0.085228	-0.143183	-0.228311	0.0579598	-0.46576	0.487732	0.251554	-0.005889	1											
Fe	0.423794757	0.140157	0.745702	0.485733	0.131053	0.407044	-0.269579	-0.570048	0.0301587	-0.498061	0.848936	0.522854	0.322341	0.633149	1										
Ga	0.051193699	-0.052292	0.905967	0.185066	0.171705	0.703916	-0.25995	-0.850247	0.13797	-0.175192	0.491375	0.296249	0.644507	0.279202	0.601075	1									
Ge	-0.279115382	0.154569	-0.434914	-0.251598	-0.088621	0.1739	0.625668	0.321236	0.0513885	0.440459	-0.410996	-0.277263	-0.193954	-0.28047	-0.404254	-0.085459	1								
Hf	-0.104842597	-0.129847	0.342765	-0.013507	0.101767	0.227208	-0.074009	-0.377642	0.0600754	0.081068	-0.051801	-0.015654	0.294239	0.047584	0.063832	0.488013	0.057825	1							
Hg	0.320624342	0.634592	-0.276431	0.364149	-0.130742	-0.21904	0.197357	0.33043	0.0384041	-0.228914	0.156628	-0.07827	-0.369858	0.258903	0.14478	-0.356696	0.186558	-0.210629	1						
In	0.093638235	0.024925	0.498474	0.101285	0.181214	0.473918	-0.050665	-0.44642	0.387921	-0.072752	0.49566	0.208347	0.399097	0.450261	0.477694	0.450115	-0.085027	0.145995	0.003926	1					
K	0.240351898	-0.063922	0.936346	0.33277	0.305985	0.482014	-0.470734	-0.773813	0.1047181	-0.303656	0.583295	0.360229	0.510236	0.442534	0.720229	0.841582	-0.408105	0.368536	-0.268715	0.469554	1				
La	-0.356899214	-0.199216	-0.388952	-0.406393	0.114895	-0.078707	0.352614	0.299736	0.0952586	0.963169	-0.535198	-0.326022	-0.100311	-0.452527	-0.561409	-0.224035	0.479155	0.073924	-0.087428	-0.110375	-0.344914	1			
Li	-0.12009843	-0.041663	0.743952	-0.011082	0.061945	0.75088	-0.123469	-0.766445	0.1798623	-0.077943	0.54688	0.253048	0.732545	0.051534	0.525252	0.779555	-0.133436	0.319225	-0.287095	0.457914	0.604841	-0.157459	1		
Mg	0.47357561	0.169185	0.203094	0.368649	0.012085	-0.043842	-0.102123	0.015244	-0.08735	-0.533575	0.65087	0.350757	-0.019189	0.57465	0.696436	0.033351	-0.350006	-0.194576	0.304957	0.149054	0.205812	-0.558854	0.026761	1	
Mn	0.292435808	0.245855	-0.263967	0.143969	-0.129233	-0.149678	0.310421	0.344095	-0.117786	-0.239547	0.158688	0.205871	-0.36744	0.266625	0.274856	-0.300752	0.021452	-0.290478	0.332699	-0.127321	-0.251929	-0.235157	-0.234591	0.71102	1
Mo	0.147499275	0.120005	0.232652	0.171326	0.217644	0.145945	0.108344	-0.138319	-0.00092	0.241397	0.173672	0.055214	0.267418	0.340322	0.221699	0.145836	0.214144	0.073744	0.288566	0.300317	0.063235	0.147522	0.183566	-0.01672	1
Na	-0.101048404	-0.227088	0.731195	0.015006	0.108598	0.493639	-0.299936	0.736082	0.148217	0.079962	0.335892	0.196149	0.556887	-0.032903	0.339328	0.72327	-0.207233	0.274831	-0.418628	0.388661	0.652031	0.022311	0.71524	-0.241366	-0.507227
Nb	0.131593601	-0.114148	0.893369	0.221308	0.322078	0.592068	-0.381798	-0.800807	0.134271	-0.201691	0.568015	0.329935	0.583873	0.32405	0.659131	0.835393	-0.358528	0.413463	-0.219286	0.481539	0.879469	-0.230505	0.672879	0.12287	-0.295051
Ni	0.122845274	-0.090096	0.528064	0.152448	0.025138	0.276748	-0.248417	-0.491876	0.0722473	-0.214302	0.639635	0.460727	0.563153	0.217936	0.500028	0.454457	-0.254868	0.075663	-0.087367	0.307582	0.465801	-0.251932	0.495973	0.328429	-0.027402
P	0.24971657	0.052448	0.636396	0.324356	0.130652	0.511203	-0.138078	-0.504857	0.0551513	-0.395505	0.73586	0.433728	0.382637	0.403879	0.749083	0.602027	-0.154969	0.075512	0.001137	0.422963	0.579468	-0.446455	0.519521	0.514755	0.165158
Pb	-0.229634233	0.371788	-0.413634	-0.319377	0.049428	0.123601	0.858501	0.283886	0.1102401	0.400122	-0.321176	-0.25559	-0.186594	-0.1519	-0.249886	-0.205653	0.611897	-0.057233	0.116931	0.043202	-0.389468	0.456261	-0.114497	-0.229632	0.176982
Rb	0.047815783	-0.123241	0.894718	0.126063	0.220401	0.590771	-0.354766	-0.804411	0.1665392	-0.095176	0.513304	0.263051	0.690688	0.237868	0.555849	0.868915	-0.250767	0.438174	-0.217463	0.477046	0.906115	-0.154835	0.753479	0.001806	-0.390527
Re	0.230178586	0.066326	0.278669	0.1364	0.021239	0.04707	-0.004207	-0.12616	-0.004657	-0.180846	0.485841	0.212287	0.096265	0.353731	0.448455	0.146979	-0.165453	-0.114213	0.01652	0.27609	0.293522	-0.22845	0.143028	0.383149	0.068191
S	0.026859109	-0.15499	-0.378664	0.044335	-0.139668	-0.553574	-0.321593	0.392514	-0.0837	-0.0874	-0.082845	-0.203564	-0.279512	-0.131887	-0.254515	-0.595843	-0.382103	-0.290321	0.122818	-0.216563	-0.347478	-0.07742	-0.407046	0.017443	-0.06975
Sb	-0.287377155	0.24075	0.043988	0.336119	0.028367	0.03755	-0.141839	-0.100762	-0.060558	-0.192166	0.085698	0.442311	-0.083063	0.122934	0.141887	0.040612	-0.062438	-0.072092	0.151572	-0.050963	0.051903	-0.190998	-0.013614	0.074962	0.092073
Se	-0.019905905	0.009955	0.137347	0.08998	-0.047587	0.19034	0.030157	-0.179265	0.1421111	0.067916	-0.010101	0.000705	0.071221	0.098661	0.031758	0.251113	0.283798	0.28053	0.066609	0.217321	0.16998	0.059219	0.137578	-0.109103	-0.161168
Sn	0.132073342	-0.006796	0.532439	0.15569	0.100081	0.264426	-0.261767	-0.471888	0.0287702	-0.190761	0.457239	0.282059	0.403946	0.313006	0.452978	0.454923	-0.270711	0.14825	0.020657	0.304553	0.53337	-0.213283	0.420677	0.181646	-0.115964
Sr	-0.187730816	-0.090264	-0.203488	-0.271554	0.125719	-0.061487	0.224622	0.149786	0.0705163	0.694279	-0.372595	-0.221423	0.01402	-0.372506	-0.427003	-0.101515	0.287723	0.063334	-0.289217	-0.088203	-0.142574	0.64749	-0.026854	-0.546217	-0.33143
Ta	0.171104579	-0.084559	0.819277	0.244973	0.299606	0.541394	-0.408108	-0.711895	0.1221554	-0.280996	0.623647	0.349342	0.519674	0.29693	0.667828	0.696692	-0.43783	0.219688	0.082484	0.469994	0.80416	-0.300255	0.589882	0.214139	-0.208189
Te	0.434464362	0.631984	0.161895	0.484614	0.188273	-0.081708	-0.239257	-0.001001	-0.082878	-0.499688	0.282732	0.110831	-0.098047	0.441071	0.343218	-0.008521	-0.333862	-0.096912	0.705985	0.033212	0.229844	-0.47832	-0.061002	0.381333	0.133018
Th	-0.00152124	-0.088889	0.586247	0.07031	0.259003	0.379911	-0.221899	-0.564698	0.1106243	-0.017223	0.159394	0.106181	0.408072	0.20543	0.296834	0.644386	-0.119117	0.854051	-0.056912	0.296276	0.625527	-0.001911	0.433025	-0.080001	-0.337918
Ti	0.303060966	-0.076503	0.862063	0.40341	0.216	0.491991	-0.458593	-0.710243	0.0753572	-0.424411	0.81262	0.469255	0.505621	0.446872	0.863659	0.71294	-0.484188	0.130882	-0.042071	0.47524	0.816838	-0.48448	0.622759	0.474684	-0.033656
Tl	0.039102534	-0.104126	0.829968	0.250021	0.18563	0.61494	-0.253679	-0.811495	0.1553216	-0.079335	0.472393	0.268809	0.596837	0.084661	0.500929	0.81454	-0.22384	0.271315	-0.319823	0.425586	0.751038	-0.122889	0.762369	-0.124335	-0.413324
U	-0.104824681	0.117832	0.132499	-0.069179	0.112163	0.364113	0.423469	-0.189873	0.3873209	-0.399476	-0.006284	-0.071123	0.174759	-0.103624	-0.011732	0.317927	0.484893	0.184114	-0.099679	0.228387	0.14402	0.314806	0.292091	-0.227385	-0.114437
V	0.528542562	0.056318	0.742616	0.528186	0.177851	0.315737	-0.423294	-0.520909	0.0225899	-0.531497	0.840924	0.445303	0.431874	0.5											

GHC-747-D: Pearson's Correlation Coefficients Con't

GHC-747-D	Mo	Na	Nb	Ni	P	Pb	Rb	Re	S	Sb	Se	Sn	Sr	Ta	Te	Th	Ti	Tl	U	V	W	Y	Zn	Zr
Au																								
Ag																								
Al																								
As																								
Ba																								
Be																								
Bi																								
Ca																								
Cd																								
Ce																								
Co																								
Cr																								
Cs																								
Cu																								
Fe																								
Ga																								
Ge																								
Hf																								
Hg																								
In																								
K																								
La																								
Li																								
Mg																								
Mn																								
Mo	1																							
Na	0.092939	1																						
Nb	0.282889	0.688958	1																					
Ni	0.155564	0.361015	0.433385	1																				
P	0.212272	0.33952	0.625087	0.468489	1																			
Pb	0.099942	-0.221267	-0.25213	-0.271512	-0.146888	1																		
Rb	0.253428	0.759245	0.814807	0.504109	0.486705	-0.281271	1																	
Re	0.521442	0.136006	0.195197	0.222051	0.270599	-0.144956	0.227694	1																
S	-0.205404	-0.310998	-0.359349	-0.124566	-0.318175	-0.327562	-0.396111	-0.02263	1															
Sb	-0.047987	-0.058261	0.007412	0.037437	0.052959	-0.134332	-0.038861	-0.044408	-0.124318	1														
Se	0.279074	0.049312	0.055281	0.033163	-0.013636	0.011187	0.238205	0.008576	-0.195839	0.022584	1													
Sn	0.112045	0.400503	0.472058	0.825303	0.398292	-0.251371	0.533414	0.174475	-0.148288	0.030809	0.024262	1												
Sr	0.097236	0.117612	-0.06269	-0.202789	-0.377407	0.263243	-0.037146	-0.020328	-0.045903	-0.067781	0.02737	-0.152548	1											
Ta	0.203031	0.611301	0.949726	0.434342	0.645855	-0.272794	0.692104	0.199576	-0.238626	0.035619	-0.073225	0.474503	-0.114439	1										
Te	0.195572	-0.125533	0.077887	0.020098	0.137718	-0.250572	0.034192	0.156292	0.143112	0.308341	0.013667	0.112336	-0.231477	0.150197	1									
Th	0.298912	0.471142	0.697011	0.238021	0.278018	-0.145268	0.640083	0.025212	-0.342786	-0.046454	0.179583	0.33608	-0.010611	0.559173	0.022623	1								
Ti	0.213482	0.53985	0.866032	0.532422	0.780022	-0.392741	0.685924	0.303314	-0.209998	0.079804	-0.015989	0.486479	-0.299108	0.895216	0.208418	0.41666	1							
Tl	0.113444	0.789208	0.78202	0.400851	0.482414	-0.160229	0.789165	0.152111	-0.372797	0.057472	0.140742	0.441066	0.016888	0.707091	-0.035565	0.470768	0.670142	1						
U	0.347579	0.219324	0.180933	0.024756	0.181998	0.424928	0.250863	0.138154	-0.509431	-0.096521	0.371823	-0.00784	0.323488	0.075278	-0.159362	0.182914	-0.008726	0.325711	1					
V	0.175019	0.320794	0.666373	0.539585	0.718471	-0.435515	0.545578	0.340189	-0.169376	0.173995	-0.02958	0.452831	-0.421432	0.703187	0.403785	0.313262	0.879634	0.468502	-0.104688	1				
W	0.03553	0.391853	0.36853	0.776524	0.247927	-0.149565	0.461219	0.096571	-0.165834	-0.021566	0.001392	0.94223	0.013277	0.36282	-0.027453	0.269584	0.331366	0.407596	0.072459	0.293756	1			
Y	0.045564	-0.229764	-0.244977	-0.214696	0.033361	0.623334	-0.213178	-0.113911	-0.481091	-0.059639	0.01052	-0.19829	0.13442	-0.285416	-0.266982	-0.103309	-0.315477	-0.208075	0.420666	-0.24464	-0.1284	1		
Zn	0.074739	0.301608	0.1549	0.157945	0.138289	0.278023	0.210892	0.098642	-0.190429	-0.079342	0.032246	0.100063	0.13047	0.178952	-0.134109	0.042877	0.123856	0.252438	0.262504	0.057793	0.14722	0.127456	1	
Zr	0.09132	0.502883	0.597604	0.182892	0.174717	-0.071756	0.621192	-0.128683	-0.380244	-0.089379	0.162842	0.231368	0.10793	0.406725	-0.151987	0.590649	0.28213	0.491778	0.236377	0.153317	0.236206	-0.071462	0.034307	1

GHC-747-D2: Pearson's Correlation Coefficients

GHC-747-D2	Au	Ag	Al	As	Ba	Be	Bi	Ca	Cd	Ce	Co	Cr	Cs	Cu	Fe	Ga	Ge	Hf	Hg	In	K	La	Li	Mg	Mn
Au		1																							
Ag	0.166493502	1																							
Al	0.480699319	0.165023	1																						
As	0.625279258	0.39968	0.50987	1																					
Ba	0.004984633	-0.141814	0.2844	0.073678	1																				
Be	-0.083220436	-0.085097	-0.129073	-0.093412	0.065575	1																			
Bi	-0.033129791	0.629282	-0.159178	-0.072367	0.005817	-0.055451	1																		
Ca	-0.508774362	-0.311153	-0.945303	-0.571561	-0.258932	-0.041914	-0.015421	1																	
Cd	0.327333671	0.532543	0.138135	0.228559	-0.090057	0.002057	0.513938	-0.24395	1																
Ce	-0.460891984	-0.22423	-0.693709	-0.451847	-0.081163	0.014776	0.131316	0.709157	-0.172916	1															
Co	0.42888729	0.387485	0.750027	0.630184	0.125271	0.185704	0.019029	-0.751197	0.3080973	-0.556916	1														
Cr	0.41088678	0.331648	0.671532	0.65116	0.055717	0.024549	-0.040818	-0.69026	0.3740703	-0.449116	0.669086	1													
Cs	0.089205063	-0.007071	0.615311	0.033386	0.108695	0.523111	-0.09741	-0.522587	0.085705	-0.307547	0.532698	0.359702	1												
Cu	0.39116363	0.475146	0.665974	0.652509	0.080232	0.026316	0.030119	-0.687086	0.243899	-0.611442	0.823963	0.568463	0.236794	1											
Fe	0.46992285	0.392582	0.747869	0.695063	0.160249	0.065402	0.027795	-0.768914	0.289605	-0.528868	0.954502	0.686314	0.418731	0.84526	1										
Ga	0.437769904	0.137184	0.932488	0.40459	0.185188	0.195098	-0.120244	-0.878802	0.1915025	-0.644883	0.618002	0.620909	0.673442	0.505703	0.595083	1									
Ge	-0.212852802	-0.047703	-0.225207	-0.255995	-0.20764	0.1239	0.095371	0.242886	0.1831685	0.194973	-0.132472	-0.074792	0.138634	-0.262315	-0.190176	-0.093541	1								
Hf	-0.084589378	-0.246342	0.097689	-0.324088	0.013	0.069317	0.073168	-0.041419	-0.064077	0.008933	-0.182365	-0.074749	0.453706	-0.332933	-0.239829	0.311221	0.24926	1							
Hg	-0.07152217	0.847681	0.137933	0.230435	-0.462394	-0.150821	0.432028	-0.321643	0.396492	-0.187459	0.333819	0.169973	-0.132658	0.385862	0.318029	0.110515	-0.141565	-0.301228	1						
In	0.457024297	0.405528	0.628557	0.500696	0.217562	0.03282	0.270124	-0.702762	0.4474022	-0.43511	0.789073	0.52146	0.341663	0.748824	0.800927	0.498619	-0.24826	-0.155637	0.357819	1					
K	0.44896077	0.172293	0.919873	0.505202	0.258436	-0.026323	-0.148892	-0.876107	0.1725516	-0.610579	0.642745	0.654426	0.489369	0.580895	0.660737	0.850526	-0.236722	0.066817	0.106421	0.541888	1				
La	-0.490693917	-0.266439	-0.715369	-0.479709	-0.050474	-0.022244	0.131109	0.72904	-0.200773	0.981696	-0.572134	-0.500026	-0.337942	-0.596431	-0.536719	-0.683052	0.194448	0.008161	-0.252142	-0.422309	-0.653448	1			
Li	0.463753316	0.110682	0.773937	0.411044	-0.029758	0.072537	-0.194231	-0.760301	-0.018824	-0.623623	0.682191	0.44261	0.513413	0.599748	0.668223	0.702766	-0.213491	0.031864	0.093554	0.514191	0.616554	-0.619648	1		
Mg	0.174510905	0.10887	0.409312	0.25104	0.314836	0.055438	0.104002	-0.42282	0.1453156	-0.149534	0.57741	0.342305	0.34014	0.445393	0.650184	0.267221	-0.074821	-0.146147	-0.018393	0.590067	0.361392	-0.147889	0.24795	1	
Mn	-0.43244614	-0.273589	-0.552985	-0.343656	0.021899	0.003627	0.080566	0.577573	-0.317167	0.648778	-0.369613	-0.339016	-0.230088	-0.355338	-0.294041	-0.53971	0.177183	-0.018655	-0.488698	-0.29063	-0.514554	0.66808	-0.543956	0.297414	1
Mo	0.039252941	0.255264	0.060736	0.180755	0.043196	-0.009076	0.168854	-0.098681	0.2278443	-0.127146	0.331177	0.218501	-0.043145	0.266248	0.299656	-0.069442	0.045903	-0.375334	0.31302	0.244495	0.068898	-0.110045	-0.068959	0.264682	0.038584
Na	0.428044952	0.13619	0.80919	0.352201	0.255382	-0.102125	0.030165	-0.794886	0.2122501	-0.574573	0.500142	0.54992	0.452846	0.470966	0.517122	0.792494	-0.245033	0.282039	0.066263	0.594499	0.816442	-0.590098	0.558019	0.319298	-0.439754
Nb	0.386820335	-0.015535	0.851994	0.399126	0.320474	0.282243	-0.122883	-0.790175	0.0203905	-0.592099	0.635294	0.468092	0.704005	0.462388	0.564491	0.853454	-0.176966	0.362336	-0.03758	0.520103	0.742114	-0.609367	0.689006	0.321844	-0.442939
Ni	0.241073455	0.138679	0.379467	0.259281	-0.122014	0.171745	-0.041243	-0.394006	0.3157851	-0.436328	0.517228	0.51956	0.471934	0.304822	0.449303	0.40457	0.186846	0.159031	-0.072132	0.348802	0.329711	-0.469888	0.36428	0.236357	-0.287357
P	0.467763984	0.251943	0.803636	0.643221	0.148298	0.05598	-0.138334	-0.7876	0.1098088	-0.532164	0.868764	0.639333	0.464246	0.780619	0.894864	0.645794	-0.264446	-0.162663	0.270351	0.687992	0.720162	-0.547981	0.77682	0.572163	-0.347463
Pb	-0.203682332	0.437849	-0.418644	-0.226547	-0.105911	-0.102889	0.684302	0.317905	0.2221682	0.386522	-0.172435	-0.27822	-0.242514	-0.164547	-0.146376	-0.416146	0.151913	-0.0827	0.358356	-0.05465	-0.4056	0.397053	-0.289122	0.027108	0.31767
Rb	0.34426307	0.168446	0.804997	0.330124	0.088724	0.054105	-0.103772	-0.750402	0.2605319	-0.478043	0.555598	0.582984	0.597411	0.391762	0.539083	0.806062	-0.076528	0.141628	0.150736	0.43928	0.894431	-0.551427	0.519874	0.357659	-0.441725
Re	0.086957916	0.200412	0.151726	0.271376	-0.01621	0.004611	0.058779	-0.180178	0.1757156	-0.161896	0.342385	0.194204	-0.028554	0.307815	0.297981	0.067655	-0.036742	-0.32786	0.151735	0.202035	0.116659	-0.132621	0.098936	0.076696	-0.165863
S	0.437471257	0.404334	0.581385	0.570654	0.147177	-0.073525	0.112709	-0.712759	0.241812	-0.634206	0.641575	0.529342	0.153088	0.606526	0.655708	0.468415	-0.304934	-0.234123	0.462657	0.579943	0.569845	-0.666961	0.553808	0.276451	-0.508781
Sb	0.255275516	0.381404	0.237932	0.500086	0.072332	0.002449	-0.058931	-0.245427	0.2111134	-0.104379	0.314532	0.461158	0.015109	0.375689	0.326555	0.196473	-0.099219	-0.283831	0.680374	0.201436	0.329154	-0.150011	0.008529	0.036433	-0.134042
Se	-0.103586222	0.159261	-0.181688	-0.033977	-0.033218	0.140797	0.191115	0.230268	0.184224	0.195618	0.087416	0.009141	0.027172	0.022282	0.053192	-0.14874	0.63812	-0.088436	-0.013709	-0.06782	-0.217905	0.198376	-0.208591	0.092854	0.314826
Sn	0.391083228	0.302081	0.837042	0.543863	0.125693	0.252684	-0.057903	-0.795666	0.1812156	-0.58915	0.888715	0.63989	0.629995	0.757752	0.873698	0.746619	-0.096825	-0.07302	0.17921	0.672288	0.708181	-0.595718	0.736922	0.531514	-0.35701
Sr	-0.392646902	-0.043607	-0.576818	-0.233659	0.034443	-0.099109	0.200503	0.536473	-0.220191	0.548309	-0.502361	-0.290271	-0.386432	-0.469765	-0.519829	-0.501245	0.05835	0.085762	0.125359	-0.464565	-0.453322	0.517507	-0.61087	-0.354914	0.36444
Ta	0.316234582	-0.091101	0.783257	0.272917	0.371276	0.266662	-0.154618	-0.712974	-0.119407	-0.518607	0.543178	0.344854	0.63665	0.392373	0.482185	0.765248	-0.221984	0.348385	-0.025798	0.451092	0.665897	-0.516792	0.66348	0.285438	-0.371116
Te	0.220369634	0.524402	0.431362	0.598344	-0.051397	-0.080499	-0.051672	-0.462717	0.0532772	-0.510197	0.550314	0.397017	0.091396	0.728388	0.594889	0.284617	-0.263761	-0.302383	0.495709	0.365577	0.403099	-0.489948	0.425486	0.181376	-0.349487
Th	-0.177568298	-0.429786	0.072809	-0.247104	0.300629	0.166891	-0.087109	0.024818	-0.354443	-0.152569	-0.116262	-0.188365	0.207501	-0.066245	-0.097016	0.120894	0.006642	0.416737	-0.633614	0.020173	-0.049461	0.225437	0.041536	0.044833	0.254753
Ti	0.475127769	0.0775	0.863856	0.502247	0.257563	0.193456	-0.188077	-0.805975	0.0493314	-0.584666	0.82147	0.544256	0.66242	0.615749	0.777625	0.757951	-0.237831	0.105952	0.033301	0.636828	0.758991	-0.593702	0.806059	0.472177	-0.451284
Tl	0.611699379	0.344869	0.900033	0.674396	0.166836	-0.049555	-0.106205	-0.919778	0.2107656	-0.709042	0.771136	0.690793	0.374843	0.714481	0.7988	0.804639	-0.291084	-0.109539	0.350494	0.678159	0.831663	-0.724665	0.808082	0.334417	-0.614786
U	0.222027055	0.136637	0.146796	0.365796	0.249113	0.103657	0.093246	-0.146133	0.2431798	0.071416	0.243754	0.264563	0.055185												




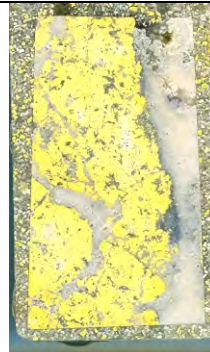











GHC-747-D2: Pearson's Correlation Coefficients Con't




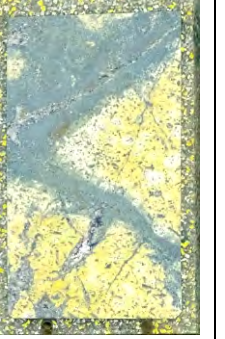


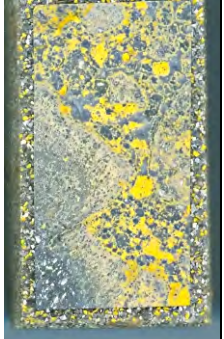




GHC-747-D2	Mo	Na	Nb	Ni	P	Pb	Rb	Re	S	Sb	Se	Sn	Sr	Ta	Te	Th	Ti	Tl	U	V	W	Y	Zn	Zr
Au																								
Ag																								
Al																								
As																								
Ba																								
Be																								
Bi																								
Ca																								
Cd																								
Ce																								
Co																								
Cr																								
Cs																								
Cu																								
Fe																								
Ga																								
Ge																								
Hf																								
Hg																								
In																								
K																								
La																								
Li																								
Mg																								
Mn																								
Mo	1																							
Na	0.03628	1																						
Nb	-0.003721	0.749815	1																					
Ni	0.016374	0.255679	0.361574	1																				
P	0.109774	0.54225	0.660492	0.387201	1																			
Pb	0.106148	-0.288432	-0.413051	-0.287192	-0.27225	1																		
Rb	0.02066	0.720193	0.618668	0.371478	0.571986	-0.311871	1																	
Re	0.71014	0.027319	0.075138	0.046695	0.193167	-0.095731	0.021327	1																
S	0.211426	0.456221	0.47789	0.374274	0.61593	-0.247833	0.419698	0.300352	1															
Sb	0.203584	0.110648	0.101106	0.06744	0.326689	-0.084083	0.205138	0.1954	0.214323	1														
Se	0.323196	-0.258234	-0.140872	-0.131593	-0.083521	0.323847	-0.184269	0.166651	-0.152173	0.236935	1													
Sn	0.241508	0.570224	0.719593	0.422089	0.842959	-0.23486	0.624704	0.29285	0.524871	0.346821	0.118369	1												
Sr	-0.065932	-0.419606	-0.378134	-0.275756	-0.483333	0.181868	-0.480749	-0.019116	-0.22705	0.047693	0.074991	-0.571173	1											
Ta	-0.040281	0.686905	0.963182	0.237464	0.59716	-0.404429	0.509211	0.058323	0.424571	0.068013	-0.14708	0.658744	-0.316088	1										
Te	0.265036	0.264923	0.242107	0.224424	0.516906	-0.153369	0.221649	0.318786	0.528438	0.287936	-0.041478	0.537635	-0.284217	0.225629	1									
Th	-0.132256	0.167789	0.303978	-0.271564	-0.048841	-0.038268	-0.159617	-0.180527	-0.313768	-0.214141	0.08905	0.020374	-0.01355	0.365965	-0.19161	1								
Ti	0.05086	0.655266	0.884467	0.421903	0.873078	-0.371653	0.610772	0.149901	0.565509	0.204503	-0.113082	0.834648	-0.486675	0.851531	0.407429	0.102546	1							
Tl	0.081502	0.685478	0.693746	0.373743	0.845312	-0.341931	0.670389	0.222981	0.699136	0.384911	-0.200811	0.795842	-0.54092	0.628007	0.534399	-0.118326	0.798317	1						
U	0.326789	0.08198	0.113482	-0.08364	0.229756	0.087232	0.113977	0.255916	0.098621	0.292997	0.142416	0.105703	0.069813	0.030199	0.002966	-0.012359	0.161719	0.16694	1					
V	0.243282	0.463946	0.508883	0.313435	0.731744	-0.157747	0.448154	0.116645	0.389236	0.289681	0.110442	0.67089	-0.515038	0.444778	0.332899	0.048535	0.705002	0.589199	0.327403	1				
W	0.120522	0.453594	0.680047	0.39586	0.756913	-0.330388	0.440475	0.183744	0.583906	0.372283	-0.046852	0.715876	-0.402798	0.643463	0.491283	-0.038155	0.837345	0.733969	0.255394	0.66879	1			
Y	-0.126383	-0.723934	-0.749633	-0.42913	-0.714998	0.447456	-0.664591	-0.276882	-0.736527	-0.266085	0.345589	-0.682568	0.35281	-0.68491	-0.44984	0.107996	-0.75794	-0.854564	-0.123347	-0.432477	-0.653424	1		
Zn	0.382286	0.365133	0.21031	0.170184	0.303728	0.276528	0.245193	0.230687	0.382158	0.288905	0.231474	0.39263	-0.136798	0.137496	0.135385	-0.054525	0.254234	0.320158	0.313481	0.446172	0.247264	-0.331335	1	
Zr	-0.321042	0.405023	0.549482	0.201962	0.049236	-0.216432	0.32215	-0.235993	-0.106618	-0.17928	-0.089286	0.119534	-0.018322	0.535546	-0.228215	0.382483	0.354637	0.069974	-0.225806	-0.004503	0.122903	-0.217535	-0.130218	1

Appendix B:
CC-2272, CC-2273, GHC-747-D, & GHC-747-D2: Stained Billets

CC-2272, CC-2273, GHC-747-D, & GHC-747-D2: Stained Billets

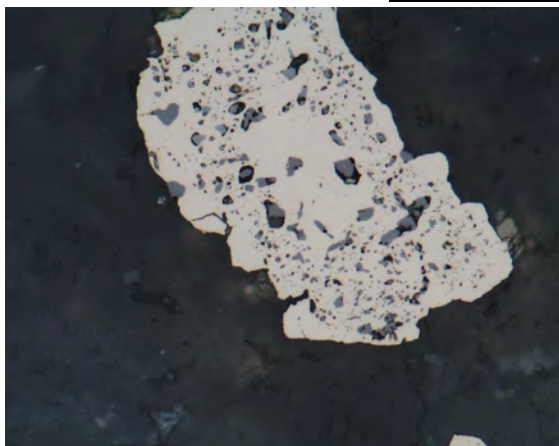
The stained billets presented below were cut from samples taken from drill core. These samples were collected from the drill holes listed above and the 26 thin sections used to define the paragenetic sequence were cut from these billets. The billets are labeled with the sample number, followed by the depth in feet, and the drill hole in parentheses.

				
1; 2641 (GHC-747-D2)	5; 2456 (GHC-747-D2)	6; 2436 (GHC-747-D2)	7; 2571 (GHC-747-D2)	8; 2880 (GHC-747-D2)
				
9; 2627 (GHC-747-D)	10; 2644 (GHC-747-D)	13; 4645 (CC-2272)	19; 4556 (CC-2272)	21; 4552 (CC-2272)
				
23; 4465 (CC-2272)	25; 4434 (CC-2272)	26; 4450 (CC-2272)	34; 2880 (CC-2272)	35; 2900 (CC-2272)

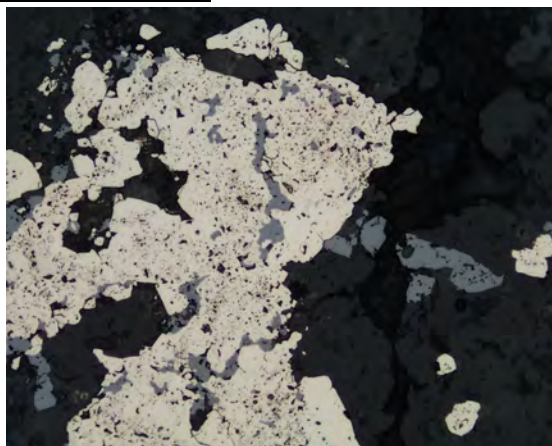
CC-2272, CC-2273, GHC-747-D, & GHC-747-D2 Stained Billets Continued				
				
38; 3008 (CC-2272)	44; 3362 (CC-2272)	51; 4742 (CC-2272)	53; 4813 (CC-2272)	53a; 4813 (CC-2272)
				
56; 3380 (CC-2273)	58; 3628 (CC-2273)	59; 3756 (CC-2273)	61; 3854 (CC-2273)	65; 4362 (CC-2273)
				
66; 2679 (GHC-747-D2)				

Appendix C:
CC-2272, CC-2273, GHC-747-D, & GHC-747-D2: Photomicrographs

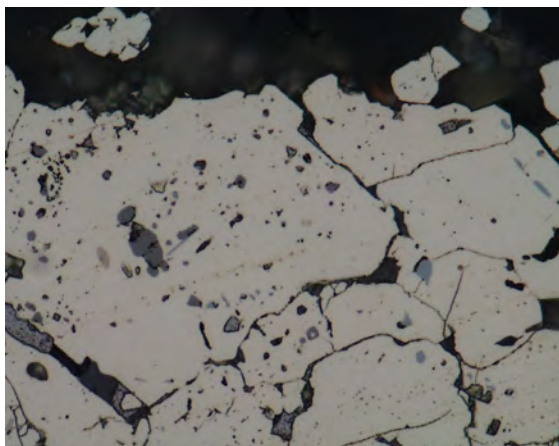
CC-2272 Photomicrographs



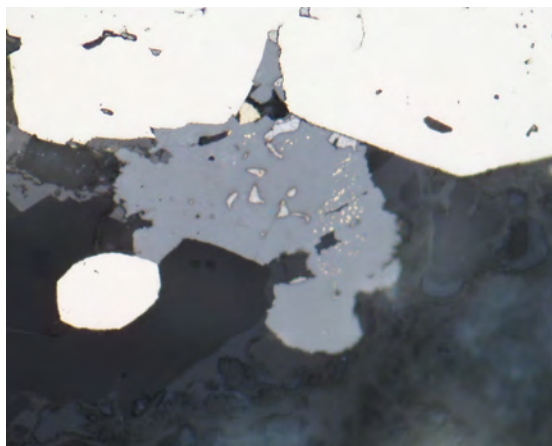
1) Sphalerite (low Fe, no chalcopyrite) replacing pockmarked pyrite. FOV= 0.43 mm; Sample 35; 2900 ft.



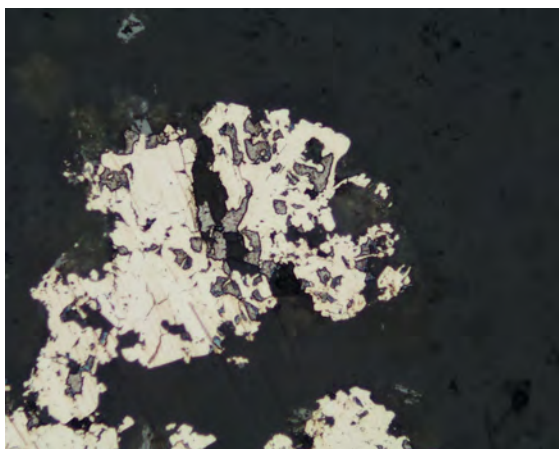
2) Sphalerite (low Fe, no chalcopyrite) replacing pockmarked pyrite. FOV= 0.43 mm; Sample 35; 2900 ft.



3) Pyrrhotite, chalcocite, and sphalerite (high Fe, no chalcopyrite) inclusions in pockmarked pyrite with interstitial galena. FOV= 0.16 mm; Sample 23, 4465 ft.



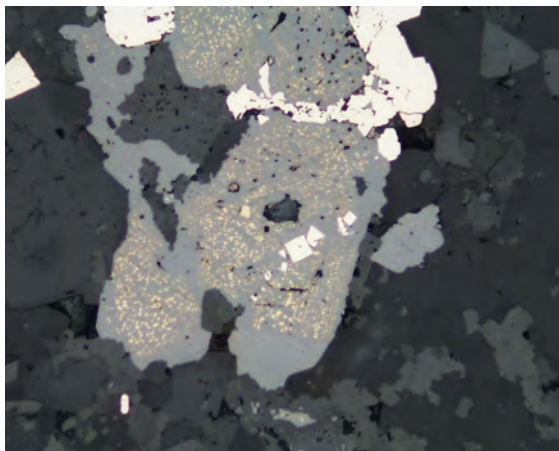
4) Sphalerite (low Fe, no chalcopyrite) intergrown with galena and rimming sphalerite (low Fe, chalcopyrite disease). FOV= 0.16 mm; Sample 23, 4465 ft.



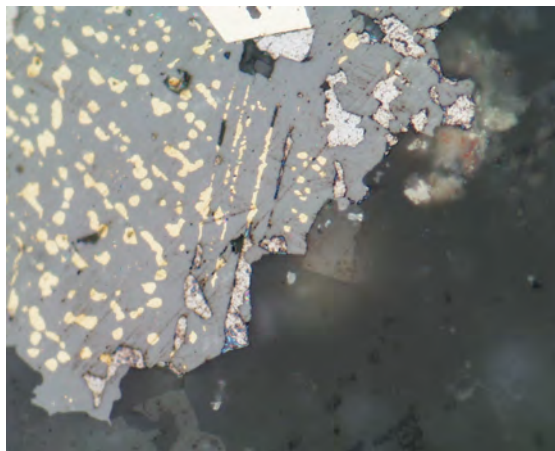
5) Galena intergrown with non pockmarked pyrite. FOV= 0.43 mm; Sample 25, 4434 ft.



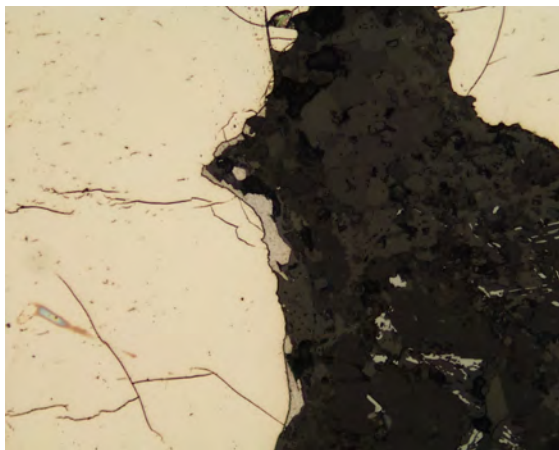
6) Galena intergrown with sphalerite (high Fe, chalcopyrite disease) and rimmed by sphalerite (high Fe, no chalcopyrite disease). FOV= 0.43 mm; Sample 44, 3362 ft.



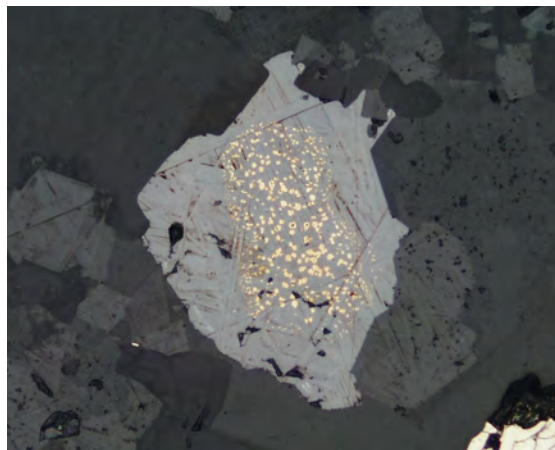
7) Sphalerite (high Fe, chalcopyrite disease) rimmed by sphalerite (high Fe, no chalcopyrite). FOV= 0.43 mm; Sample 25, 4434 ft.



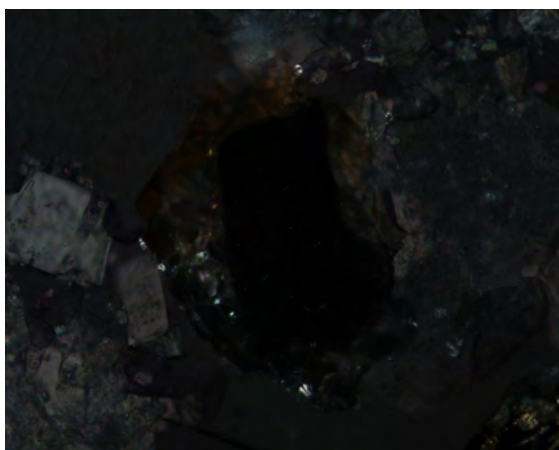
8) Galena replacing chalcopyrite along chalcopyrite veinlets in sphalerite (high Fe, chalcopyrite disease). FOV= 0.16 mm; Sample 25, 4434 ft.



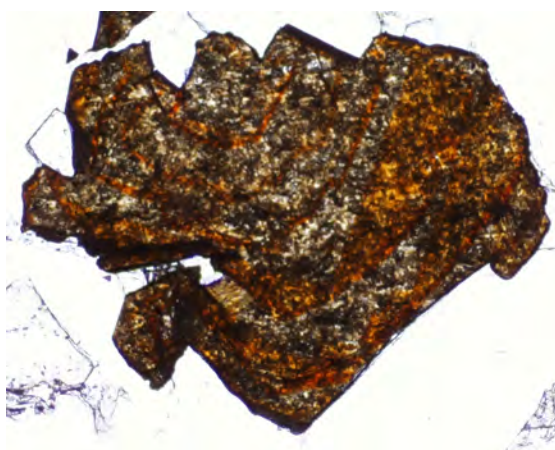
9) Galena rimming pyrite. FOV= 0.43 mm; Sample 13, 4645 ft.



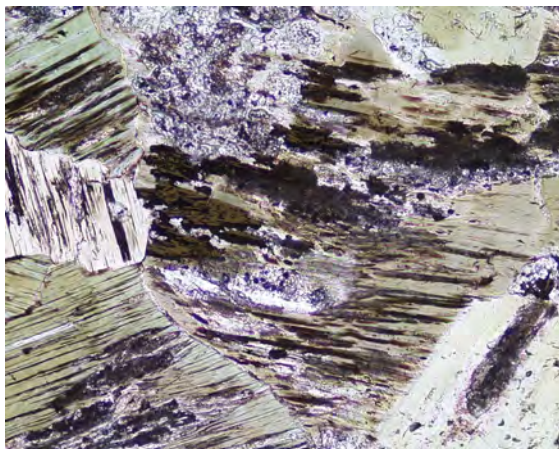
10) Sphalerite (high Fe, chalcopyrite disease) rimmed by sphalerite (low Fe, no chalcopyrite) and sphalerite (mod Fe, no chalcopyrite). FOV= 0.43 mm; Sample 25, 4434 ft.



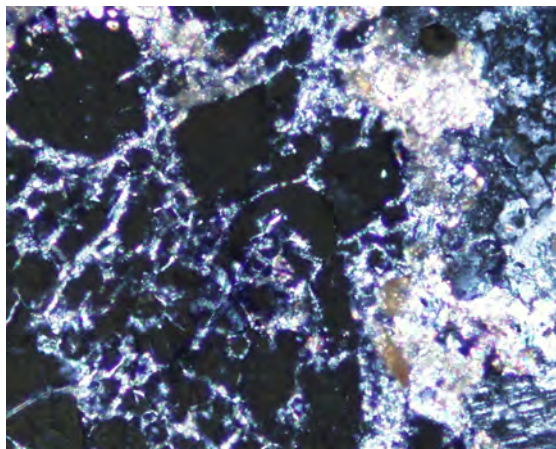
11) Crossed nichols view of previous grain showing high to low to moderate Fe zoning outward. FOV= 0.43 mm; Sample 25, 4434 ft.



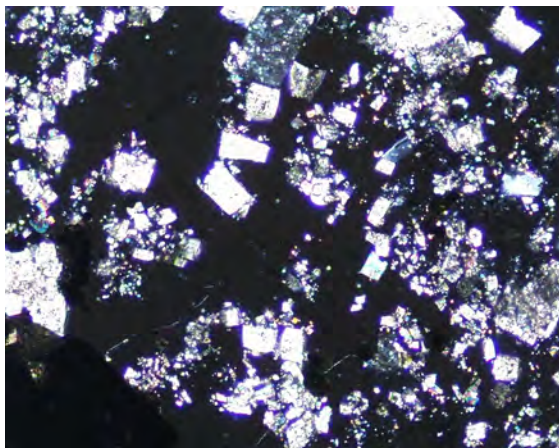
12) 12 generations of mod/low Fe sp (no cp). FOV= 1.7 mm; Sample 19, 4556 ft.



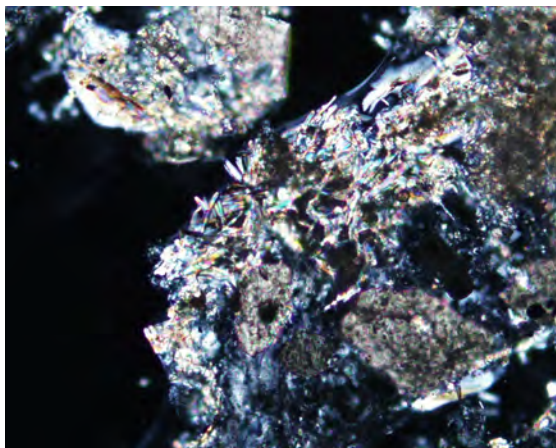
13) Biotite locally replaced by chlorite and hematite \pm magnetite. FOV= 0.85; Sample 53A, 4813 ft.



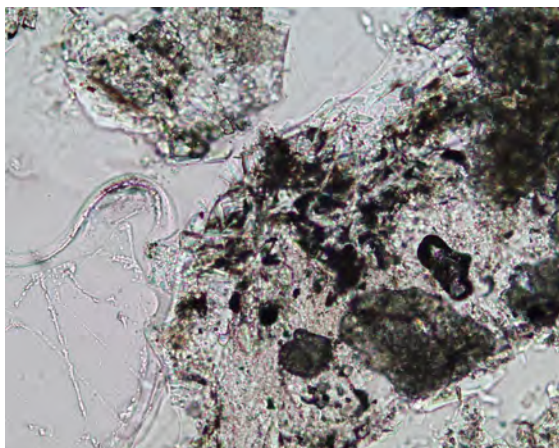
14) Carbonate interstitial to fluorite. FOV= 0.43 mm; Sample 26, 4450 ft.



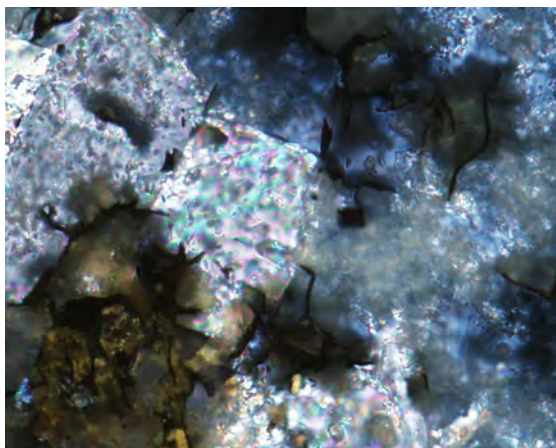
15) Euhedral carbonate entrained in fluorite. FOV= 0.85 mm; Sample 25, 4434 ft.



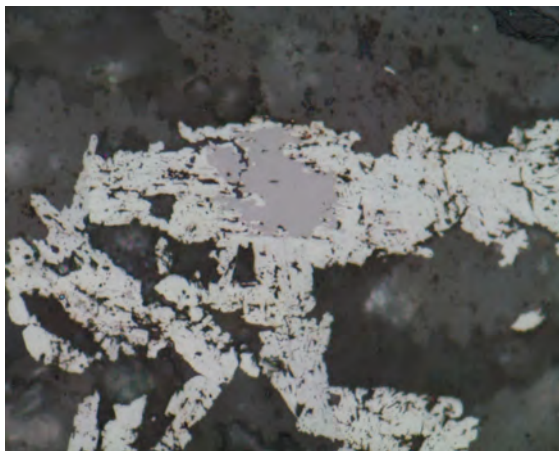
16) Carbonate entrained in quartz-clay-sericite matrix. FOV= 0.43 mm; Sample 38, 3008 ft.



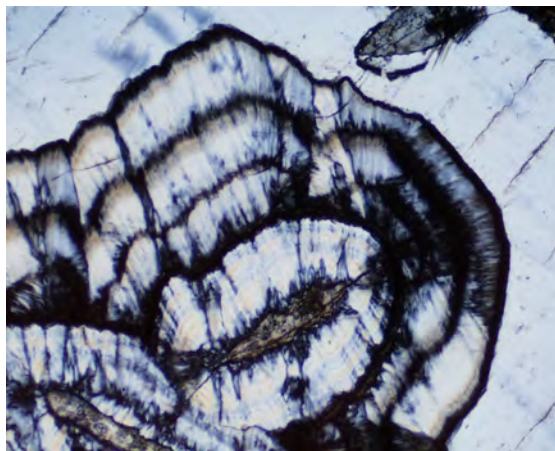
17) Same view as previous in plane light. FOV= 0.43 mm; Sample 38, 3008 ft.



18) Molybdenite and intergrown sulfate/Fe carbonate mineral replacing carbonate. FOV= 0.16 mm; Sample 26, 4450 ft.



19) Intergrown hematite and magnetite, possibly magnetite replacing hematite. FOV= 0.16 mm; Sample 53, 4813 ft.

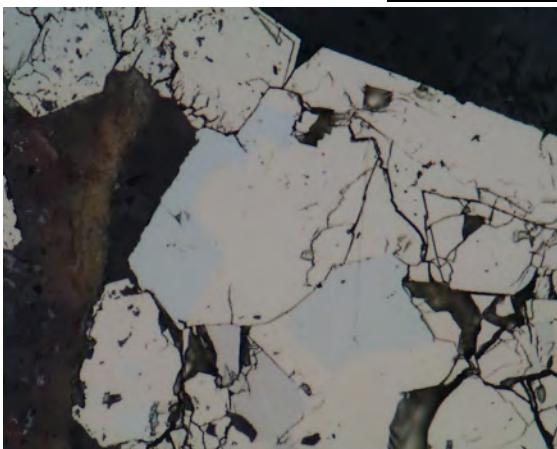


20) Chalcedony nodules in gypsum vein. FOV= 1.7 mm; Sample 34, 2880 ft.

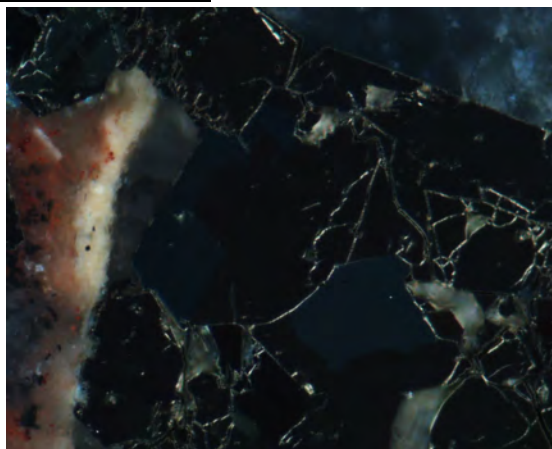


21) Tennantite intergrown with galena rimming/intergrown with pyrite. FOV= 0.16 mm; Sample 44, 3362 ft.

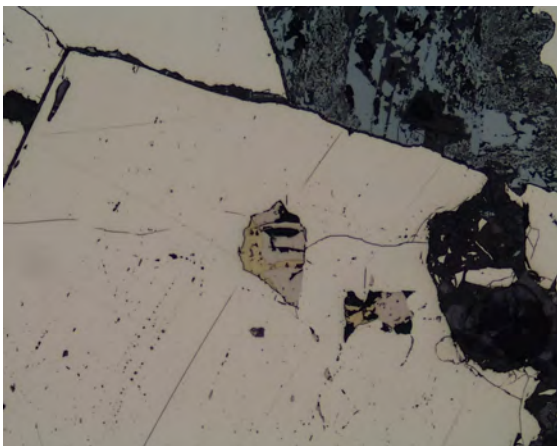
CC-2273 Photomicrographs



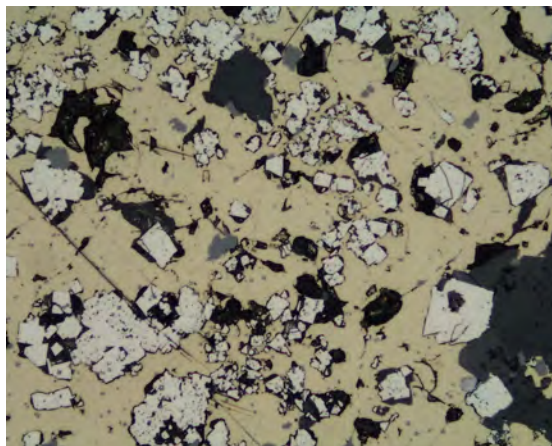
1) Arsenopyrite fragments intergrown with pyrite. FOV= 0.16 mm; Sample 56, 3380 ft.



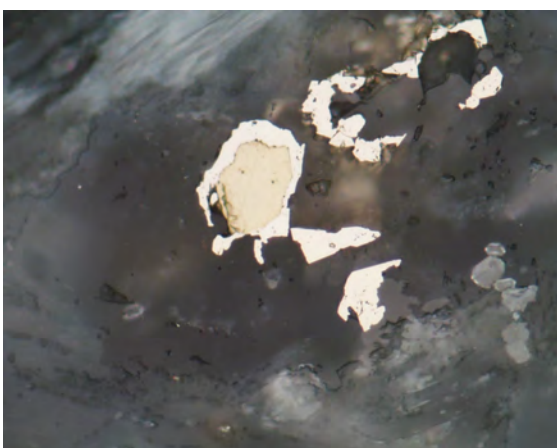
2) Same view as in previous picture (1) with crossed nichols. FOV= 0.16 mm; Sample 56, 3380 ft.



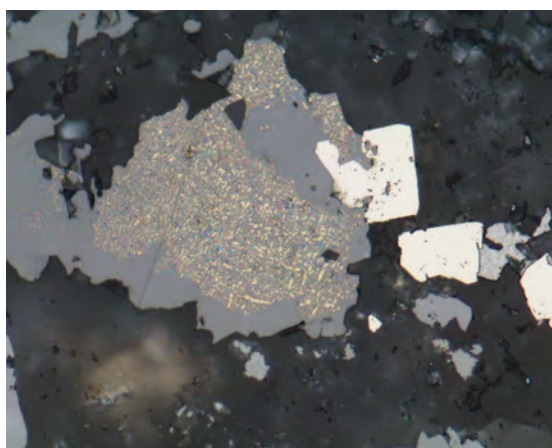
3) Pyrrhotite inclusion in pyrite being replaced by chalcopyrite. FOV= 0.85 mm; Sample 65, 4362 ft.



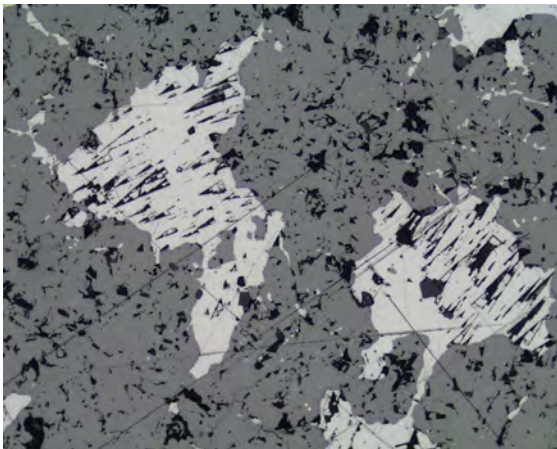
4) Euhedral to subhedral pyrite surrounded by chalcopyrite all being replaced by sphalerite and galena. FOV= 0.83 mm; Sample 61, 3854 ft.



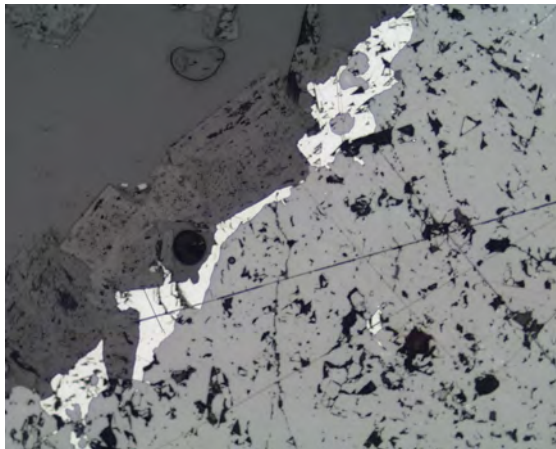
5) Chalcopyrite rimmed by pyrite. FOV= 0.83 mm; Sample 56, 3380 ft.



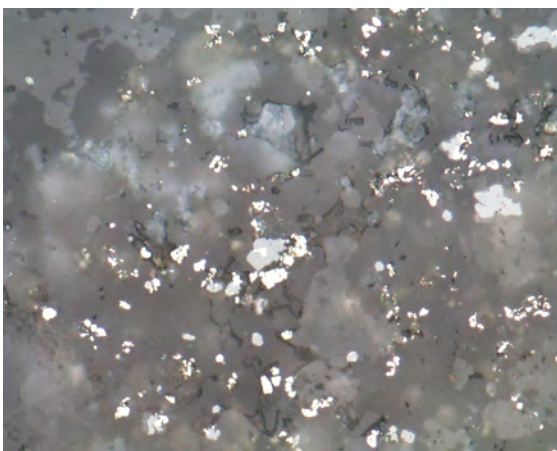
6) Sphalerite (low Fe, chalcopyrite disease) rimmed by sphalerite (low Fe, no chalcopyrite) and replacing pyrite. FOV= 0.16 mm; Sample 61, 3854 ft.



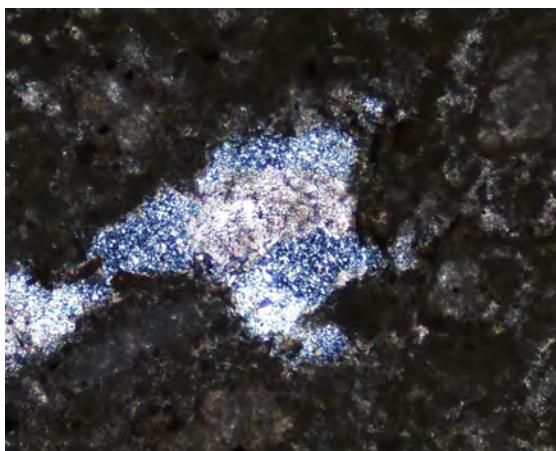
7) Sphalerite (low-no Fe, no chalcopyrite) intergrown with galena. FOV= 0.43 mm; Sample 61, 3854 ft.



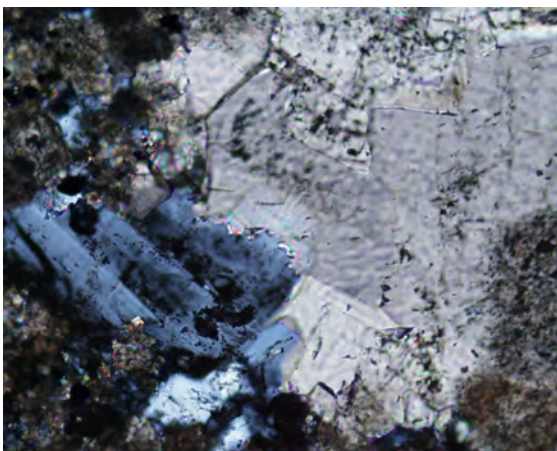
8) Galena rimming sphalerite (low-no Fe, no chalcopyrite). FOV= 0.43 mm; Sample 61, 3854 ft.



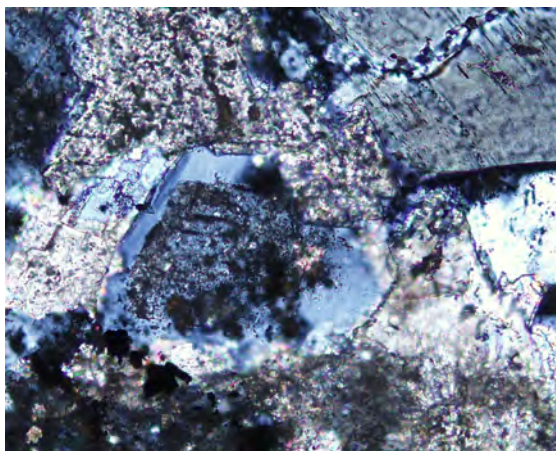
9) Sulfate/Fe carbonate mineral rimming pyrite. FOV= 0.16 mm; Sample 59, 3756 ft.



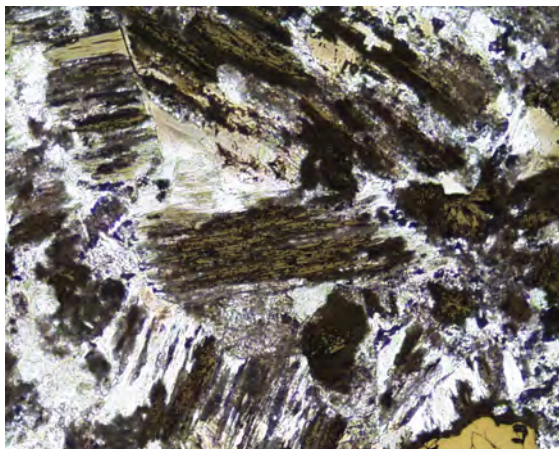
10) Sericite, carbonate, and clay growing in vug. FOV= 0.85 mm; Sample 58, 3628 ft.



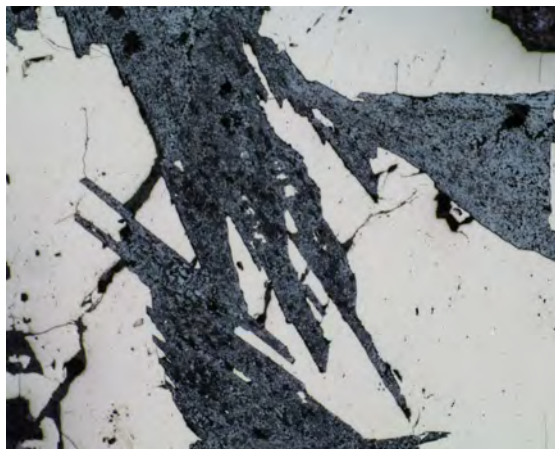
11) Potassic flooding replacing carbonate. FOV= 0.85 mm; Sample 58, 3628 ft.



12) Potassic rim on altered orthoclase grain. FOV= 0.43 mm; Sample 59, 3756 ft.

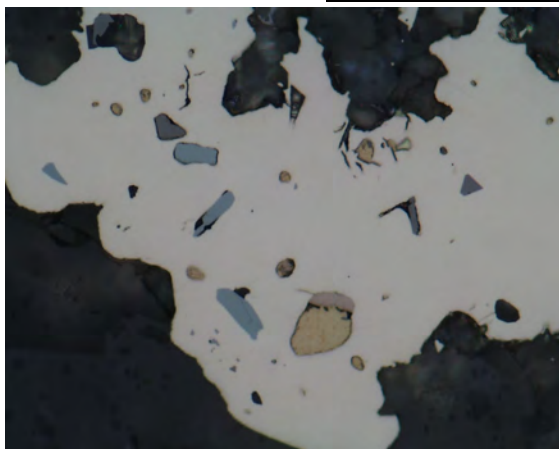


13) Euhedral biotite (secondary, in vein) partially replaced by hematite \pm magnetite. FOV= 0.85 mm; Sample 65, 4362 ft.

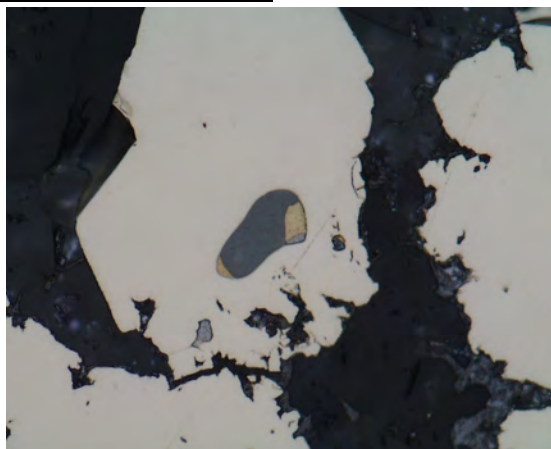


14) Hematite \pm magnetite replacing pyrite. FOV= 1.7 mm; Sample 65, 4362 ft.

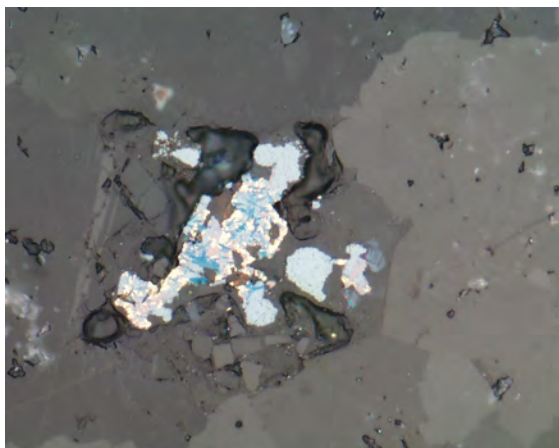
GHC-747-D & D2 Photomicrographs



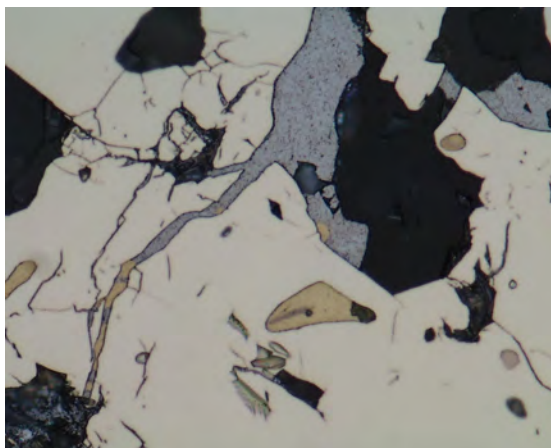
1) Chalcocite, chalcopyrite, and pyrrhotite included in and replacing pyrite. FOV= 0.16 mm; Sample 1, 2641 ft.



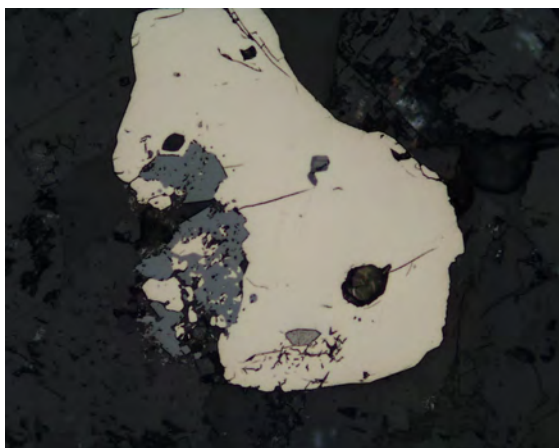
2) Sphalerite (low Fe, no chalcopyrite) partially replaced by chalcopyrite and included in pyrite that is intergrown with galena. FOV= 0.16 mm; Sample 9, 2627 ft.



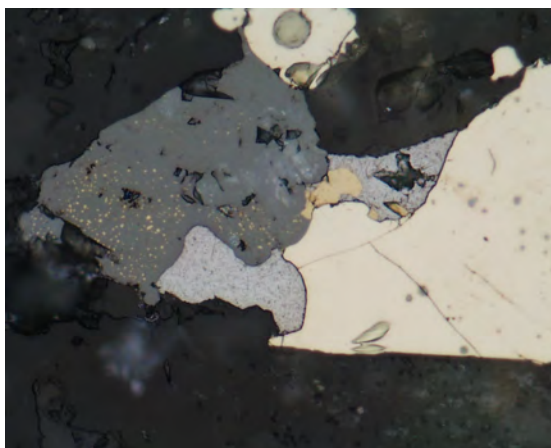
3) Covellite and bornite intergrown with chalcopyrite. FOV= 0.16 mm; Sample 66, 2678 ft.



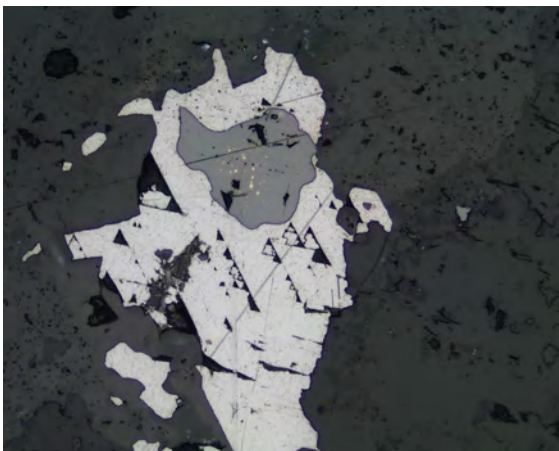
4) Galena growing in fracture in pyrite, partially replaced by chalcopyrite. FOV= 0.43 mm; Sample 1, 2641 ft.



5) Sphalerite (low Fe, no chalcopyrite) replacing pyrite intergrown with galena. FOV= 0.43 mm; Sample 10, 2644 ft.



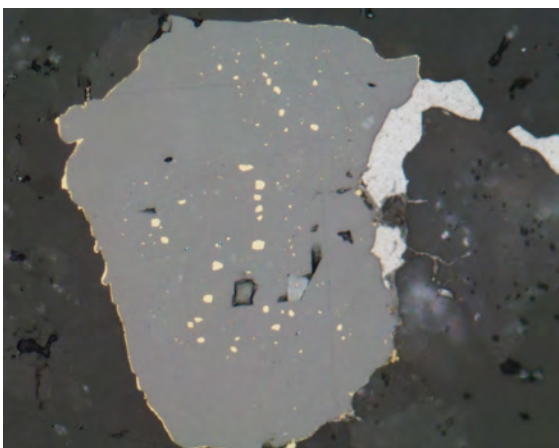
6) Pyrite replaced by galena being replaced by sphalerite (low Fe, chalcopyrite disease) with chalcopyrite replacing galena and sphalerite. FOV= 0.16 mm; Sample 6, 2436 ft.



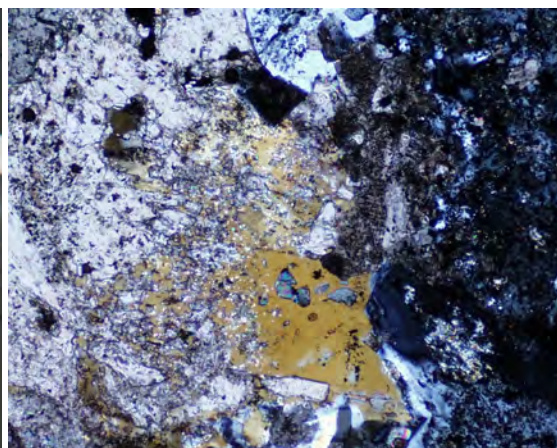
7) Sphalerite (high Fe, chalcopyrite disease) rimmed by sphalerite (high Fe, no chalcopyrite) rimmed by sphalerite (mod Fe, no chalcopyrite) all enclosed in galena. FOV= 0.43 mm; Sample 66, 2678 ft.



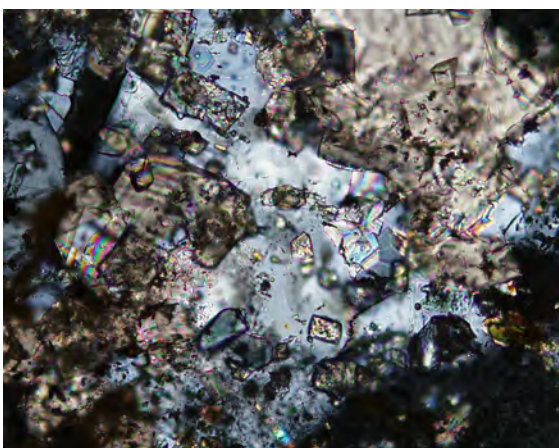
8) Same grain as previous picture in crossed nichols. FOV= 0.43 mm; Sample 66, 2678 ft.



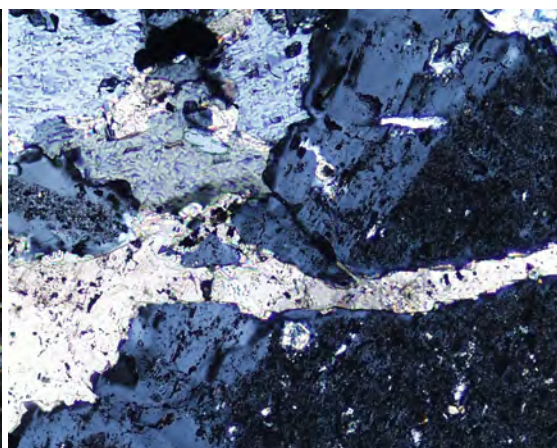
9) Sphalerite (low Fe, chalcopyrite disease) enclosed in sphalerite (high Fe, no chalcopyrite) rimmed by chalcopyrite. FOV= 0.16 mm; Sample 66, 2678 ft.



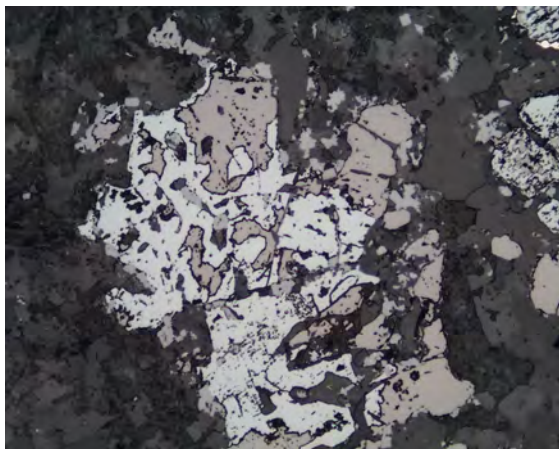
10) Biotite being replaced by carbonate. FOV= 1.7 mm; Sample 8, 2880 ft.



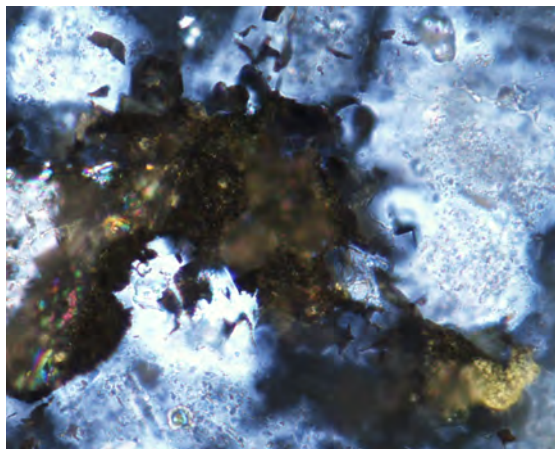
11) Euhedral carbonate entrained in potassium flooding. FOV= 0.43 mm; Sample 8, 2880 ft.



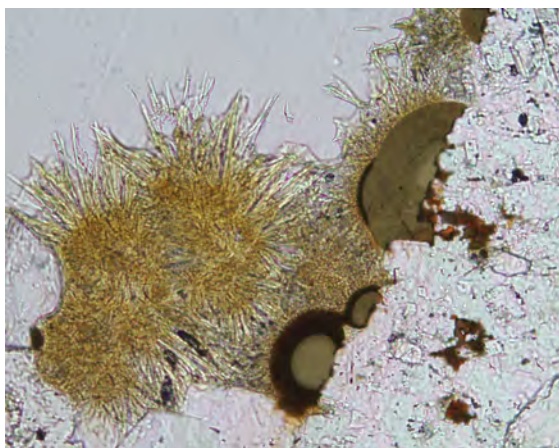
12) Potassic rim on altered orthoclase cut by carbonate veinlet. FOV= 0.85 mm; Sample 1, 2641 ft.



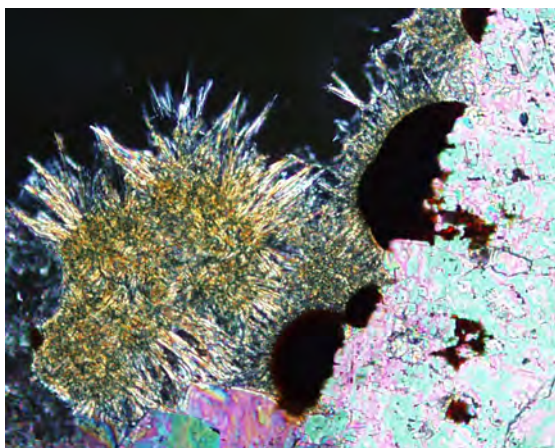
13) Magnetite replacing hematite. FOV= 0.43 mm; Sample 8, 2880 ft.



14) Molybdenite and sulfate/Fe carbonate mineral intergrown and replacing potassic feldspar. Sample 5 FOV= 0.16 mm; 2456 ft.

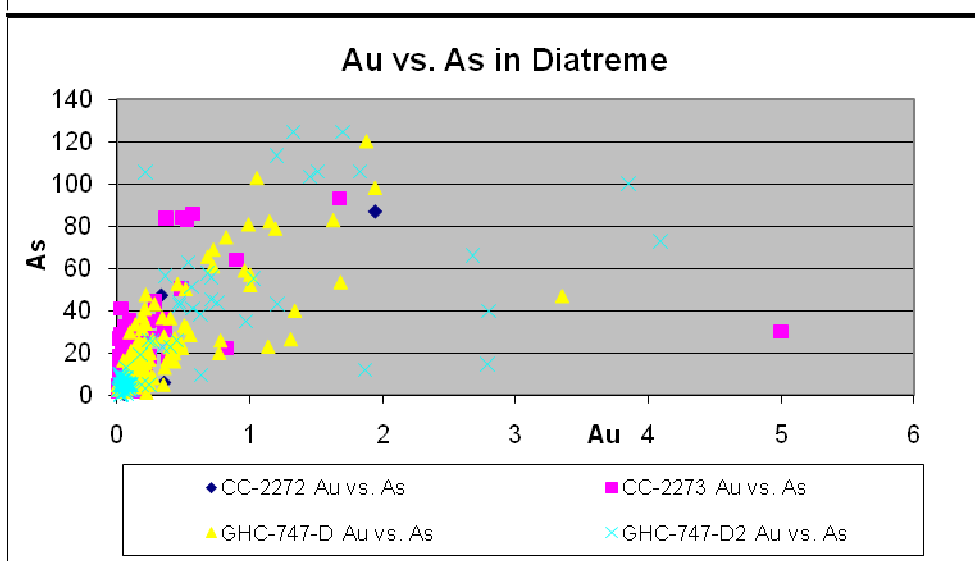
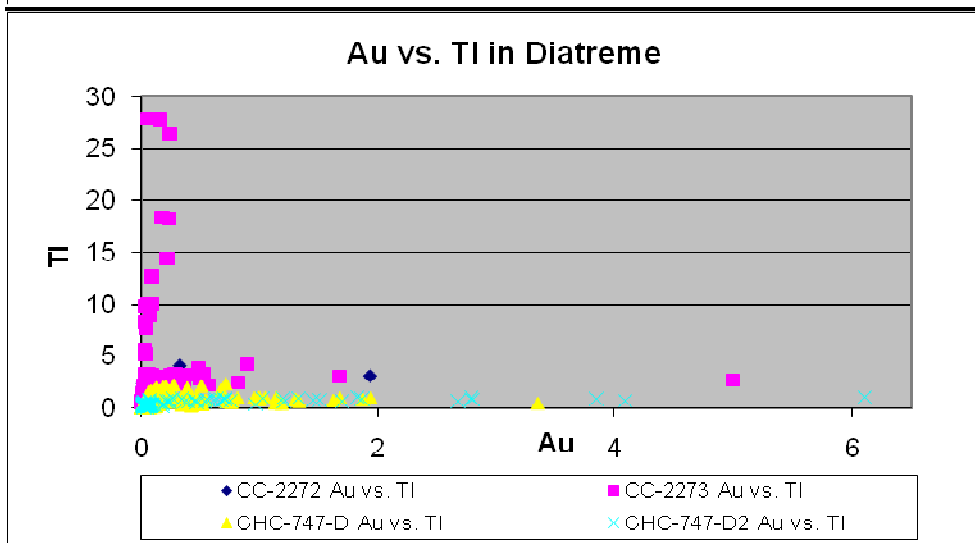
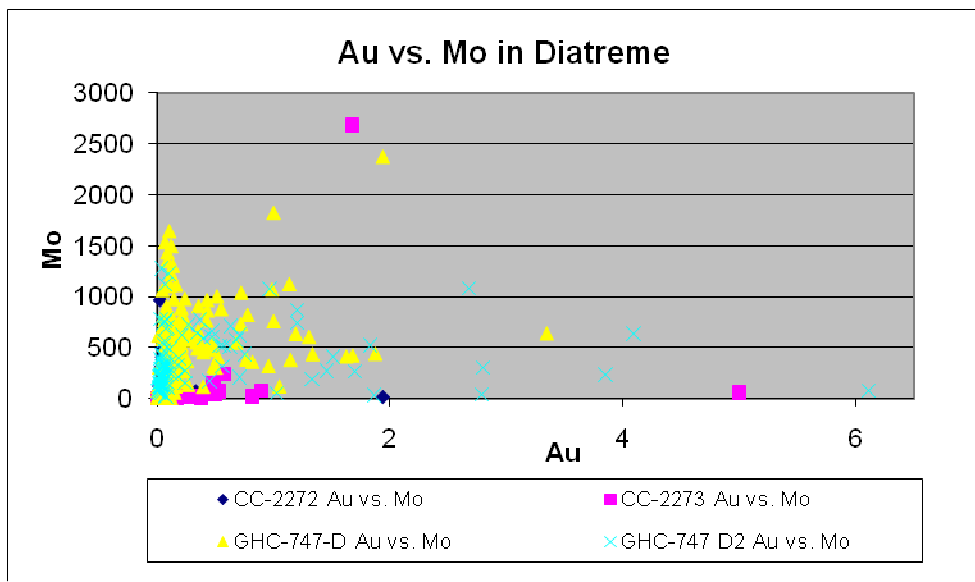


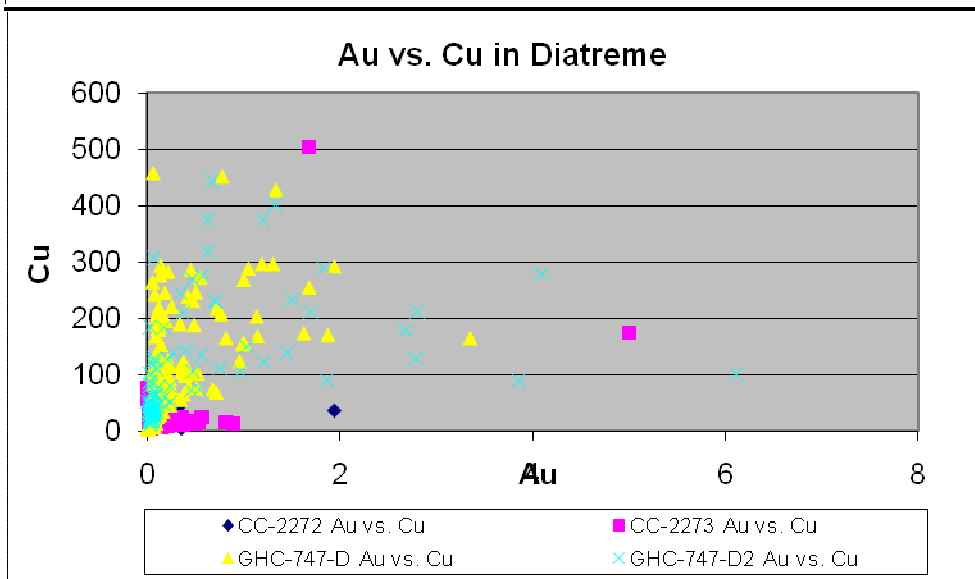
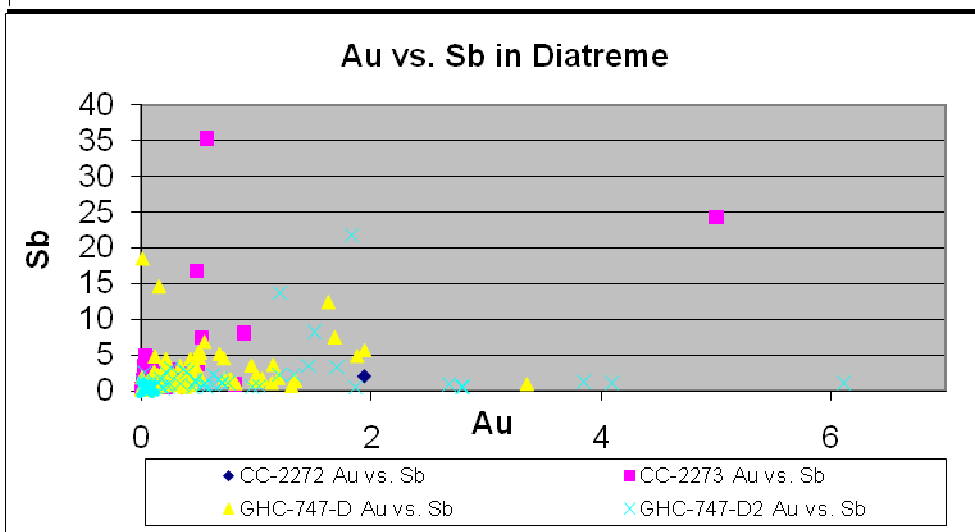
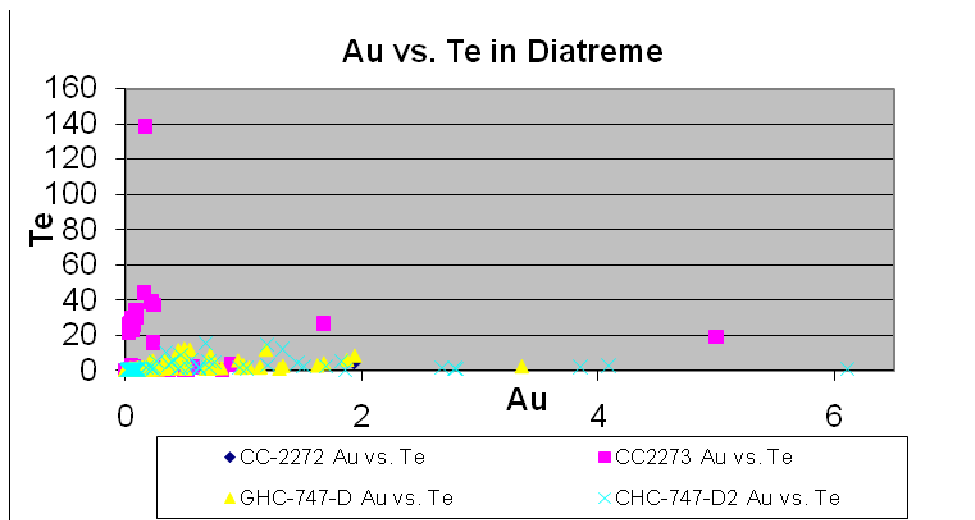
15) Botryoidal hematite growing into vug and rimmed by crystalline sericite. FOV= 0.43 mm; Sample 66, 2678 ft.

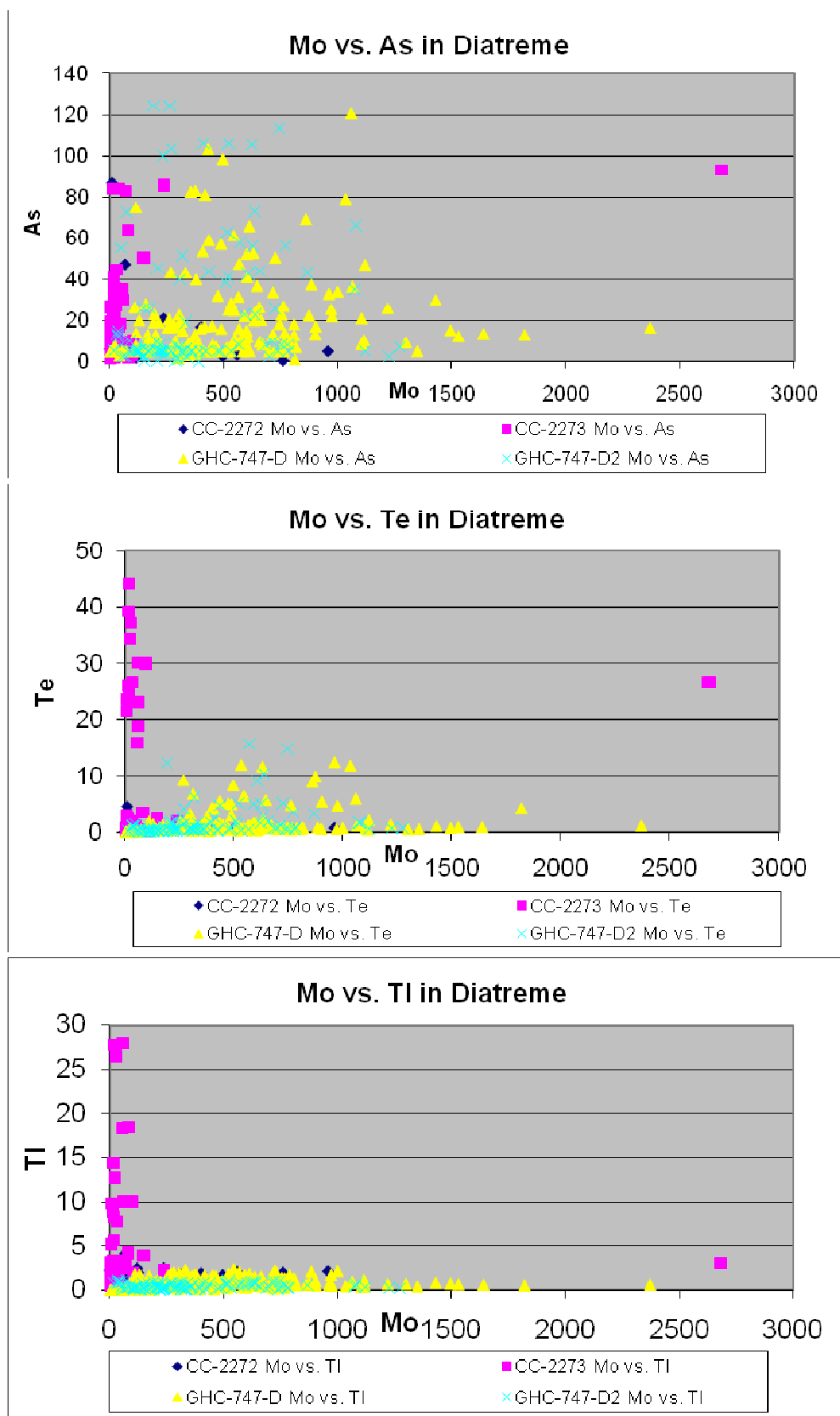


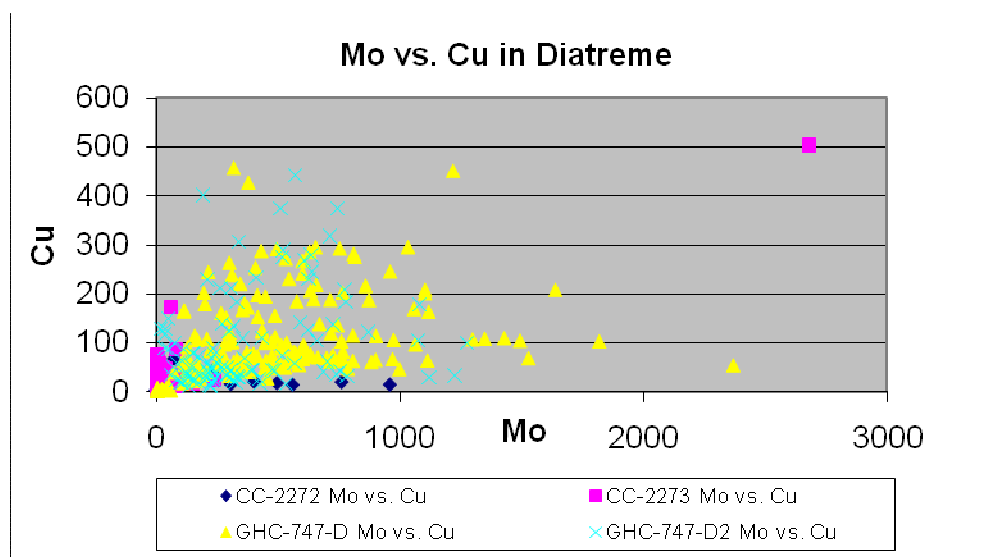
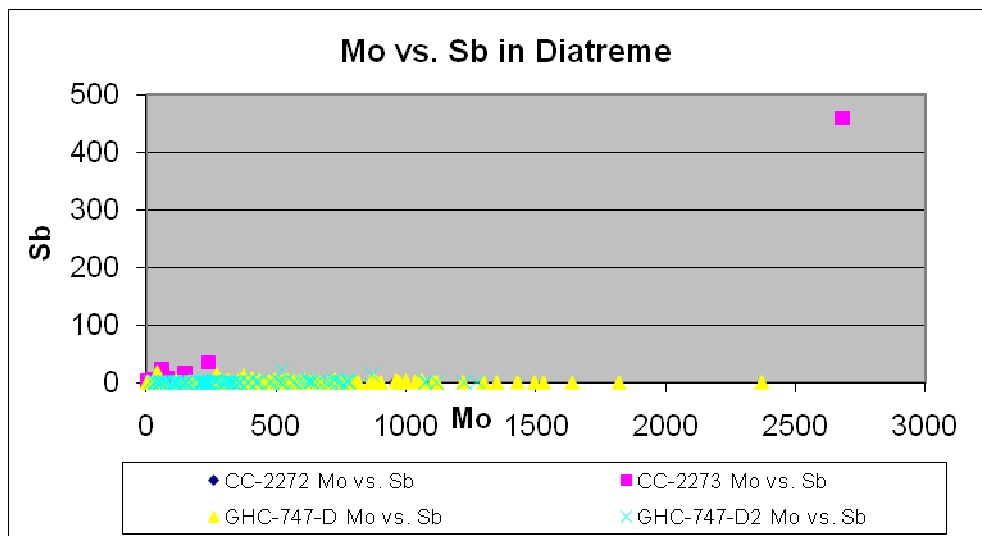
16) Same as previous under crossed nichols. FOV= 0.43 mm; Sample 66, 2678 ft.

Appendix D:
CC-2272, CC-2273, GHC-747-D & D2 Geochemical Graphs

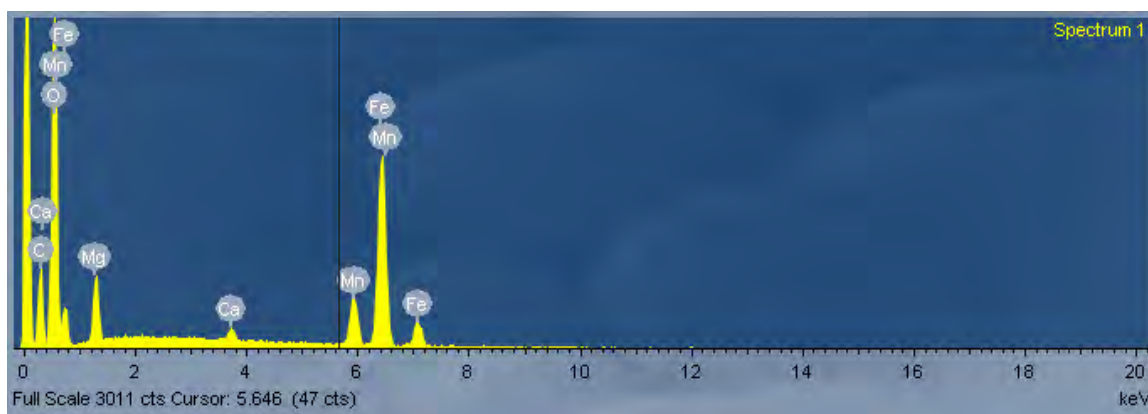
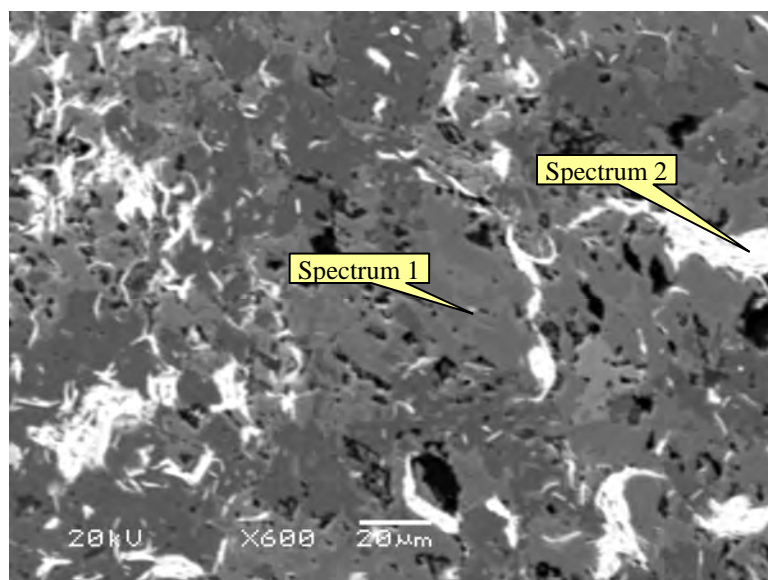




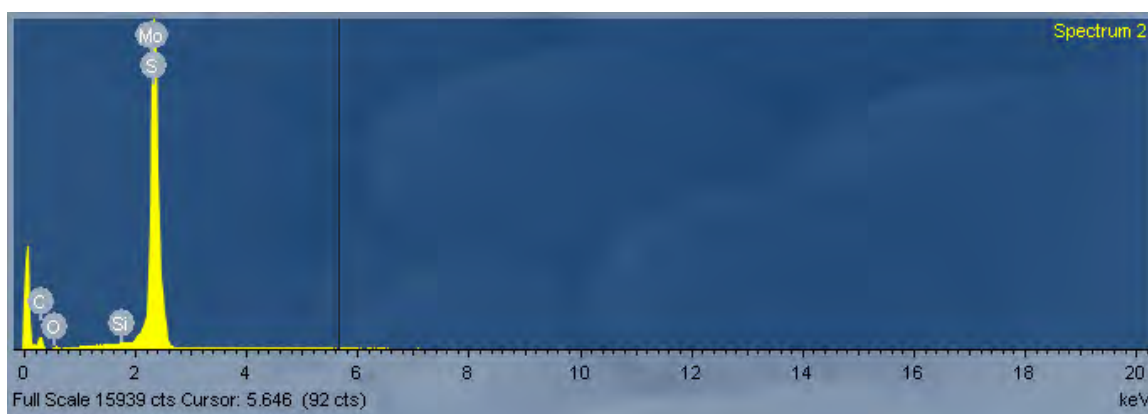




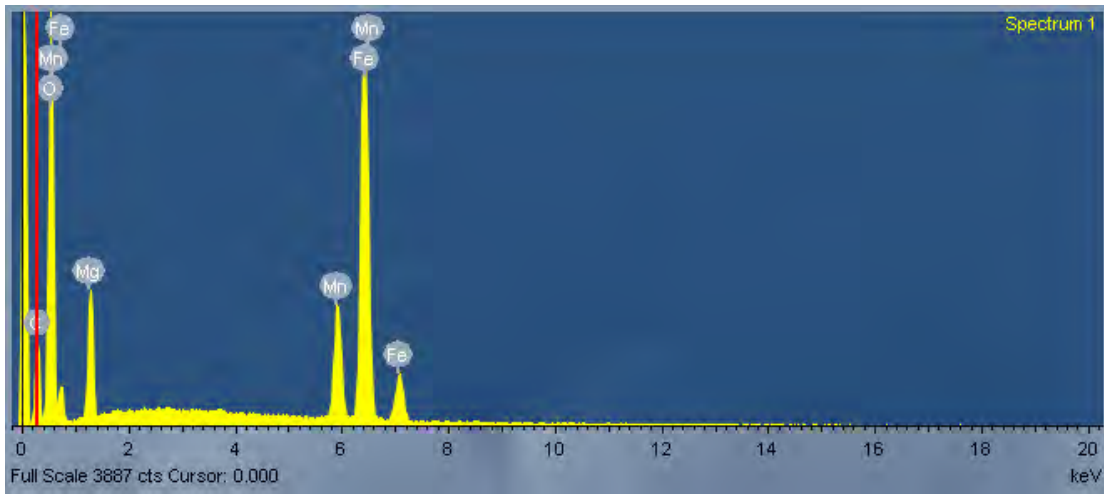
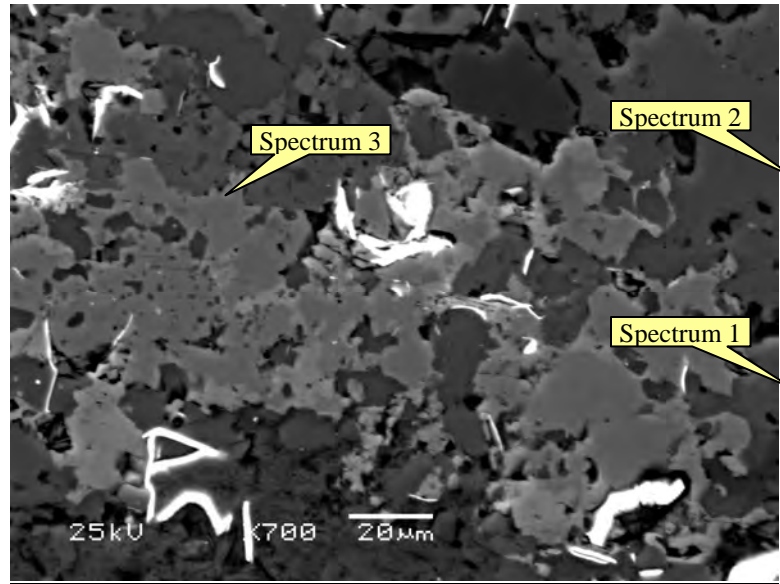
Appendix E:
SEM Images and EDS Spectra



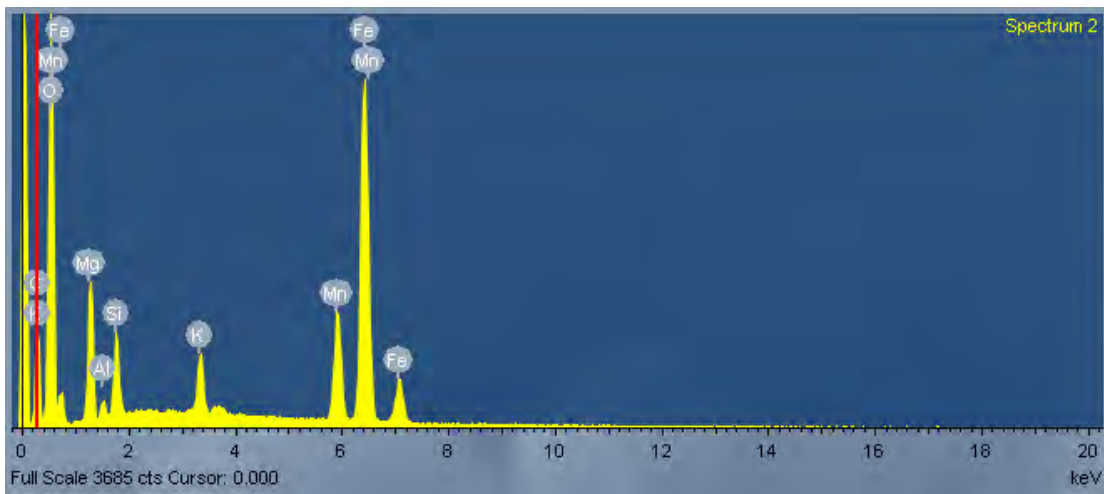
EDS spectrum for ankeritic mineral intergrown with molybdenite.



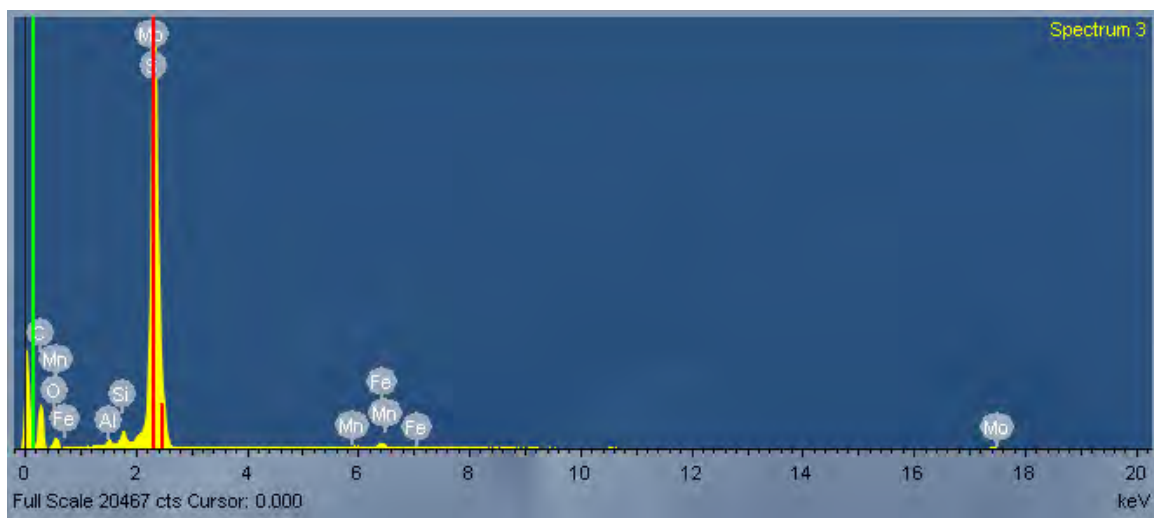
EDS spectrum for molybdenite.



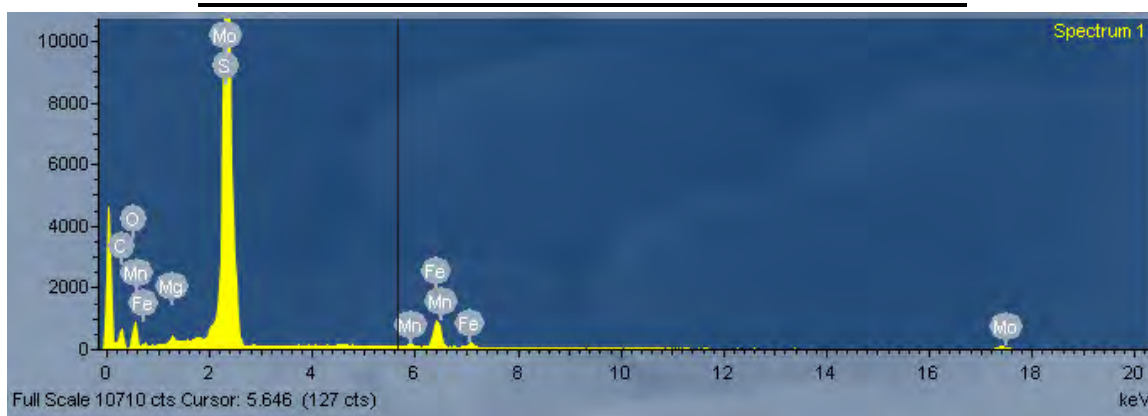
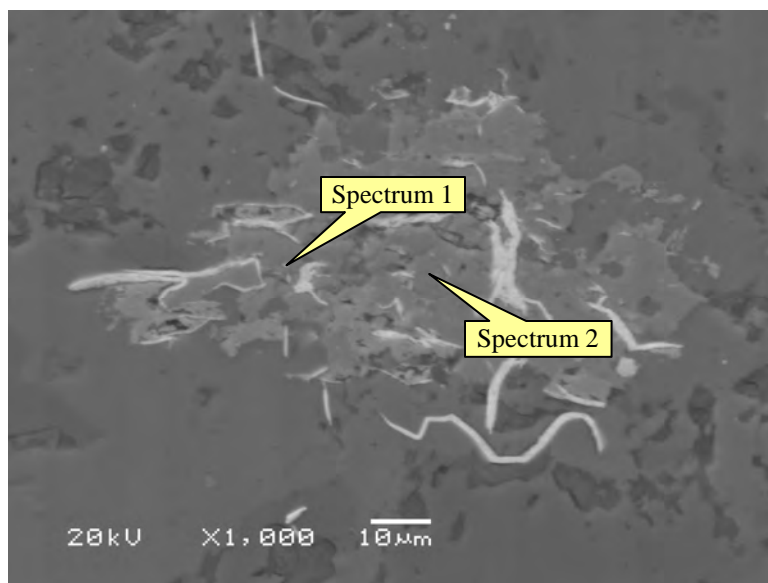
EDS spectrum for ankeritic mineral intergrown with molybdenite.



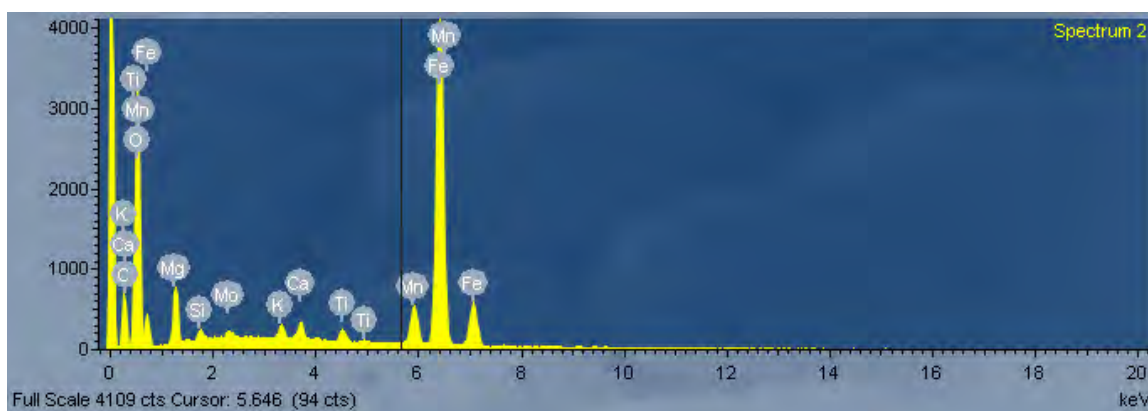
EDS spectrum for ankeritic mineral intergrown with molybdenite.



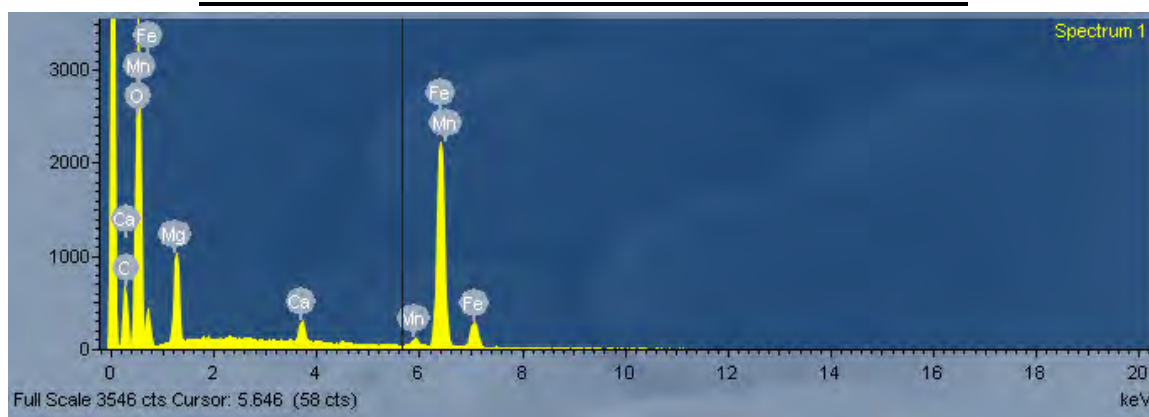
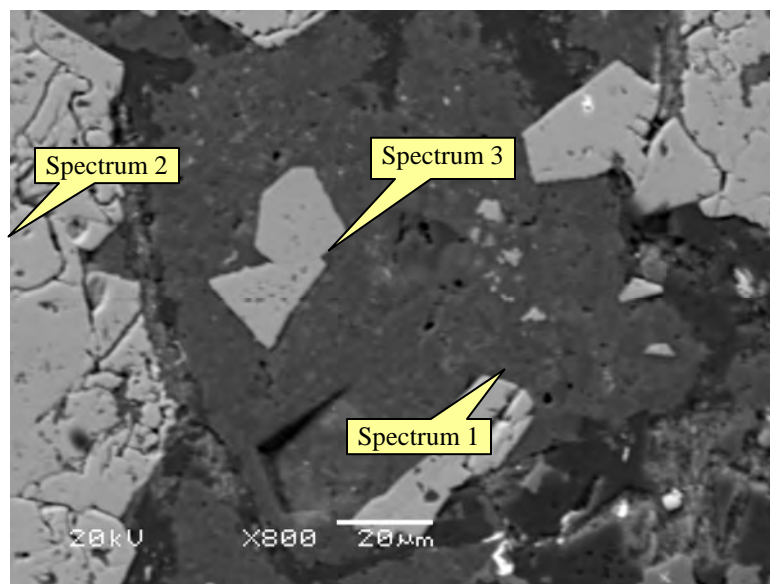
EDS spectrum for molybdenite.



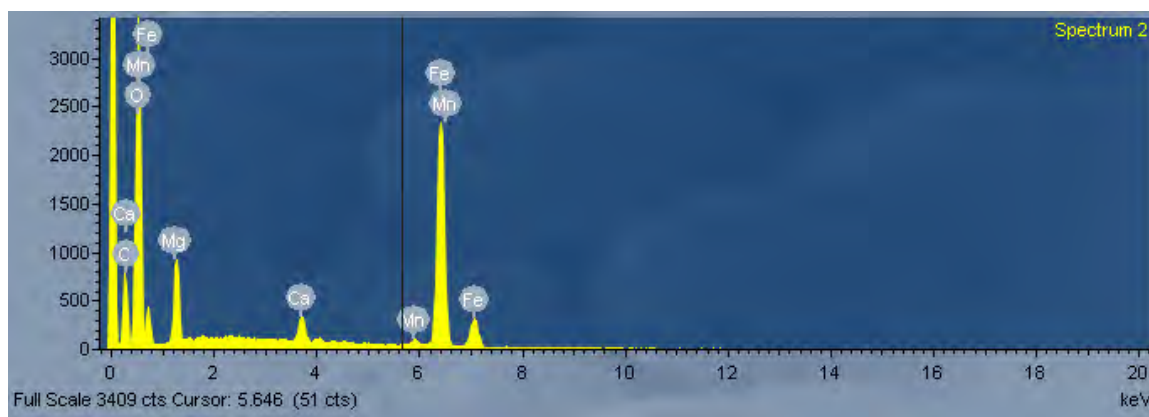
EDS Spectrum for molybdenite.



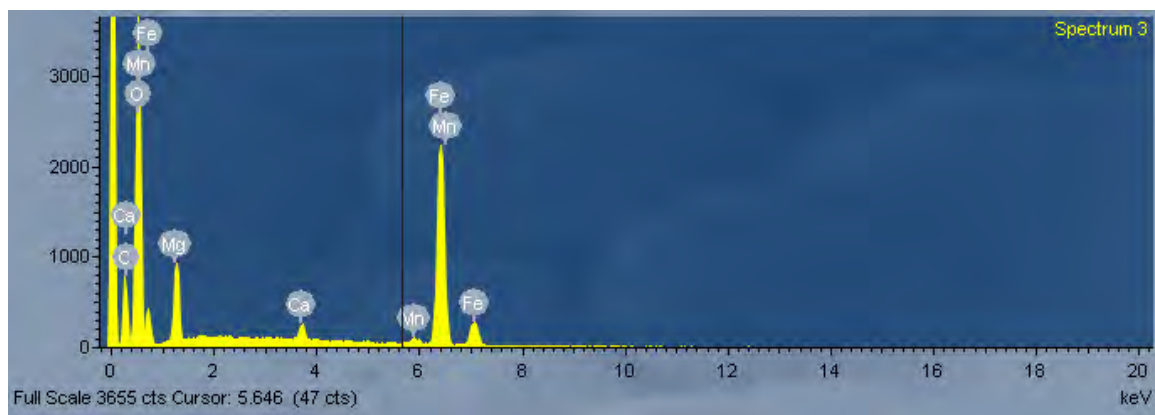
EDS spectrum for ankeritic mineral intergrown with molybdenite with some local contamination from matrix.



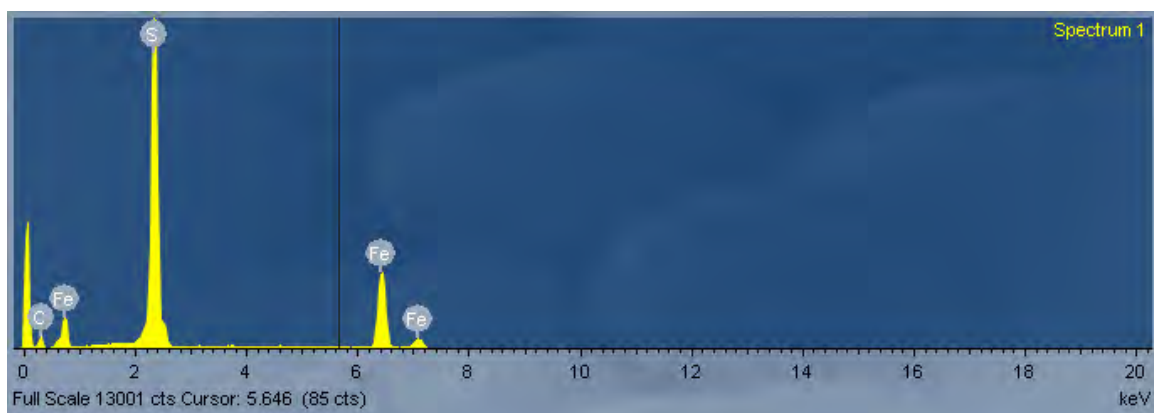
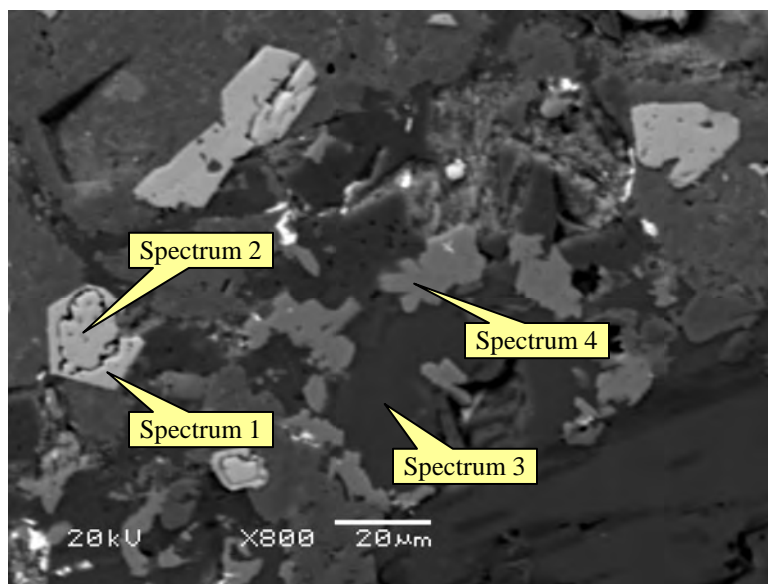
EDS spectrum for ankeritic mineral intergrown with molybdenite.



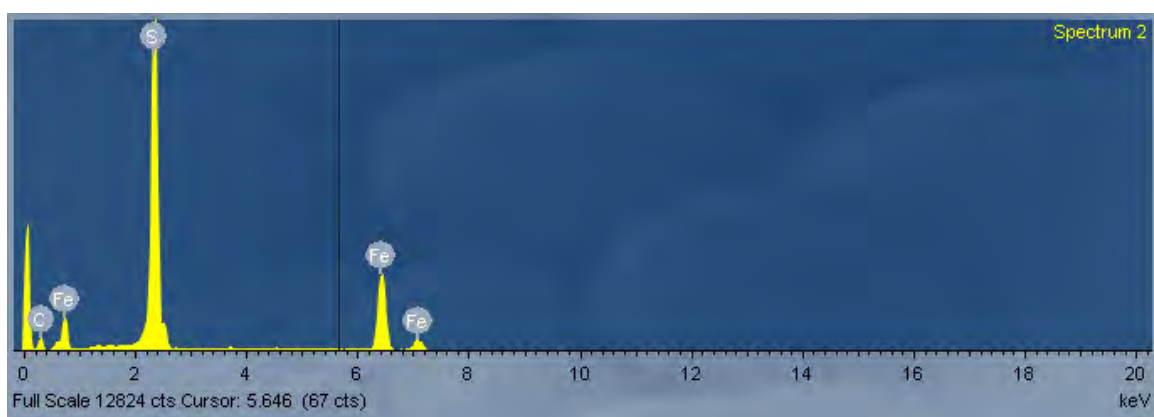
EDS spectrum for ankeritic mineral intergrown with molybdenite.



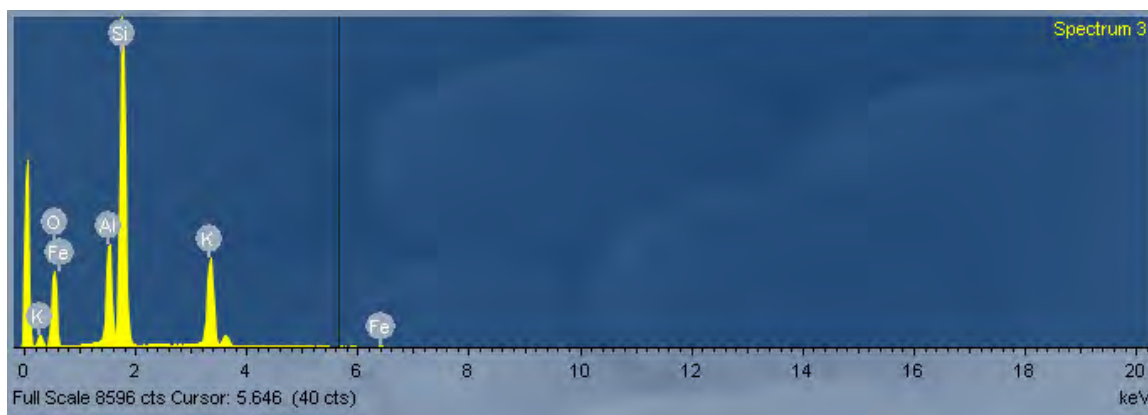
EDS spectrum for ankeritic mineral intergrown with molybdenite.



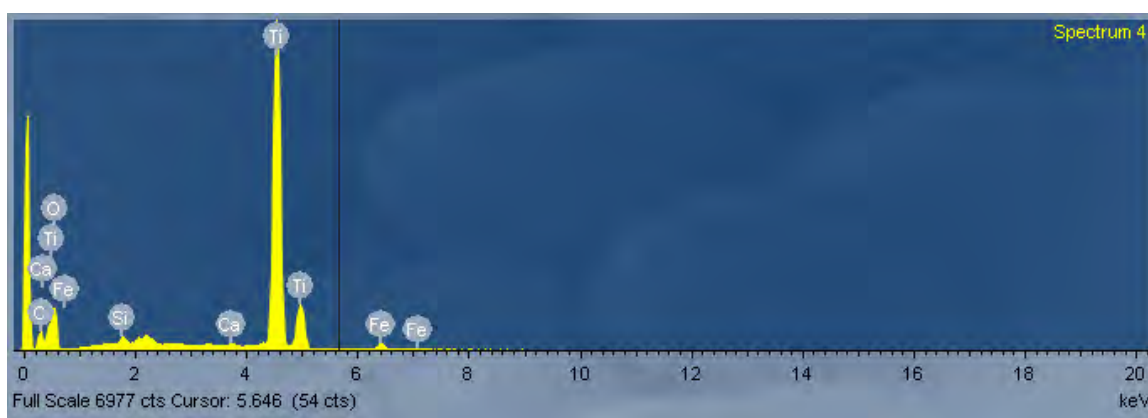
EDS spectrum for pyrite core.



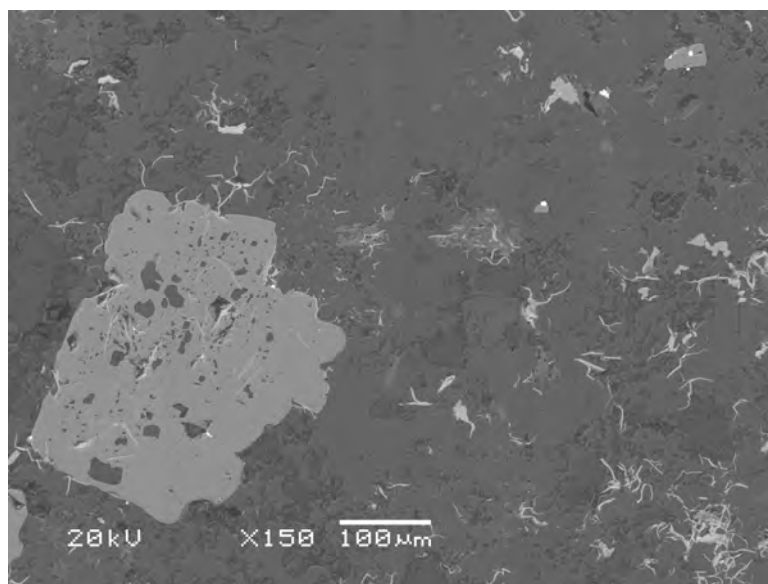
EDS spectrum for pyrite rim.



EDS spectrum for feldspar.



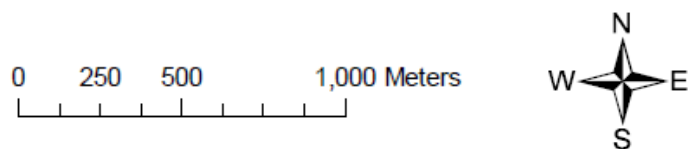
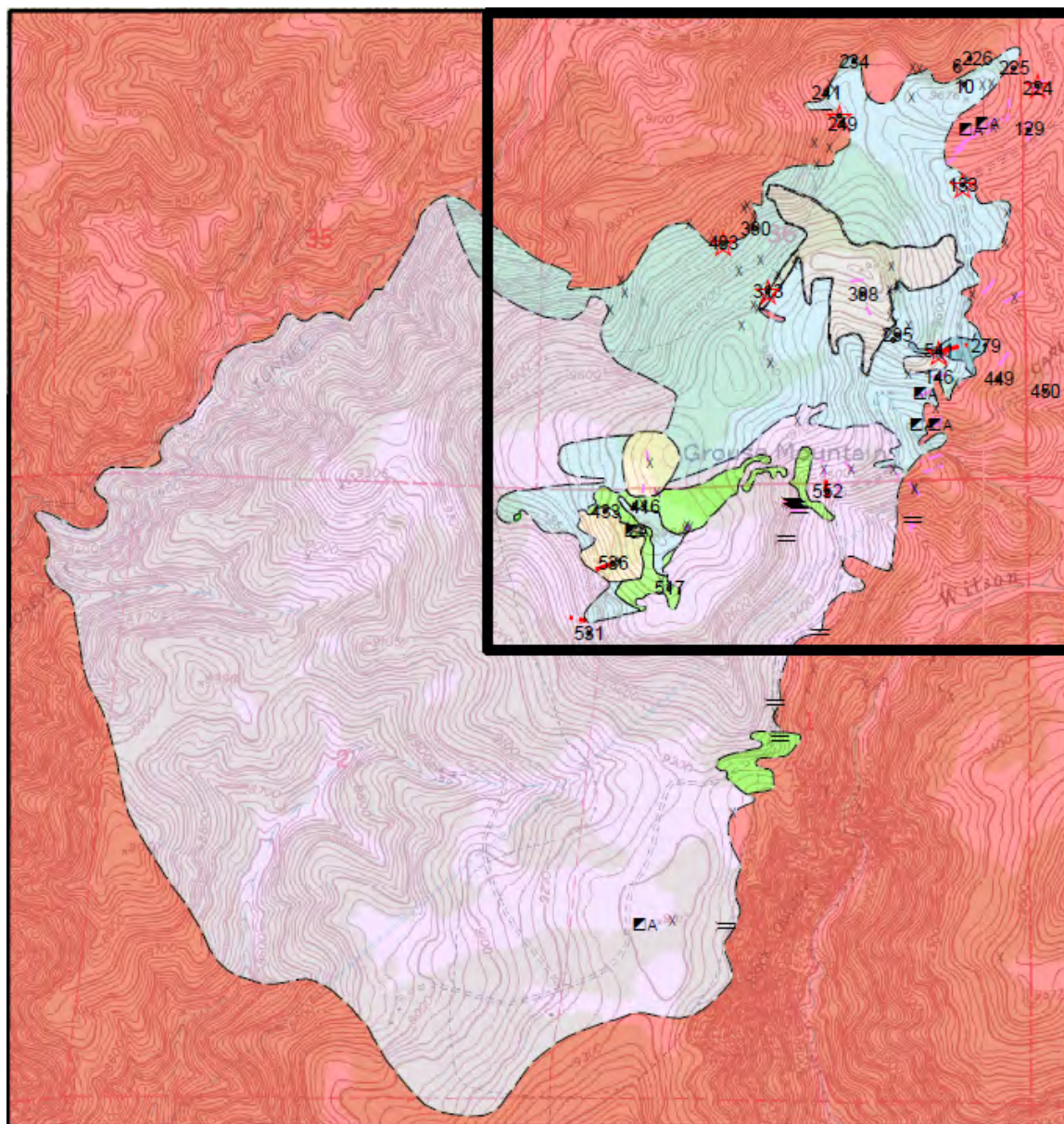
EDS spectrum for ankeritic mineral with matrix contamination.



Backscatter image showing pyrite grain being replaced by molybdenite and molybdenite in matrix.

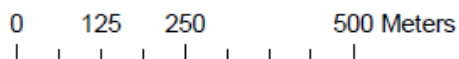
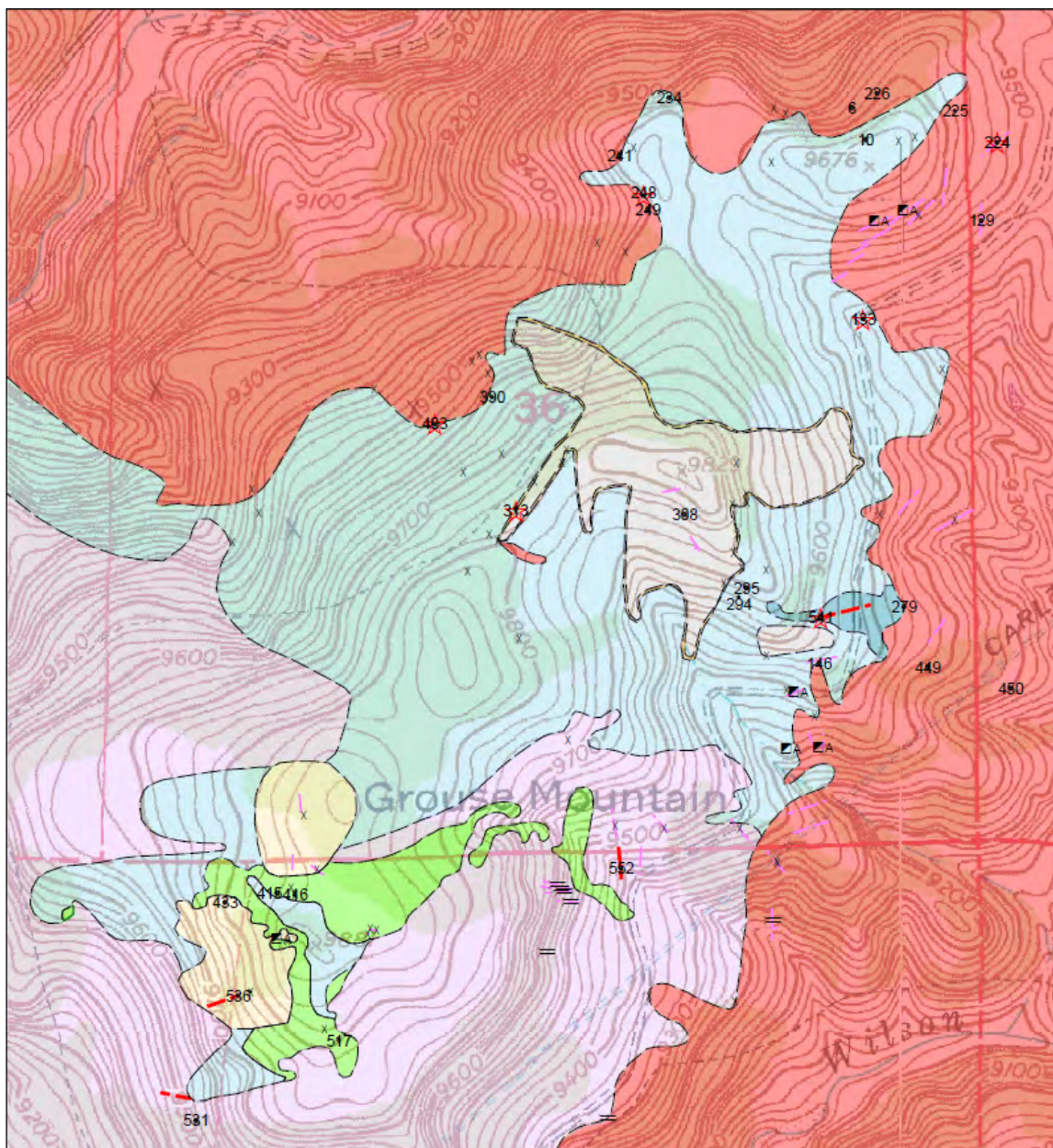
Appendix F:
Geologic Map of Grouse Mountain

Grouse Mountain Map












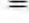







The black box indicates the area shown on the next page.

Grouse Mountain Inset



Grouse Mountain, Cripple Creek District, Teller County, Colorado

Legend

	Tph- Phonolite: Light gray to tan aphanitic to locally porphyritic phonolite that may contain euhedral cubic voids or lath-like voids in locally porphyritic regions. Oxidation rings are common and local bleaching, often accompanied by abundant sericite and/or clay is found near dikes and structures. Potassic flooding is moderate to strong and minor quartz veining is present though rare and usually associated with structures.		Samples above 0.005 oz/t gold, which is the current cutoff grade at the Cresson mine
	Tpca- Altered Clinopyroxene Phonolite: Light gray to gray porphyritic, locally glassy (due to strong potassic alteration) cpx phonolite. Phenocrysts are dominantly pyroxenes (rounded to lath-shaped) or sanidines. Local trachytic texture and measurable foliation may be present. Minor to moderate sericite was observed in thin section but is not usually detectable in hand sample. Unit is locally rimmed by 10-30 ft of oxidized, matrix to clast supported phonolite breccia at contact with surrounding unit. The clasts in the breccia are dominantly phonolite and matrix is strongly oxidized, mainly composed of goethite.		Approximate fault
			Approximate contact
			Dike
			Known contact
			Known fault
			Shafts
			Portals
			Prospect Pits
	Tpc- Clinopyroxene Phonolite: Light gray to gray, medium-grained porphyry with euhedral to subhedral clinopyroxene crystals and local alkali feldspar phenocrysts. Trachytic texture is common and foliation is not measurable as few outcrops exist (material is dominantly found in prospect pits and as float). Minor to moderate sericite is visible in thin section and local, minor clay development may be present. Potassic alteration is moderate to strong.		
	Tbx- Grouse Mountain Breccia: Unit is generally poorly sorted with minor, localized bedding and subrounded to angular clasts. Matrix consists of quartz flooding and sand-sized particles. Local fragments of phonolite are present and fragments of Wall Mountain Tuff are common. Potassic flooding is strong in Wall Mountain Tuff and phonolite clasts but is not present in matrix. Locally, fragments exhibit a "puzzle-breccia" texture (appearing to fit back together).		
	Tw- Tallahassee Creek Conglomerate: Fluvially derived conglomeritic layer with clasts of various lithologies. Clasts generally range from sand-sized to cobble size. Local bedding and sorting are present. Clasts are generally rounded. Unit also overlies the Wall Mountain Tuff and may contain fragments of the Wall Mountain Tuff.		
	Twm- Wall Mountain Tuff: Moderately to densely welded tuff composed of 16-32% sanidine or plagioclase phenocrysts, 3-10% biotite, and traces of pyroxene. Quartz is absent as phenocrysts. Description modified from Chapin and Lowell, 1979. In the field area unit generally displays strong potassic alteration with significant bleaching and minor to moderate clay and/or sericite development. Local minor oxidation is also present.		
	Xgd- Granodiorite: Massive to foliated, medium to coarse-grained, biotite granodiorite. Locally occurs as augen gneiss and may contain local schistose lenses. In altered areas (generally near structures) there is abundant sericite and/or clay development. Samples of this unit were not stained for potassic alteration.		
	Tpb- Phonolite Breccia: Breccia composed almost exclusively of angular, poorly sorted phonolite fragments ranging from boulder to sand-sized. Phonolite fragments are bleached and likely contain sericite and/or clay. Potassic alteration is prevalent in phonolite clasts and weak in matrix. Matrix is dominantly iron oxides, mainly goethite.		

Appendix G:
Pearson's Correlation Coefficients for Grouse Mountain Samples

The raw geochemical data are proprietary and are not included in this report. The reader interested in such data should contact the AngloGold Exploration Manager of the Colorado division, currently Tim Brown.

Grouse Mountain: Pearson's Correlation Coefficients

Grouse	Au	Ag	Al	As	Ba	Be	Bi	Ca	Cd	Ce	Co	Cr	Cs	Cu	Fe	Ga	Ge	Hf	Hg	In	K	La	Li	Mg	Mn	
Au	1																									
Ag	0.239662	1																								
Al	0.191632	0.284481	1																							
As	0.332038	0.086841	0.067687	1																						
Ba	-0.2063	0.035426	0.076412	-0.20499	1																					
Be	-0.09738	-0.05576	0.481064	-0.2171	0.006216	1																				
Bi	0.217155	-0.07482	0.474575	0.134116	-0.38033	0.450651	1																			
Bi	-0.3174	-0.22204	-0.11333	-0.23228	0.227003	0.16845	-0.33688	1																		
Cd	0.114646	0.170201	0.293973	-0.07389	0.596943	0.141253	-0.12844	-0.14368	1																	
Ce	-0.21458	-0.17287	0.011844	0.266744	0.163277	-0.06801	-0.17949	0.073749	0.141992	1																
Co	-0.28505	0.024036	0.046224	-0.25627	0.453946	0.040016	-0.40293	0.738521	0.051992	0.241532	1															
Cr	-0.18996	-0.14159	-0.90546	-0.0883	0.038919	-0.41349	-0.45699	0.166065	-0.21211	-0.07198	0.074409	1														
Cs	-0.07588	0.077588	0.225861	-0.31038	-0.0273	0.260254	0.232068	0.059876	0.007077	-0.25836	-0.10125	-0.22384	1													
Cu	0.19006	0.80819	-0.10213	0.003383	0.065761	-0.34433	-0.27495	-0.09255	0.07352	-0.28365	0.100078	0.229597	0.115399	1												
Fe	-0.03714	-0.01491	0.178899	-0.04128	0.296686	0.182314	-0.22772	0.535506	0.253247	0.426557	0.706546	-0.11405	-0.17401	-0.113	1											
Ga	0.192337	0.154791	0.824426	0.094147	-0.19711	0.627482	0.778189	-0.14417	0.044527	-0.06656	-0.08767	-0.71616	0.203848	-0.16943	0.064281	1										
Ge	-0.18517	-0.13498	-0.1668	0.239153	0.173707	-0.25151	-0.47873	0.112089	0.069845	0.875613	0.302686	0.054106	-0.27777	-0.10152	0.477011	-0.31343	1									
Hf	0.19103	-0.07679	0.548657	0.264691	-0.38187	0.414244	0.884698	-0.37106	0.000786	0.105204	-0.39252	-0.53756	0.089441	-0.35638	-0.07331	0.79156	-0.22425	1								
Hg	0.22801	0.064873	-0.12127	0.429113	-0.08996	-0.20053	-0.15029	-0.19247	0.077036	0.581737	-0.06141	0.075875	-0.12602	0.060657	0.16763	-0.09025	0.64325	0.042224	1							
In	-0.04691	-0.03751	0.043078	-0.07669	0.14631	0.050826	-0.22408	0.575361	-0.08762	0.367659	0.631812	-0.0028	0.023438	0.020323	0.722094	-0.04595	0.486105	-0.2615	0.246186	1						
K	0.065027	0.051829	0.774881	0.118996	0.236291	0.261672	0.225728	0.075677	0.186415	0.028159	0.141182	-0.76659	0.172405	-0.14636	0.009939	0.564407	-0.0783	0.268897	-0.06677	0.006681	1					
La	-0.03561	-0.11398	0.225196	0.288207	-0.03825	0.124612	0.278365	-0.31631	0.145999	0.819895	-0.15503	-0.12663	-0.33527	0.113112	0.262082	0.542549	0.537602	0.456341	0.00831	0.085848	1					
Li	0.228687	-0.0762	0.332762	-0.08837	-0.31128	0.61294	0.579869	0.003692	-0.05213	-0.05326	-0.17282	-0.32781	0.49409	-0.25301	0.022689	0.584704	-0.23753	0.629026	0.055162	-0.06957	0.09795	0.241972	1			
Mg	-0.24687	-0.13948	0.068244	-0.27548	0.363069	0.230776	-0.24247	0.818417	0.037064	0.232245	0.821706	0.048594	-0.0311	-0.10289	0.756683	0.004998	0.260863	-0.29637	-0.09329	0.787497	0.04949	-0.14159	-0.04021	1		
Mn	-0.14933	0.245439	0.291429	-0.22985	0.794632	0.15175	-0.1532	0.082897	0.639518	0.136157	0.351624	-0.20625	0.148183	0.223181	0.308828	0.086846	0.131181	-0.10544	-0.05993	0.053569	0.323576	0.067436	-0.0456	0.195215	1	
Mo	0.594981	0.065775	0.112085	0.3747	-0.08281	-0.06635	0.105978	-0.28338	0.278946	0.183981	-0.18136	-0.19213	-0.12302	-0.0015	0.210996	0.072583	0.143653	0.286016	0.307444	-0.1033	0.021158	0.282266	0.161202	-0.26096	0.061772	
Nb	-0.30023	-0.13326	0.255534	-0.25567	0.03171	0.62936	0.159731	0.132428	0.091857	-0.03745	-0.09183	-0.23231	0.257011	-0.16763	-0.0681	0.263511	-0.09769	0.133725	-0.20698	-0.00147	0.220931	0.069769	0.27162	0.106681	0.207007	
Ni	0.093504	0.038586	0.647158	0.15474	-0.11728	0.532366	0.78762	-0.37859	0.235015	0.141547	-0.29649	-0.58754	0.047789	-0.36478	0.051968	0.805158	-0.19305	0.90481	0.009179	-0.21591	0.296085	0.535307	0.5485	-0.16482	0.103828	
Ni	-0.25233	0.211543	-0.27261	-0.06315	0.130685	-0.2293	-0.52327	0.44747	-0.12744	0.056225	0.668015	0.360589	-0.12163	0.366849	0.328589	-0.39018	0.19185	-0.52933	0.057905	0.27172	-0.14361	-0.28567	-0.39616	0.352803	0.038353	
P	-0.24823	-0.16755	-0.20806	-0.13292	0.205246	-0.0676	0.46135	0.676236	-0.08849	0.480357	0.700842	0.221182	-0.17799	-0.0596	0.693365	-0.27809	0.605931	-0.43672	0.295369	0.885062	-0.13426	-0.00747	-0.20977	0.831978	0.026443	
Pb	0.027656	0.593438	0.287246	0.001	0.238893	0.083462	-0.19681	-0.18192	0.485429	0.057182	0.024766	-0.19969	-0.11471	0.184914	0.125644	0.012243	-0.0234	-0.10668	-0.08086	-0.11715	0.044086	0.053482	-0.16612	-0.01199	0.193835	
Rb	0.185976	-0.03788	0.682081	0.246762	-0.21201	0.173008	0.485896	0.038224	-0.08079	0.052845	0.054237	-0.69573	0.197091	-0.17798	0.088483	0.671114	-0.10909	0.58349	-0.01619	0.040972	0.759496	0.217144	0.303513	-0.04511	-0.00362	
Re	3.2E-16	-2.6E-16	1.68E-16	1.47E-16	1.46E-16	1.37E-16	-1.4E-16	-2.6E-18	-1.6E-17	5.51E-17	9.83E-17	1.53E-17	3.02E-16	-3.9E-17	8.18E-17	-5.1E-16	6.17E-16	6.98E-16	2.41E-16	4.79E-16	1.81E-16	-1.4E-16	-3.7E-17	-3.7E-17	-4.2E-17	
S	0.334038	-0.05698	-0.07877	0.498673	-0.01525	-0.21782	0.242582	-0.19899	0.013403	0.154768	-0.32436	0.085863	-0.43609	-0.09771	-0.20552	0.095042	-0.01117	0.338754	0.250627	-0.28648	0.003095	0.281724	0.051977	-0.27681	-0.0819	
Sb	0.509077	0.533333	-0.07902	0.552481	-0.17829	-0.44454	-0.0847	-0.31472	0.064413	0.088449	-0.18433	0.101616	-0.15784	0.635144	-0.09256	-0.10212	1.38226	0.033451	0.365884	-0.12271	-0.13846	0.142313	-0.1431	-0.36693	-0.05094	
Sc	-0.15088	-0.20589	-0.27331	-0.07174	0.097307	-0.2034	-0.47559	0.564792	-0.18925	0.45971	0.561157	0.227382	-0.12625	-0.02405	0.56848	-0.36737	0.645898	-0.47981	0.365347	0.885084	-0.14258	-0.00601	-0.27568	0.688732	-0.07829	
Se	-0.06199	-0.06474	-0.20016	0.510148	0.036907	-0.36341	-0.36401	-0.12511	-0.09493	0.47185	0.032176	0.14849	-0.28688	0.007292	0.065086	-0.26616	0.647458	-0.23288	0.655591	0.174468	0.01222	0.229138	-0.34881	-0.02653	-0.1864	
Sn	-0.16314	-0.30919	-0.01728	0.038644	0.045031	0.021115	-0.16074	0.392739	-0.10551	0.706457	0.454239	-0.02507	-0.09748	-0.2742	0.609888	-0.03106	0.743736	-0.06378	0.473811	0.849249	0.02345	0.393409	-0.01036	0.604531	-0.05342	
Sr	-0.29643	-0.19665	-0.3377	-0.21316	0.554039	-0.08569	-0.57117	0.62501	0.105227	0.035769	0.591911	0.394553	-0.04306	0.097302	0.25827	-0.46648	0.174739	-0.64208	-0.22299	0.279546	-0.03279	-0.30458	0.32068	0.556129	0.244617	
Ta	-0.07298	0.165623	0.605404	0.024421	0.348255	0.443367	0.338213	-0.25853	0.566136	-0.24229	-0.05492	-0.54363	-0.06028	-0.30541	0.201092	0.512088	-0.01387	0.501757	0.000413	-0.17365	0.355192	0.470779	0.228473	-0.01056	0.416642	
Te	0.275804	0.92813	0.158448	0.038175	0.050391	-0.21901	-0.16071	-0.12504	0.098091	-0.24225	0.070269	-0.04543	0.156441	0.936956	-0.07193	0.027435	-0.12094	-0.22297	0.065782	0.041907	0.057965	-0.2456	-0.15796	-0.09404	0.254454	
Th	0.170455	-0.05332	0.565772	0.272303	-0.35879	0.453507	0.866144	-0.38613	0.032885	0.121279	-0.37014	-0.55106	0.0833	-0.35825	-0.02955	0.799328	-0.20428	0.989584	0.02469	-0.2625	0.257205	0.550633	0.614007	-0.29465	-0.06378	
Ti	-0.27022	-0.20944	-0.01806	-0.03623	0.294256	0.032557	-0.2995	0.418043	0.115864	0.752432	0.533014	-0.00437	-0.17235	-0.2675	0.707763	-0.13324	0.772467	-0.16729	0.417613	0.801601	-0.02619	0.387262	-0.10308	0.677691	0.145447	
Tl	0.503319	0.122902	0.312753	0.598656	-0.35208	-0.24998	0.399767	-0.45396	-0.00668	0.150782	-0.32174	-0.34834	-0.17204	-0.06404	-0.09999	0.315335	-0.02829	0.597851	0.254747	-0.2914	0.180868	0.410034	0.162456	-0.47684	-0.26936	
U	0.404883	-0.15361	0.318061	0.368661	-0.56481	0.19127	0.715497	-0.37937	-0.18404	0.21963	-0.424	-0.38743	0.018201	-0.30255	-0.08865	0.594469	0.006281	0.864604	0.32919	-0.13156	0.118539	0.574135	0.595747	-0.347	-0.32662	
V	-0.15346	-0.01484	0.180684	0.212051	0.305513	0.099626	-0.09924	0.438064	0.187945	0.647322	0.603522	-0.03256	-0.25194	-0.12605	0.73668											
















Grouse Mountain: Pearson's Correlation Coefficients Con't



















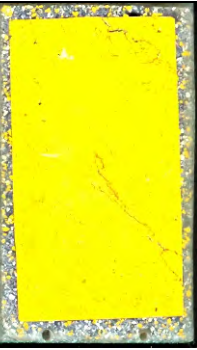
Grouse	Mo	Na	Nb	Ni	P	Pb	Rb	Re	S	Sb	Sc	Se	Sn	Sr	Ta	Te	Th	Ti	Tl	U	V	W	Y	Zn	Zr
Au																									
Ag																									
Al																									
As																									
Ba																									
Be																									
Bi																									
Ca																									
Cd																									
Ce																									
Co																									
Cr																									
Cs																									
Cu																									
Fe																									
Ga																									
Ge																									
Hf																									
Hg																									
In																									
K																									
La																									
Li																									
Mg																									
Mn																									
Mo		1																							
Na	-0.24863		1																						
Nb	0.157285	0.19611		1																					
Ni	-0.0731	-0.16472	-0.53742		1																				
P	-0.21921	-0.05107	-0.35626	0.384878		1																			
Pb	0.006308	-0.0933	0.197787	0.068979	-0.09256		1																		
Rb	0.254232	-0.03187	0.420636	-0.13622	-0.16768	-0.2213		1																	
Re	6.69E-17	-9.8E-17	-7.6E-17	5.59E-16	-8.5E-17	-2.2E-16	-1.1E-16		1																
S	0.184616	-0.22914	0.259235	-0.40552	-0.22678	-0.10699	0.033327	-2.7E-17		1															
Sb	0.597492	-0.41428	-0.13559	0.152901	-0.20534	0.045164	0.096143	2.77E-16	0.306753		1														
Sc	-0.11067	-0.05914	-0.48556	0.343549	0.940995	-0.22564	-0.14968	1.1E-16	-0.2179	-0.09394		1													
Se	0.10069	-0.31966	-0.26308	0.195841	0.270243	-0.073	-0.05939	-1.8E-16	0.092999	0.27203	0.36296		1												
Sn	-0.04038	0.020419	-0.05925	0.08947	0.835751	-0.21988	0.099664	-2.4E-16	-0.10888	-0.17085	0.858988	0.386734		1											
Sr	-0.21585	0.042903	-0.59079	0.438099	0.409203	-0.058	-0.28571	-2.3E-16	-0.212	-0.1568	0.359704	0.177566	0.155211		1										
Ta	0.08718	0.132999	0.793455	-0.32839	-0.18748	0.593838	0.178366	3.7E-16	0.125509	-0.227	-0.38262	-0.17327	-0.0653	-0.30767		1									
Te	0.032324	-0.1395	-0.18335	0.261415	-0.08422	0.354462	-0.0208	1.34E-16	-0.0888	0.598222	-0.06914	-0.04849	-0.26268	-0.06035	-0.09648		1								
Th	0.309402	0.13594	0.915363	-0.50518	-0.4459	-0.06436	0.568921	2.91E-16	0.295509	0.034298	-0.49817	-0.23545	-0.07312	-0.64934	0.536038	-0.22343		1							
Ti	-0.09415	0.012354	-0.02365	0.136302	0.863694	0.059848	-0.09683	-8.8E-17	-0.10238	-0.24872	0.805885	0.33119	0.91734	0.224878	0.170441	-0.22981	-0.16107		1						
Tl	0.584331	-0.52128	0.424028	-0.20318	-0.41065	0.042192	0.547489	-7E-17	0.450161	0.57027	-0.35775	0.139278	-0.15047	-0.53116	0.206349	0.03336	0.589693	-0.24636							
U	0.462197	-0.05954	0.653319	-0.48851	-0.29388	-0.31063	0.555548	5.08E-16	0.39125	0.249841	-0.23576	-0.00529	0.127291	-0.61793	0.181548	-0.21696	0.837532	-0.08866	0.69767						
V	0.075079	-0.1388	0.165679	0.290209	0.608517	0.130784	0.114221		0.090718	0.032398	0.464243	0.380123	0.602889	0.317996	0.277057	-0.09104	0.079237	0.687475	0.048118	0.047311					
W	0.249776	-0.26092	0.240826	-0.27156	-0.13802	-0.26397	0.31644	-2.1E-16	0.040289	0.058644	-0.07203	0.191082	0.147465	-0.44688	0.034236	-0.19117	0.400713	0.052012	0.377012	0.488031	-0.03284				
Y	0.196501	-0.17196	-0.26145	0.275933	0.484236	-0.13179	-0.03207	1.08E-16	0.04621	0.284759	0.563407	0.837478	0.633158	0.257579	-0.14906	-0.11918	-0.20745	0.594877	0.084241	0.049403	0.542266	0.205045			
Zn	0.114856	0.177213	0.307998	-0.1365	-0.02476	0.549291	-0.1119		0	-0.0583	-0.14338	-0.17361	-0.13348	-0.06426	0.154419	0.706119	0.032303	0.034922	0.208772	-0.139	-0.27718	0.255457	-0.1862	-0.07725	
Zr	0.344034	0.094638	0.898277	-0.51433	-0.44223	-0.07794	0.573138	-1.5E-16	0.310623	0.065521	-0.49033	-0.24121	-0.07225	-0.63311	0.526321	-0.21805	0.98018	-0.15801	0.62427	0.857116	0.088992	0.380754	-0.19951	0.049544	

Appendix H:
Grouse Mountain: Stained Billets

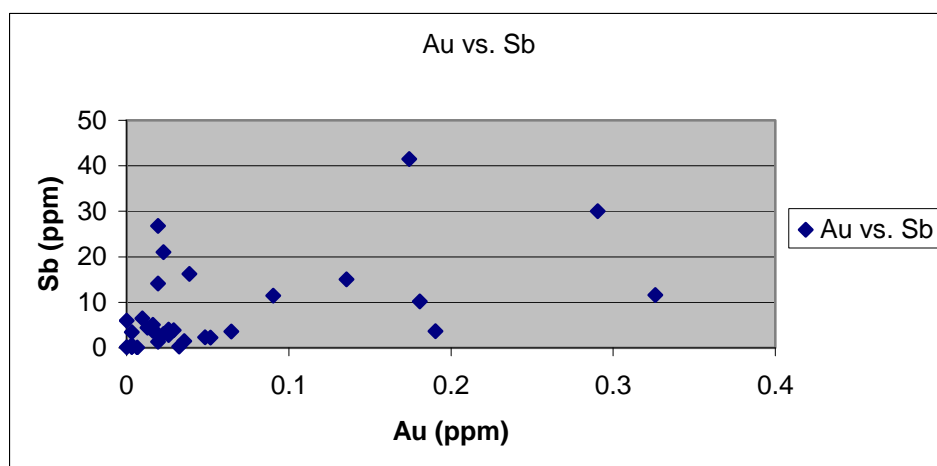
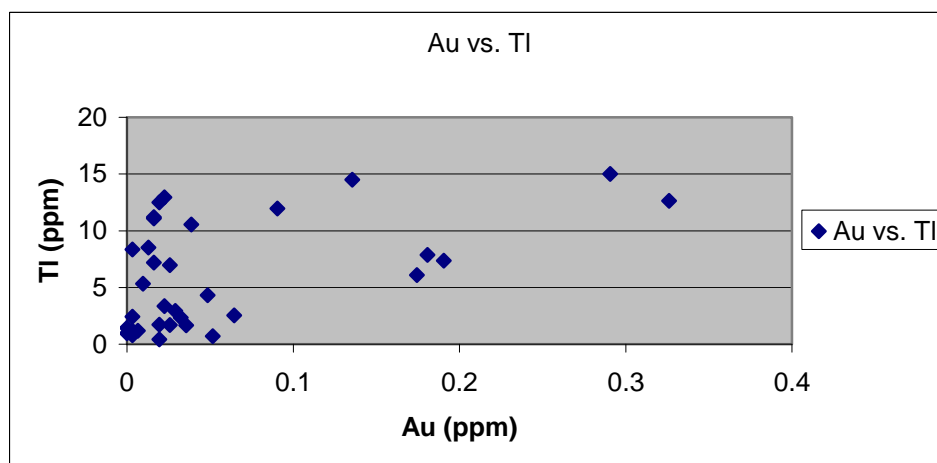
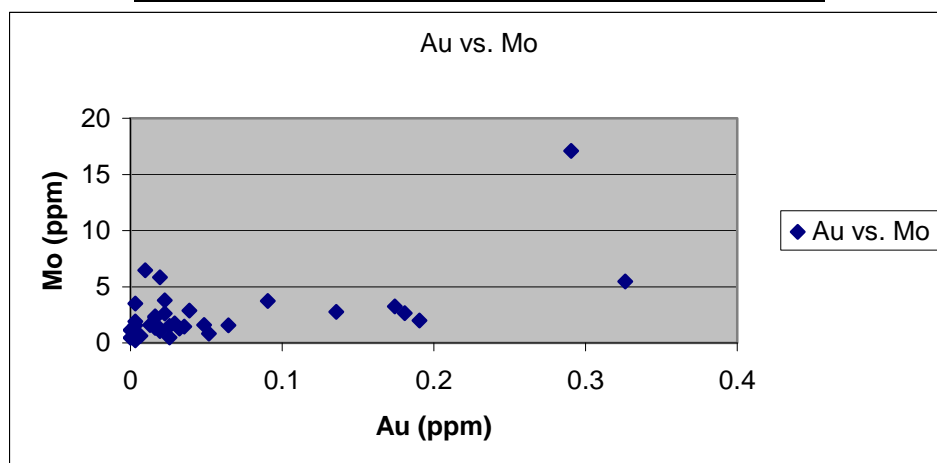
Grouse Mountain Stained Billets

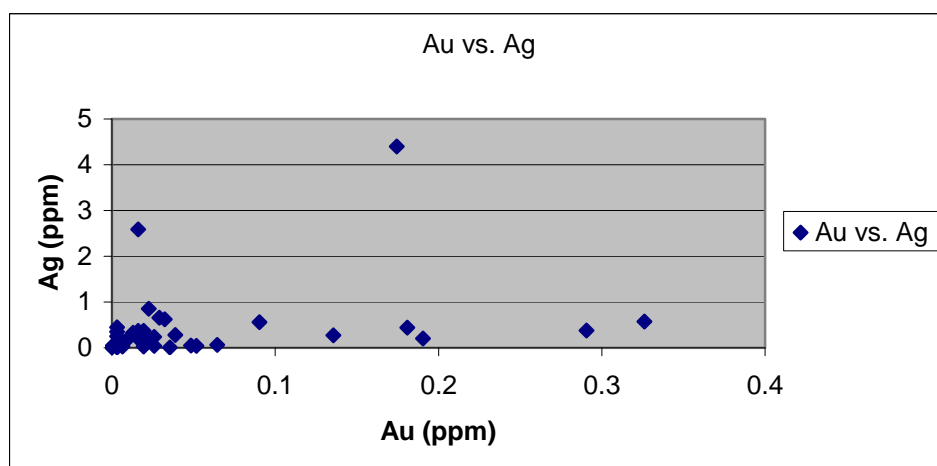
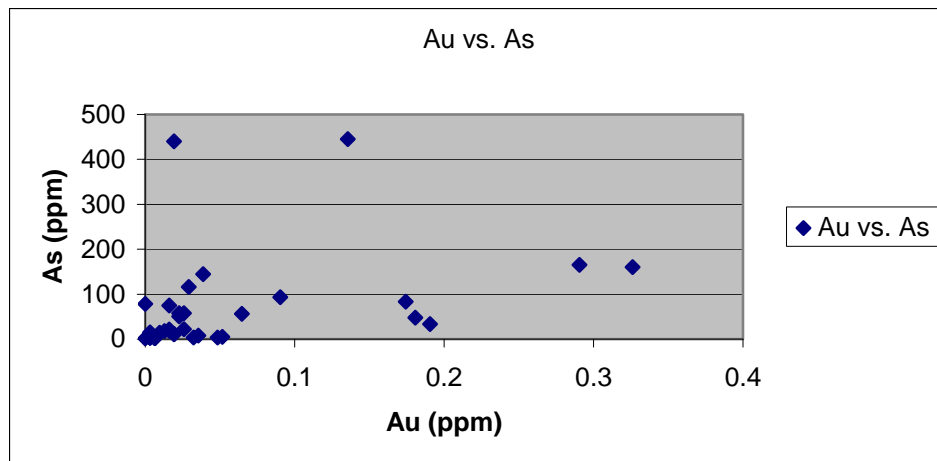
The stained billets below are labeled with three-digit sample numbers that correspond to the sample sites labeled on the Grouse Mountain map. An A, B, or C on the label indicates multiple samples at that site and an underscore followed by a number indicates more than one billet stained from a particular sample. A range such as 306-309 means the sample was one of several collected along a traverse between those waypoints. Due to poor exposure, most samples were collected from prospect pits or dumps.

				
129B	129B_2	133	133_2	146
				
224B	224B_2	234	248	295A
				
295B	295C	295C_2	306-309	306-309_2

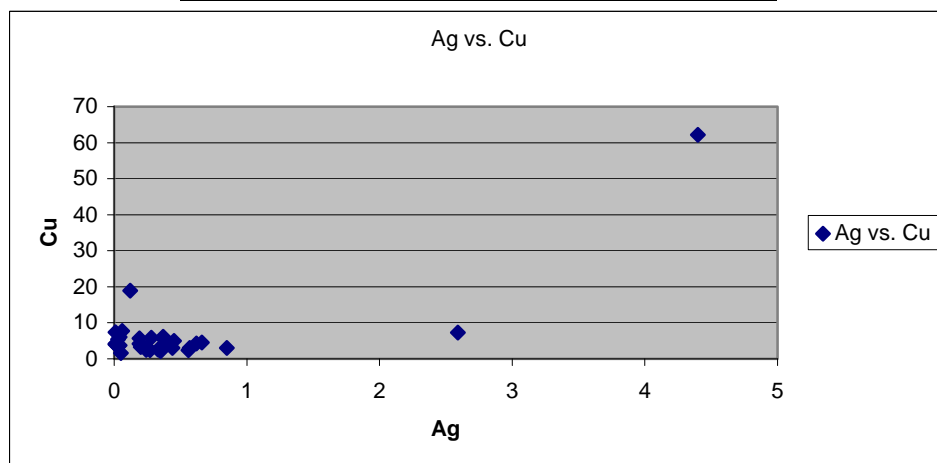
Grouse Mountain Stained Billets Continued				
				
306-309A	308A	308A_2	308B	313B
				
390	415B	416A	416A_2	416B
				
433	517	531	531B	535
				
541A	552	Bx1_416	Bx2_297	

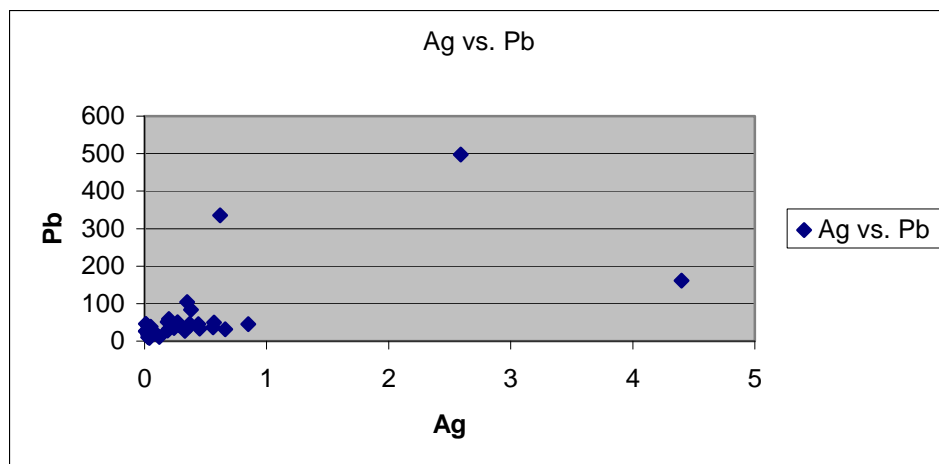
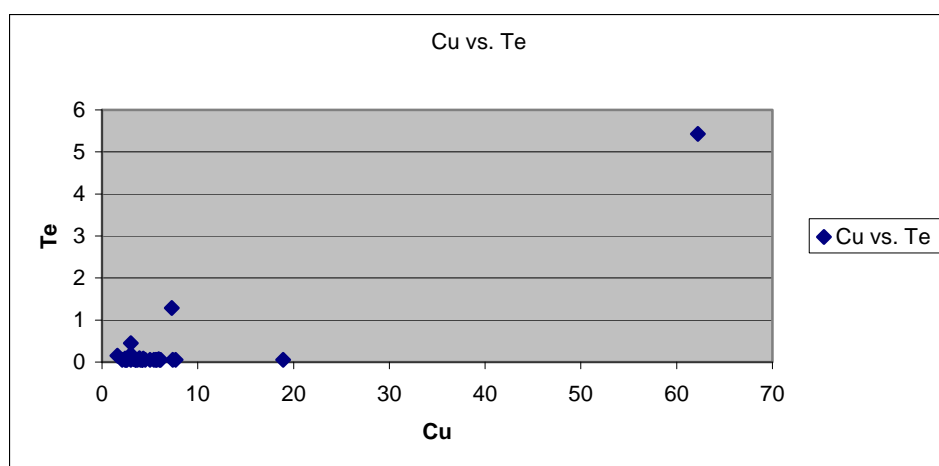
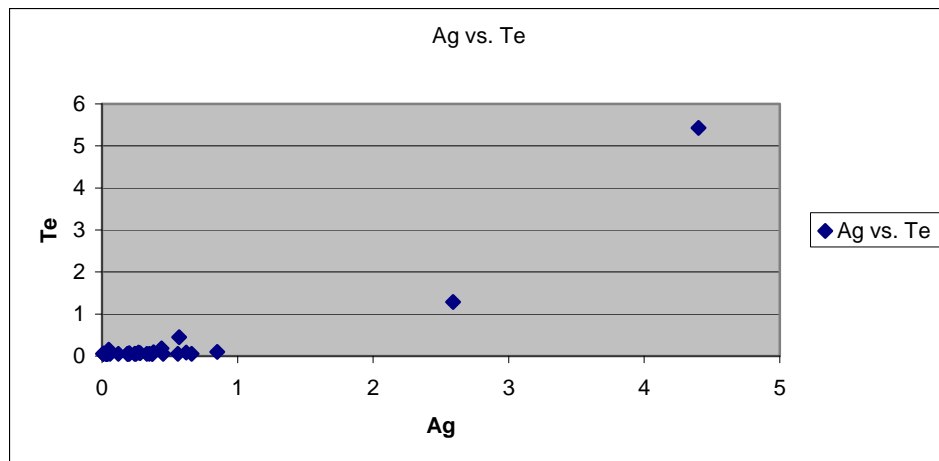
Appendix I:
Grouse Mountain Geochemical Graphs

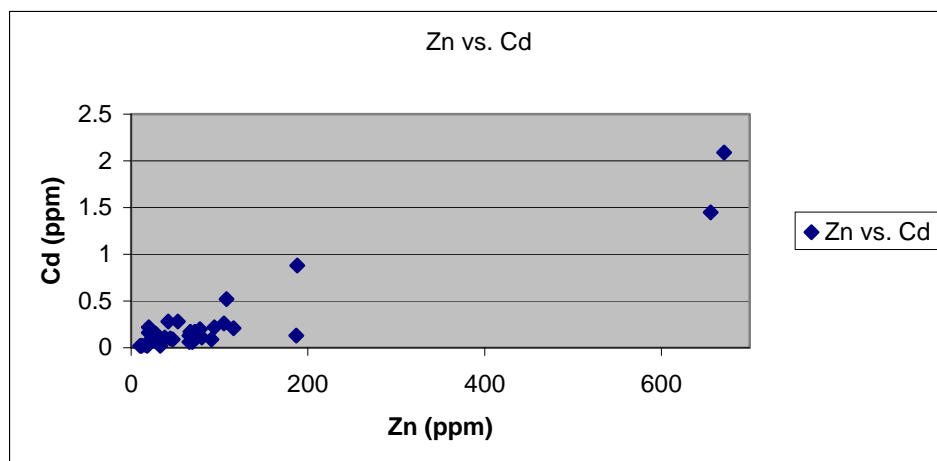
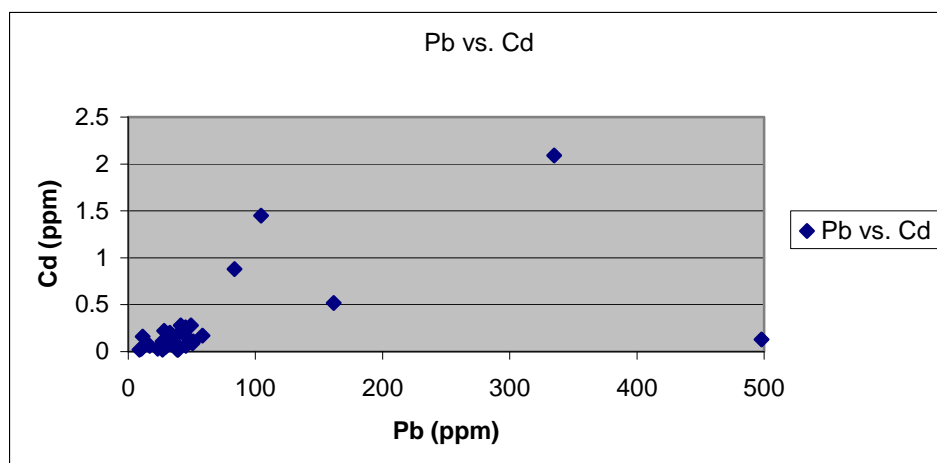
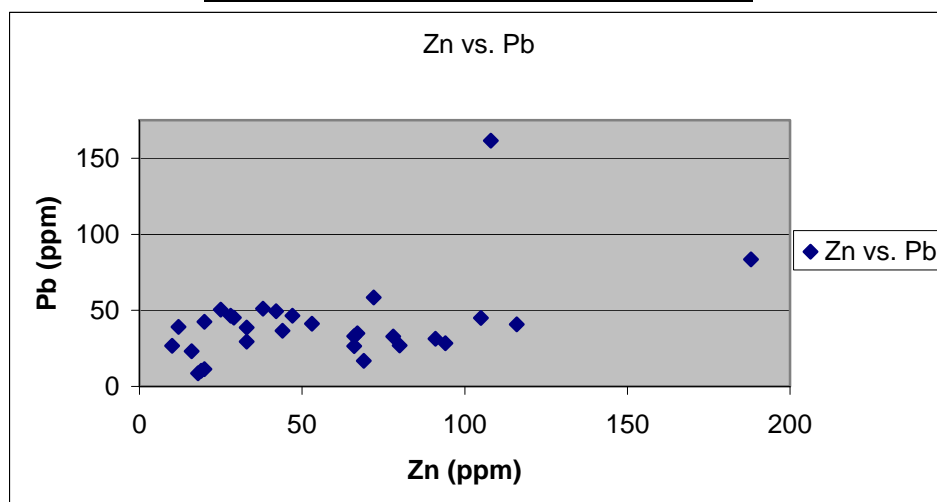
Hydrothermal Fluid #1: Au-Mo \pm Tl, Sb, As, S, Ag



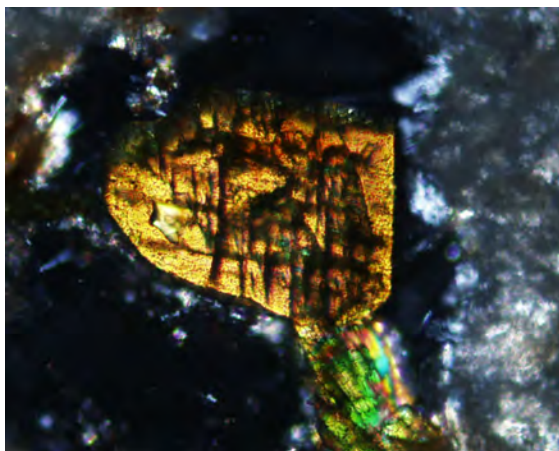
Hydrothermal Fluid #2: Ag-Cu-Te ± Pb, Sb



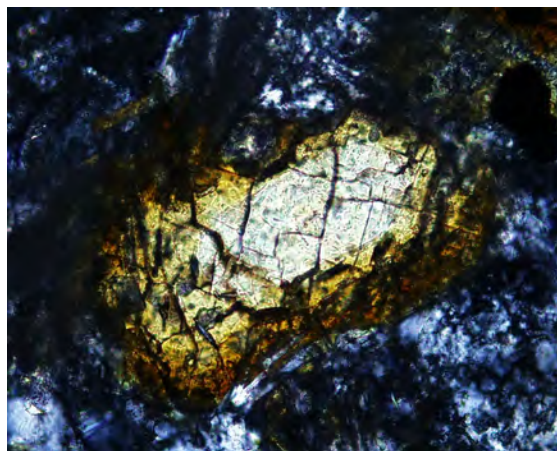


Hydrothermal Fluid #3: Pb-Zn-Cd \pm Ag

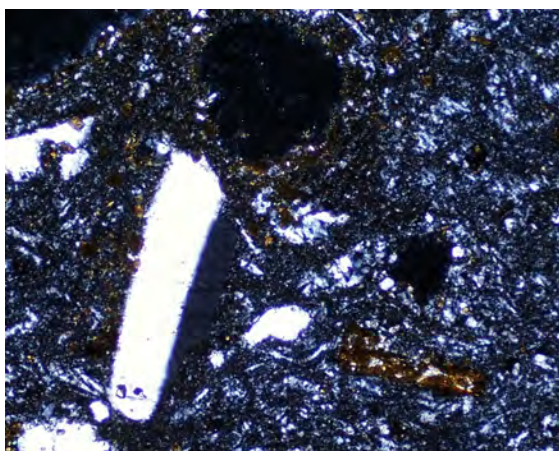
Appendix J:
Grouse Mountain Photographs and Photomicrographs



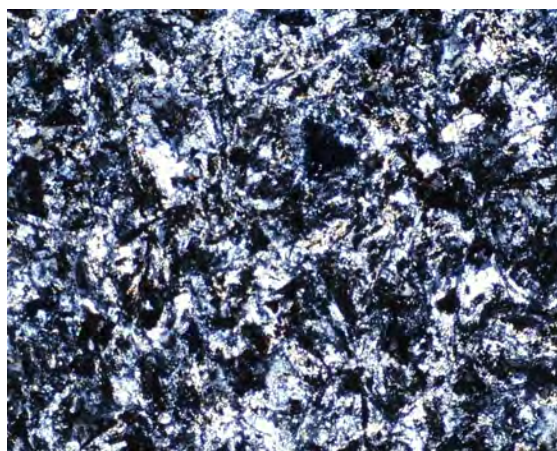
1) View of 90° cleavage in clinopyroxene grain from waypoint 416.



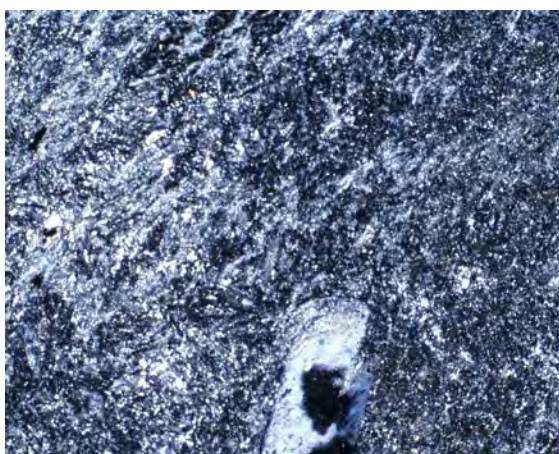
2) View of 90° cleavage in clinopyroxene grain from sample collected between waypoints 306-309.



3) Altered Wall Mountain Tuff from Bx2.



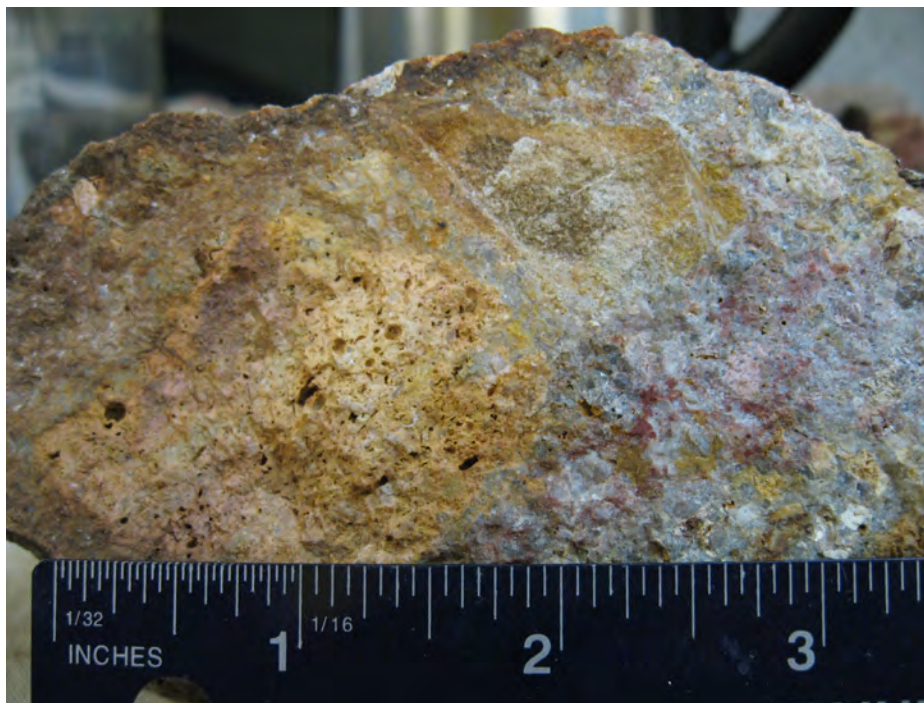
4) Mildly altered phonolite clast in Bx2.



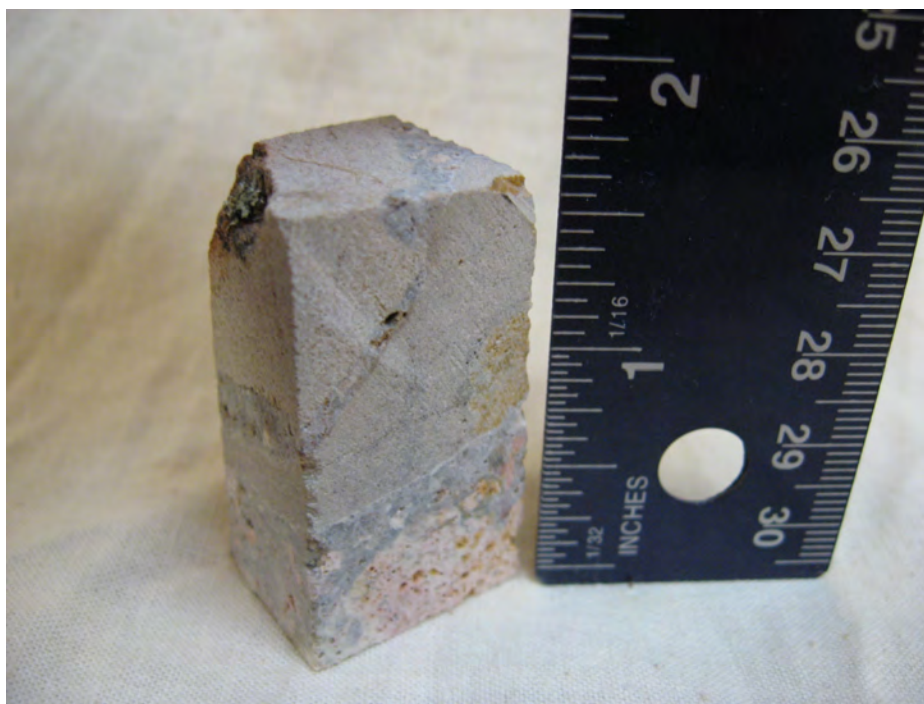
5) Mildly altered porphyritic phonolite from waypoint 535.



6) Aphanitic phonolite from a dike at waypoint 248.



Sample Bx2 with altered Wall Mountain Tuff clast adjacent to phonolite clast surrounded by a heterolithic breccia matrix.



View of the billet cut from sample Bx2 showing the brecciated phonolite clast and adjacent Wall Mountain Tuff clast.